Synthesis of zeolites from coal fly ash for the extraction of chromium from wastewater treatment plants

By

Malete Emmanuel Marakalala

Student no: 11617888

A dissertation submitted to the Department of Chemistry, University of Venda in fulfilment of the requirement for the degree of Masters in Science in Chemistry

April 2021

Declaration

I, **Malete Emmanuel Marakalala** (Student number 11617888), hereby declare that this dissertation entitled “Synthesis of zeolites from coal fly ash for the extraction of chromium from wastewater treatment plants” is my own work. This work has not been submitted for any degree at any other university or institution and that all reference materials contained therein have been duly acknowledged.

Student’s signature Date

06 - 07 - 2021

Mr Marakalala ME

Abstract

South Africa consumes more than 100 million tons of low-grade coal annually to produce electricity. This process results in generation of vast amounts of waste ash in coal fly ash (CFA) which is voluminous and is a source of toxic particulate matter into the atmosphere. In this work, a zeolite was synthesized from CFA for the selective and efficient extraction of chromium ions from wastewater treatment plants (WWTPs).

The first part of the study was directed at characterization of CFA and performing optimization studies for the dissolution of the CFA aluminosilicate matrix. The dissolution conditions studied were concentration of NaOH activating agent (0.5 - 2.5 M), ageing time (24 h - 72 h) and the solid/liquid ratio (15 g/30 mL - 15 g/100 mL). The optimized concentration of activating agent was 2.5 M NaOH, aged for 24 h at a solid/ liquid ratio of (15 g/100 g/mL).

The second stage was focused on optimization of crystallization conditions of the CFA/NaOH slurries for the synthesis of zeolite. The effect of changing the water content, crystallization time, and crystallization temperature was studied, and the optimized conditions were H_2O/SiO_2 molar ratio of 1.81 crystallized at 140°C for 24 h. FT-IR studies revealed the formation of zeolitic bands as a result of asymmetric stretching of Al-O and Si-O, indicating conversion of the CFA aluminosilicate phase.

Characterization of CFA using X-ray fluorescence (XRF) analysis indicated that CFA was class C with a Si/Al ratio of 1.19 and a loss on ignition (LOI) of 3.29%. Batch adsorption and kinetic studies revealed that Cr (VI) adsorption onto zeolites particles followed a Freundlich adsorption isotherm as well as a pseudo-second-order adsorption model.

This study indicated that the binding surface energies on the zeolites were heterogeneous, resulting in multiple interactions via chemisorption. Removal efficiencies for Cr (VI) during applications studies from Makhado and Rietviei WWTPs using inductively coupled plasma atomic emission spectroscopy (ICP-OES) were found to be 69.25% and 70.02%, obtained for zeolite.

Dedication

I would like to dedicate this work to my father, Koena France Marakalala, my Mom, Mperekeng Magrath Marakalala, my siblings, Nare Lebepe and Maboloka Jimmy Marakalala. To them I say thank you for your motivation, encouragement, and financial support to keep me going.

Acknowledgements

- First, I would like to thank God the Almighty for granting me strength to successfully completing this research dissertation.
- I am indebted to my supervisor Dr N.T Tavengwa for the support and guidance. Without him, this research would not have been possible.
- I owe my deepest gratitude to my lovely parents and siblings for their endless love, prayers, support, and encouragement. You are my rock.
- I wish to thank Miss R Murovhi for her continuous support.
- I would also like to express my gratitude and deepest appreciation to the Department of Chemistry for their insightful comments and ideas. Many thanks.
- I am indebted to the University of Venda for its material support.
- Many thanks to all who helped me to complete this work but not mentioned here.
- I am thankful to Sasol INZALO Foundation / National Research Foundation (NRF) for financial support that made this project a success.

Table of contents

List of figures

List of tables

List of abbreviations

AAS	Atomic absorption spectroscopy
CFA	Coal fly ash
DWAF	Department of Water Affairs and Forestry
EC	Electrical conductivity
FAAS	Flame atomic adsorption spectroscopy
FT-IR	Fourier Transform Infra-Red
ICP-OES	Inductively coupled plasma atomic optical emission spectroscopy
LOI	Loss of ignition
Mt	Million tons
NaOH	Sodium hydroxide
PFO	Pseudo-first order
pH	Hydrogen ion concentration in aqueous media
PSO	Pseudo-second order
RT	Room temperature
S A	South Africa
TDS	Total dissolved solid
TDS	Total dissolved solids
WHO	World Health Organization
WWTP	Wastewater treatment plant
XRF	X-ray fluorescence

Chapter one

Introduction and background

This chapter provides an overview of the research and its context. The problem statement is outlined, as are the study's aim and objectives.

1. **Introduction**

1.1 **Background of the study**

Coal fly ash (CFA) is a coal combustion by-product abundant in elements such as Al and Si, with traces of Ca, K and Na amongst others (Mokgehle et al., 2020; Gollakota et al., 2019). CFA, which is produced during the combustion of coal, is an industrial by-product (Elavarasan et al., 2019), and it has mainly been disposed as solid waste in landfills (Zhang et al., 2020).

CFA production is estimated to be more than 500 million tons, a figure that is expected to rise as power demand rises (Feng et al., 2019; Ozdemir et al., 2019; Yang et al., 2019; Yang et al., 2019). If not properly handled, this massive amount of industrial waste could cause significant environmental and ecological problems (Ozdemir et al., 2019).

The sustainable management of the large volumes of CFA produced from coal-fired power plants utilizing second rate coal to produce power is a significant concern to the climate. By and large, coal mining, transportation, arrangement, burning, and CFA stockpiling exercises bring about a few natural effect (Akinyemi et al., 2019). Due to its high silicon and aluminum content, South African CFA could address significant optional asset of refined silica and alumina, given appropriate financially practical cycles can be created (Aphane et al., 2019).

The utilization of CFA as a starting material for the synthesis of zeolite is an investigation of interest due to zeolite's its numerous industrial applications as a sorbent for the removal of heavy metal particles and natural impurities from wastewaters, gas partition, and as substitution for phosphates in cleansers (Dudley et al., 2011; Gadore at el., 2021; Harizi et al., 2020; Sarti, et al., 2014.). The conversion of CFA into zeolite helps CFA to be harmless to the environment in a way that is economically viable.

In recent years, there has been a broad writing on the utilization of low-cost adsorbents to eliminate poisonous metals from water and wastewater (Joseph et al., 2019; Quesada et al., 2019; Chakraborty et al., 2020; Siddiqui et al., 2019; Nasar et al., 2019). Aside from the financial benefit, the usage of low-cost adsorbents allows the revalorization of waste or dismissed materials, accordingly, adding an environmental benefit to this approach. Adsorption is one of the promising methods that has been widely studied and applied for removing heavy metals from wastewater (Tahir et al., 2019; Hui et al., 2005; Tamjidi et al., 2019; Zhu et al., 2019;).

In most cases, adsorption is a reasonable process and does not require cutting edge innovations (Sen et al., 1987; Verrecchia et al., 2020; Angaru et al., 2021; Reshadi et al., 2020). A developing number of studies as of late have proposed different low-cost sorbents (Ren et al., 2014). CFA, naturally occurring zeolites, and engineered zeolites from low-cost starting materials, containing Si and Al, are examples of such adsorbents (Azizi et al., 2013; Cai et al., 2014).

According to Xu et al. (2013), CFA particles have a permeable surface and enormous specific surface zone bringing about high adsorption movement and arrangement of efficient and compelling adsorbents from CFA look good for high esteem reusing. CFA has extraordinary potential in the treatment of wastewater, gas, and oil in ecological remediation (Luo et al., 2020; Li et al., 2021; Nadeem et al., 2021; Wang et al., 2020; Liu et al., 2020).

The utilization of CFA as an adsorbent of metals from water has been reported by a few studies (Ochedi et al., 2020; Mushtaq et al., 2019; Gadore et al., 2021; Rojas et al., 2020; Asl et al., 2019; Rech et al., 2019). To expand its sorption dynamic and capacity, CFA is regularly submitted to a basic treatment at high temperature, subsequently improving its active surface region, or changing it into an engineered zeolite-type material (Azizi et al., 2021; Chen et al., 2018; Doumit et al., 2019). The basic nature of CFA compounds normally makes them more effective in the removal of cationic metals (Zhou et al., 2019; Visa et al., 2014; Singureanu et al., 2017; Futsaeter et al., 2013; Ren et al., 2020; Lin et al., 2019).

Zeolites are 3D aluminosilicate frameworks, hydrated (Feng et al., 2019) with porous crystalline structures (Ozdemir et al., 2019) that have wide ranging usage in the fields of adsorption, catalysis (Bai et al., 2019) and ion exchange (Joseph et al., 2019; Bai et al., 2019). Zeolites have been effectively utilized in the fields of oil refining, environmental security, and methanol to light olefins due its customizable surface acidity, micropore structure, and hydrothermal stability (Odlare et al., 2014).

Nowadays, it is still of crucial significance to decrease expenses to blend this zeolite with a more affordable silica and aluminum crude materials (Feng et al., 2019). The use of CFA in this project is an advantage because it is readily available, and it is rich in both silica and aluminium.

Adsorptive removal is quite possibly the most generally utilized methodology (Sajid et al., 2014; Annadurai et al., 2003). The adsorption method stays the best and normal material innovation broadly utilized over different procedures in worldwide environment protection areas (Chen et al., 2015). Adsorption has benefits over the customary techniques which includes reusability of biomaterial, low working expense, selectivity for specific metal, short operation time and no chemical sludge (Rahmani et al., 2009; Shah et al., 2009).

In the adsorption cycle, three phases usually happen, including the adsorption for the surface, the reversal, and the moderate adsorption inside the microcrystal (Irannajad et al. 2020). Studies on the adsorption of heavy metals by natural zeolites are yet attractive to scientists (Irannajad et al. 2020).

The contamination of water resources with heavy metals pose danger to the human and the natural life as referenced here. Various techniques have been adopted to decontaminate the water by eliminating the load of heavy metals (Zhu et al., 2016). A few zeolites have restricted metal adsorption limit and may require a chemical treatment before use in water or wastewater treatments. As of late, the chemical modification of zeolites has been investigated with the purpose of expanding metal binding capacity of these materials (Jiménez-Castañed et al., 2017).

Because of their high ion exchange capacity, adsorption molecule sieving capacity, and low cost (He et al., 2000), zeolites are potential adsorbents used for water remediation. Synthetic zeolites are aluminum silicates characterized by three-dimensional organizations of tetrahedral units of silica and alumina connected by the sharing of all oxygen atoms, with channels.

Zeolites show great affinity for metal cations and adsorption and catalytic properties (Dursun el at., 2007). Moreover, cations of sodium, calcium, and potassium that are regularly present in the channels of the zeolite design can be replaced by other metal cations, including lead, cadmium, zinc, copper, nickel, iron, chromium, and manganese (Apreutesei et al., 2008; Gupta et al., 2013).

Heavy metals are naturally occurring elements with a high atomic weight and a density that is at least multiple times that of water (Tchounwou et al., 2012). The toxicity of heavy metals varies. While some are lethal even at low concentrations, others are lethal due to bioaccumulation; poisonous effects range from nervous system disruption to carcinogenic potential, as referenced above (Joseph et al., 2019).

One of the harmful heavy metals is chromium and is viewed as a priority pollutant (Tavengwa et al., 2013). The name Chromium is derived from the Greek word "Chroma" which means color due to its nature of giving color to its compounds (Gautam et al., 2016). People are exposed to chromium through breathing, eating, or drinking and through skin contact with chromium or chromium compounds (Rangabhashiyam et al., 2018).

Chromium exists in numerous oxidation states of which hexavalent chromium (Cr (VI)) and trivalent chromium (Cr (III)) are the most stable. Trivalent chromium is fundamental for digestion in mammals (Velempini et al., 2017; Zhou et al., 2020; Chen et al., 2015).

For the vast majority. Eating food that contains chromium (III) it is the primary course of chromium uptake, as chromium (III) occurs normally in many vegetables, organic products, dietary enhancements (Tang et al., 2018; Shanker et al., 2005) meats, yeasts, and grains (Vincent., 2020). This is because of the low solubility retains Cr (III) in the solid phase as colloids or precipitates.

Cr (III) in low dosages is a fundamental dietary mineral and found in drinking water just as in most fresh food sources including breads, meats, and vegetables as referenced above (Swaroop et al. 2019). Besides, mounting evidence has shown the beneficial impacts of chromium supplementation on bodyweight, glycemia and fasting plasma glucose in patients with diabetes mellitus (Tang et al., 2018). This makes Cr (III) less harmful to human health and biological system (Jobby et al., 2018; Ou et al., 2020).

On the other hand, excessive uptake of Cr (VI) could prompt negative health impacts. Cr (VI) is experimentally affirmed to be 100 times more harmful than Cr (III); Cr (VI) is more soluble and versatile in water (about 500 times), more poisonous and is genotoxic, mutagenic, and carcinogenic to people, and Cr (VI) likewise causes birth defects and decreases productive health. Ingestion of chromium in enormous portions may cause death in creatures and humans.

Chromium is a poisonous contaminant, even in low concentrations. Chromium compounds are broadly utilized in a few modern processes, like printing, electroplating, concrete residue (Banat et al., 2005; Farzadkia et al., 2016) leather tanning (Tariq et al., 2005), fertilizers (Zeremski-Škorić et al., 2010; Poznanović Spahić et al., 2019).

Polishing and pigment businesses (Jacobs et al., 2005), lead to the emission of Cr (VI) and thus add to heavy metal contamination. More specifically, the wastewater produced by these industries normally contains Cr (VI) at high concentrations (Vasileiou et al., 2019).

Inhalation of hexavalent chromium compounds can bring about ulceration and hole of the mucous layers of the nasal septum, disturbance of the pharynx and larynx, asthmatic bronchitis, bronchospasms and edema. Chromium can prompt malignant growth in the lungs and stomach related lot (Ngah et al., 2008; Bayuo et al., 2019). Respiratory side effects may include hacking and wheezing, windedness, nasal tingle, liver harm, spewing and pneumonic blockage (Qi et al., 2017; Taghizadeh et al., 2017; Pakade et al., 2011; Gautam et al., 2016).

Cr (VI) enters the body through food, breathing, or skin contact and accumulates in the liver, kidneys, and other vital organs. Cr (VI) inhaled during the respiratory interaction can accumulate in the lungs, causing rhinitis, pharyngitis, and various types of inflammation (Wu et al., 2018).

On the opposite, Cr (III) is vital for glucose resilience factor (GTF) and significantly affects lipid digestion, protein digestion, growth, and development (Coedo et al., 2000). To secure individuals' health, the highest content of Cr (VI) in drinking water is confined to be 0.05 mg L^{-1} as per World Health Organization (WHO) (Qi et al., 2017).

Various treatment strategies have been presented for removing heavy metals from the environment, Cr (VI) content in water. To begin with, the expansion of decreasing specialists to lessen the profoundly poisonous Cr (VI) to its low harmful partner, Cr (III) (Zhang et al., 2019; Kwak et al., 2018; Schlautman et al., 2001). These techniques include adsorption, oxidation, ion exchange, evaporation, flocculation, chemical precipitation, and electrochemical treatment.

The other technique includes the utilization of biomass adsorbents, like nut shells, banana strips (Ali et al., 2016; Cai et al., 2019) mineral adsorbents, like bentonite, montmorillonite, and clinical stone, to adsorb Cr (VI) and reduce its concentration in the wastewater. Nonetheless, this technique neglects to eliminate Cr from the system, and consequently, Cr (III) can at last oxidize back to Cr (VI) within the presence of oxides and oxide oxygen. In addition, the cost to remove the Cr precipitate is high (Saputro et al., 2014).

The above methods are simple to execute and has high adsorption proficiency. They are not good in decreasing the toxicity of Cr (VI), these techniques are likewise costly and wasteful to eliminate heavy metals. Among these, adsorption is the best and normally utilized technique to remove heavy metals owing to the simplicity in operation, proficiency, and minimal effort (Marella et al., 2020).

1.2 **Problem statement**

Heavy metal pollutants are non-biodegradable (Latif et al., 2020) and diligent in the environment and as such, accumulate in the environment over a long time, arriving at extremely toxic levels in many cases (Gautam et al., 2016). Heavy metal pollutants can likewise accumulate and arrive at poisonous levels in the bodies of living organisms, because of their expected negative effect on the human health whenever consumed unknowingly from contaminated food and water sources bringing about death (Gupta et al., 2010; Muchuweti et al., 2006; Suganya et al., 2019; Vardhan et al., 2019).

Some heavy metal pollutants occur in trace amounts in the environment and are extremely hard to detect. Heavy metals are transported by runoff from industries, regions, and metropolitan regions. A large portion of these metals wind up gathering in the soil and sediments of water bodies (Bhat et al., 2020). The releases from these industries comprise biohazard to man and other living organism in the environment since they contain poisonous substances negative to health (Anyakora et al., 2011).

CFA is voluminous material which led to this waste material to have a removal challenge for countries, such as South Africa whose primary source of power generation remains coal burning. The rate at which the CFA is delivered is greater than its application, delivering it environment unreasonable (Makgabutkane et al., 2020). This enormous amount of industrial waste could cause significant environmental issues if not treated (Ozdemir et al., 2019).

CFA is generally stored as stockpiles in coal fired power stations. These reserves are exposed to various climate conditions including wind and rain. CFA turns into a source of emission of particulate make a difference to the atmosphere, accordingly, influencing air quality (Ríos et al., 1998).

CFA is exceptionally abundant in South Africa and is therefore a low- cost alternative for the synthesis of zeolites for adsorption of heavy metals in wastewater. Of interest is the adsorption of Cr (VI) in the WWTPs, the overall impact of the pollutants is also shown in brackets such as Cr (VI) (ulcer, allergic dermatitis, lung cancer and liver necrosis).

There are numerous issues that are affecting WWTPs today, such as tighter guidelines for discharge into sewers or surface waters. Simultaneously, the test is on the best way to redesign existing technology and distinguish new advances for modern wastewater refinement for reuse. The growing demand for water for industrial, agricultural, environmental, and domestic purposes has increased the need for advancements in water treatment methods (Levantesi et al., 2010).

However, effluent discharge from treatment process can be a significant source of pathogenic bacteria in surface waters (Auerbach et al., 2007; Okoh et al., 2007). Due to specific factors like opposition of microbial community (Zhi et al., 2016; Owoseni et al., 2017; Dungeni et al., 2010) glitch or helpless administration of wastewater frameworks (Ahmed et al., 2005), effluent containing bacteria are released into receiving water bodies (Geary et al., 1998; Wakelin et al., 2008).

Different wastewater treatment techniques have recently been developed, both to reduce the amount of wastewater delivered and to improve the quality of the treated effluents. A portion of those treatment techniques include chemical precipitation is broadly utilized in the removal of heavy metals from the wastewater since it inexpensive and it is moderately easy to operate (Charerntanyarak, 1999; Izadi et al., 2017; Charerntanyarak, 1999; Izadi et al., 2017).

Coagulation–flocculation (Li et al., 2003), sorptive flotation (Doyle et al., 2003), ion exchange, membrane (Kurniawan et al., 2006), and separation membrane division has been progressively utilized as of late for the treatment of inorganic effluent. There are various sorts of membrane filtration like ultrafiltration (UF), nanofiltration (NF) and reverse osmosis (RO) (Juang et al., 2000).

The above treatment methods have limits and are not 100% effective in removing heavy metals. The chemical precipitation requires a lot of chemicals to decrease the metals to a sufficient level for discharge into the environment (Kostrubiak et al., 2017). Other disadvantages include a large amount of sludge generation, increasing sludge removal cost, more slow metal precipitation, poor settling, and the long-haul ecological effects of sludge removal (Yang et al., 2001).

However, these techniques have been investigated less widely because of the high operational expenses brought about by energy consumptions. Although numerous techniques can be utilized for the treatment of inorganic effluent, the ideal treatment ought to be reasonable, suitable, and relevant to the nearby local conditions.

To take benefits of the abundant CFA, there is a need to research the optimum procedure to synthesize financially viable zeolites and investigate their expected applications. In this regard, a synthesized zeolite will be utilized for the sequestration of heavy metal pollutants from WWTPs. Presently, there are very few value end strategists for the use of CFA in South Africa which make it hard for CFA to compete with other customary raw materials. The circumstance requires a more worth added high innovation use of CFA, for example, zeolite synthesis to overcome this barrier.

The synthesis of zeolites from CFA is still a research area of interest and receiving attention in academia and industry (Musyoka, 2009). The rate at which the CFA is delivered is greater than its application. In any cases, CFA has been utilized as a zeolite precursor considering its pervasive alumina and silica content (Makgabutlane, 2020).

More research is needed to improve the application and quality of zeolites made from CFA. This is due to insufficient experimentation on the optimization of zeolite synthesis methods to improve the purity of the zeolites formed. Exceptionally restricted research has been conducted on South African CFA under laboratory conditions which would lay a reason for enormous scale transformation of the CFA to zeolites with specific commercial applications.

The zeolite was chosen as a synthesis goal and subject of study because it can be synthesized without using templates under mild hydrothermal synthesis conditions, making zeolites potentially financially suitable. Because of the high polarity of zeolites and pores in their structure, it is not difficult to isolate heavy toxic metals, chemical pesticides, or other compounds due to the narrow particle size distribution combined with micron sized crystallites and the abnormal structure flexibility.

Regardless of whether the concentration of these materials in the environment is extremely low, zeolites have an extremely high potential for suction and absorption of water and other polar materials (Kianfar, 2019). Furthermore, scientific advances in the extraction of silica and alumina from aluminosilicate-rich raw materials (Missengue et al., 2018) support the synthesis of zeolites from CFA without the addition of additional silica or alumina sources.

This study attempts to synthesise zeolite to exploit the CFA properties and hydrothermal chemistry to remove heavy metals from wastewater and increase the body of knowledge on the utilization of zeolites for the extraction of heavy metals and reduce cost. It is also hoped that the experiments will contribute to a better understanding of the synthesis of zeolites from CFA. The study also serves as a foundation for understanding the prerequisites for future large-scale synthesis conditions and looks at potential areas for future research in the advancement of successful zeolites synthesis.

Unfortunately, the greater part of studies done to assess the presence of heavy metal contaminations in wastewater effluent have been done outside the geographical areas covered by Vhembe district. This study will without a doubt add on to the scant body of knowledge regarding heavy metal pollutants in Vhembe district.

This study can also serve as a model for similar studies in other rural areas of South Africa and the continent as a whole, as well as the rest of the world. This project is focused on the synthesis of zeolite from CFA for the extraction of heavy metal ions Cr (VI) from a WWTPs in Vhembe district (Makhado) Limpopo Province South Africa, taking advantage of the abundant CFA produced by South African coal-fired power stations or steam plants such as Modderfountein steam plant.

1.3 **Aim and objectives**

1.3.1 **Aim**

- Synthesis and application of zeolites from CFA for adsorbents in the removal of Cr (VI) and contained in the effluents of WWTPs from Makhado and Rietviei.

1.3.2 **Objectives**

- To synthesize zeolites from CFA using ageing and hydrothermal approach.
- To perform characterization studies: XRF, ICP-OES and FT-IR, on CFA and zeolite.
- To perform, batch study on zeolites sorbent where parameters such as temperature, initial concentrations, contact time, pH, and mass of adsorbent (zeolite) and percentage removal of respective parameter is calculated.
- To analyze Makhado and Rietviei WWTPs effluent water using ICP-OES.

1.4 **Research approach**

To achieve the above-mentioned objectives and selecting the right strategy for synthesizing and optimizing zeolite from CFA, the following approaches were considered:

- Explore the type of synthesis procedure to adopt by carrying out literature review.
- Choose the parameters to optimise and understand the effects of different variables on product purities based on literature review.
- Understand and quantify the effects of the varying synthesis parameters.
- Investigate the removal of toxic elements from wastewater using the zeolite synthesized.

1.5 **Dissertation structure**

This dissertation is organized into five chapters (including this one) and is structured as follows:

Chapter one, which is the introduction, presents the study's objectives, provides an outline of the research framework, and contextualizes the study by providing a brief overview of the background, problem statement, and general zeolites literature.

Chapter two This chapter reviews about coal. The chapter gives a detailed information about CFA, properties of coal fly ash, and the impact of fly ash into the environment, it also presents some methods that have been used to analyse CFA. Types of zeolites, properties of zeolites and zeolite synthesis.

Chapter three describe the research design and methodology.

Chapter four contain the results as well as the reference to relevant literature. The findings are summarized, followed up by discussion of the main trends and how they relate to the literature survey, as well as any correlation found in the data.

Chapter five concludes this dissertation by summarizing the main points, emphasizing the research's novelty, and providing conclusions and recommendations. An outline of aspects that require additional research is provided, as well as information on the significance of the study of zeolites synthesis.

Chapter two

Literature review

This chapter provides a short description about coal. In addition, the chapter gives information about CFA, properties of CFA, and the impact of CFA into the environment, types of zeolites, properties of zeolites, zeolite synthesis, metal ions (sources, toxicity, maximum permissible limits, and metal removals).

2. **Literature review**

2.1 **Coal**

Coal can also be classified according to rank into four groups: anthracite, bituminous, subbituminous, and lignite coal based on the percentage of carbon content and the heating value the amount of energy released when burned. The reserve of coal in South Africa is estimated at 53 billion tonnes, an average value of 224 million tons of marketable coal is produced annually, uplifting South Africa economy, and as well as making it the world's fifth largest coal producer. South Africa is the third largest coal exporting country in the world, with 23% of the coal produced being exported internationally, and 53% of the coal produced being used for electricity generation, with electricity produced through coal combustion covering 77% of the country's primary energy needs (Eskom, 2017).

Coal is a major source of energy all over the world (Yang et al., 2019). Coal supplied 29 % of global energy in 2015; despite increased use of renewables, the share of coal is expected to remain around 24 % by 2035. (Bhatt et al., 2019). In South Africa, the indigenous power utility company (ESKOM) generates 37 Mt of CFA annually (ESKOM, 2009), of which approximately 1.85 Mt is currently beneficially utilized, while approximately 35.15 Mt is unused and dumped in landfills, ponds, or ash dams (Akinyemi et al., 2019).

South Africa is largely dependent on the combustion of coal for electricity production (Akinyemi et al., 2019). Significant coal deposits in South Africa occur within the Great Karoo basin. This basin stretches for about 200 km from west to east across northern Free State Province and in the south and east of Mpumalanga Province, and for about 400 km from southern Mpumalanga Province in the north to the center of Kwazulu-Natal in the south. The recent energy crisis, which was largely caused by economic growth and social integration, has resulted in the construction of new coal power plants in South Africa. (Musyoka et al., 2009).

2.2 **CFA**

CFA is a byproduct of coal combustion (Akinyemi et al., 2019; Makgabutlane et al., 2020; Gollakota et al., 2019) that is produced in large quantities by thermal power plants such as Eskom in South Africa (SA) and the Modderfountein steam plant (Muriithi et al., 2020). Bottom ash, boiler slag, flue gas desulphurization material, fluidized bed combustion ash, and scrubber residues are all examples of waste (Hower, 2012).

It is widely available and is typically discarded as waste (Alzeer et al., 2018), in South Africa and many other parts of the world where electricity is produced by coal-fired power plants.

Coal is one of the most important fossil fuels used on a global scale (Yang et al., 2019). In most countries, coal-fired power plants are the primary source of energy, accounting for roughly 40% of total electricity generation (Ozdemir et al., 2019). In India, for example, thermal power plants that use coal generate approximately 71% of the country's electricity (Elavarasan et al., 2019). Large amounts of fly ash are produced by power generation or industrial coal combustion as the world economy develops and energy demand rises (Yang et al., 2019).

CFA is primarily composed of inorganic metal oxide minerals such as SiO_2 and Al_2O_3, expressed as $SiO_2 – Al_2O_3$ - EaO, where EaO are metal oxides of group 1 (Na_2O and K_2O), metal oxides of group 2 (CaO and MgO), and transition metal oxides such as MnO and ZnO. Because of its Si and Al content, this coal combustion by-product can be used as a feedstock for the synthesis of zeolites (Ameh et al., 2017).

The chemical composition of CFA varies depending on geographical location and coal source, but the predominance of SiO_2 and Al_2O_3 is consistent. Typically, the phases in fly ash include crystalline structures such as mullite, hematite, magnetite, and quartz. Zeolite could be used to stabilize and immobilize heavy metals and organic pollutants in water to reduce environmental harm (Zhang et al., 2019).

2.2.1 **Sources of CFA**

CFA, which is waste product from coal combustion and mining activity (Blissett et al., 2012), is produced in massive quantities due to the high demand for energy around the world by thermal power plants such as Eskom in South Africa and Modderfountein steam plant.

Every year, a significant amount of CFA is generated as solid waste around the world (Angaru et al., 2021). Because of the leaching of toxic chemicals from dumped fly ash into groundwater, disposing of such large amounts of ash has become a pressing environmental issue. Flay ash materials have serious environmental consequences. CFA production is expected to rise, making disposal of this waste by-product a concern.

CFAs are produced at temperatures ranging from 1200°C to 1700°C from the various inorganic and organic constituents of the feed coal. CFAs are one of the most complex anthropogenic materials that can be characterised due to the scale of the variety of components (Vassilev et al., 2005).

2.2.2 **Uses of CFA**

The use of fly ash in this synthesis process has the advantage of being a waste material, while its chemical composition is dominated by the formation of an amorphous aluminosilicate glass, which serves as a substrate in the synthesis of zeolites. This type of aluminosilicate is highly reactive and allows for rapid alkalization of the reaction solution, which is advantageous in terms of the costs associated with the synthesis process (Ameh et al., 2017; Kobayashi et al., 2020).

CFA can also be used as an adsorbent material to solve environmental problems such as reducing air pollution and treating wastewater (He et al., 2020; Kobayashi et al., 2020). (Sangaroon et al., 2019). The hydrothermal modification of CFA with NaOH solution resulted in increased pore volume and surface area, significantly improving adsorption capacity (Mushtaq et al., 2019). Colored impurities in wastewater have been removed using modified CFA (Mushtaq et al., 2019).

2.2.2.1 **Treatment of acidic soils**

CFA addition to soils has been shown to increase its water-holding capacity, which has contributed its increased utilization. In the reclamation of mine spoil or damaged soil, CFA is used alone or in combination with organic or inorganic materials. Certain properties of CFA make it suitable for agricultural use, including a favorable pH, significant concentrations of many essential plant nutrients, low bulk density, and silt-sized particles (Ram et al., 2010).

However, because CFA has the ability to release trace metals and/or soluble salts into the surrounding environment, this application is limited. To make this process more efficient, certain inorganic or organic alterations that render CFA metals and other salt ions biologically inactive must be added (Ram at el., 2010).

2.2.2.2 **Treatment of AMD**

Because of its neutralization capacity, CFA has been used in the treatment of AMD (Petrik et al., 2003), as an absorbent, and as a precursor for activated carbon for water purification (Mishra et al., 2010). Because both are waste materials, AMD neutralization with CFA is always a cost-effective process, and CFA is an economically viable absorbent with good adsorption efficiencies in certain applications, CFA is sometimes compared to commercial activated carbon (Ayanda et al., 2014).

2.2.2.3 **Cement and concrete making**

South African CFA was discovered to be a strong additive to Portland cement, with a few positive effects on the resulting concrete, including a reduction in concrete water demand (Nkongolo et al., 2020). The addition of CFA to ordinary Portland cement improves compressive strength and increases the cement's resistance to chemical corrosion (Tkaczewska et al., 2012), because the pozzolanic activity of CFA is affected by factors such as ash chemical composition, mineral phase composition, glass structure, and ash fineness. Because of its larger surface area and the presence of multiple components, it is used in soil amendments to improve texture.

Because of its cementitious or binding properties, the use of CFA as a concrete mixture has several advantages on the resulting concrete, including improved consistence, lower heat of hydration, higher strength, and durability performance. It can also be used as a binder in concrete (Nkongolo et al., 2020). CFA has been used as an additive in the production of cement and concrete, and it is the most widely used technique in the world (Teixeira et al., 2016).

Furthermore, the small particle size of the CFA particle reduces air entrainment in the concrete when compared to aggregate. CFA increases corrosion resistance and corrosive liquid entry by reacting with calcium hydroxide in cement to form stable cementitious silicate hydrate gel. The less soluble calcium silicate hydrate lessens the likelihood of calcium hydroxide leaching from the concrete (Fatoba et al., 2013). Paving, mine backfilling, cement, concrete, and low-end building materials account for approximately 56% of total CFA production (Luo et al., 2020). Construction products account for a relatively small percentage (10 - 20%) (Mushtaq et al., 2019).

CFA can be used as a raw material or as an additive in the manufacture of cement. As previously stated, increased human population growth leads to increased demand for electricity, which necessitates the continuous burning of coal to achieve this goal. Huge amounts of CFA are produced as a result of coal combustion, and only a small portion of it is used, with the remainder disposed of in ash dams and dumps, as previously discussed.

2.2.2.4 **Treatment of wastewater**

CFA particles have a porous surface and a large specific surface area, which results in high adsorption activity and the production of cost-effective adsorbents (Xu et al., 2013). CFA has great potential in the treatment of wastewater, gas, and oil in environmental remediation; in this regard, zeolites from CFA have been studied and applied to cleaning of printing and dyeing wastewater (Wang and Zhu., 2005), coking wastewater (Luo et al., 2020), wastewater containing heavy metals such as bivalent mercury and hexavalent chromium (Yang et al., 2019), and ammonia nitrogen wastewater (Chen et al., 2012).

CFA has been used to adsorb sulfur compounds (Matjie et al., 2018) and organic pollutants from wastewater (Ahmaruzzaman, 2009). CFA-based adsorbents are still in the early stages of research. Post-treatment of used CFA-based adsorbents is currently the most critical bottleneck impeding industrialization. If the adsorbents are not properly handled after use, more serious secondary pollution may occur. On the bright side, the synthesis of adsorbents is critical to CFA recycling.

As a result, rather than disposing of this waste, research should focus on its utilization. A good understanding of CFA's chemical composition, mineralogy, surface chemistry, and reactivity can aid in developing utilization options. Finding uses for CFA can help to ease its disposal and reduce its negative environmental impact.

2.2.3 **Physical and chemical properties of CFA**

One of the physical properties of CFA is its color, which is determined by the percentage of unburned carbon in it after the coal combustion process (Gollakota et al., 2019). The color of CFA ranges from dark brown to light grey. The lower the carbon content, the lighter (darker) the color. In general, lignite or sub-bituminous CFA has a lower carbon content and traces of calcium or lime, making it greyish in color (Mainganye et al., 2012; Gollakota et al., 2019). The surface area of CFA is determined by the combustion conditions rather than the type of coal used to produce it (Sarbak et al., 2004).

The size distribution and surface area of CFA particles are critical parameters because they affect the texture and sorptivity of CFA when used as a medium for soil improvement (Gollakota et al., 2019). Another primary application of CFA is in the preparation of zeolites, which is the primary goal of this study.

Because of its ability to reduce soil's affinity to absorb water and thus prevent soil swelling, CFA is used as a soil stabilizer. Swelling can be severe in soils with a high montmorillonite content; they tend to expand when wet and shrink when dry, exerting pressure and resulting in cracked pavements, basement floors, driveways, pipelines, and foundations.

Because of the pozzolanic reaction, the addition of CFA to the soil changes its mineralogy, making the soil more granular and allowing it to retain less water (Nalbantoglu., 2004; Zha et al., 2008). Other important physical characteristics of CFA include particle size distribution and surface area. CFA particles are predominantly spherical, solid or hollow, and amorphous, depending on the coal grade (Gollakota et al., 2019).

CFA's chemical composition reveals that it is made up of a variety of elements from a large portion of the periodic table. Some of the elements found in CFA, such as As, Hg, Cd, Al, and Ba, are toxic to humans, causing cancer and neurological illness (Gottlieb et al., 2010; Nkongolo, 2020).

CFA contains some elements that are thought to be beneficial to plant development, but the value of these benefits pales in comparison to the negative environmental impact caused by CFA. According to (Du Plessis et al., 2013), the presence of toxic and trace elements in CFA made it a potentially hazardous material (Nkongolo et al., 2020).

CFA is mostly made up of the oxides SiO_2 (58.44%), Al_2O_3 (31.25 %), CaO (3.21%), and Fe_2O_3 (3.09%). CFA is typically composed of elements such as Si, Ca, Al, Fe, Mg, C, and many trace elements found in the ash such as Co, Cd, As, Se, Zn, Mo, Mn, Pb, B, Cu, and Ni.

Because of their high melting point and the short time that ash particles remain in the furnace during combustion, inorganic minerals liquefy and become fluid or volatile, or react with oxygen during the combustion process. when the components cool, they form crystalline solids, spherical amorphous particles, or condense as a coating on the particles (Nkongolo et al., 2020).

2.2.4 **Classification of CFA**

ASTM standards categorize fly ash based on the content of its major elements (Si, Al, Fe and Ca). The chemical composition of fly ash may determine its important properties, but this varies greatly depending on the coal type. The well-known classification method divides fly ashes into two classes: class C (SiO_2 + Al_2O_3 + Fe_2O_3 > 50% and CaO > 10%) and class F (SiO_2 + Al_2O_3 + Fe_2O_3 > 70% and CaO 10%) (Akn et al., 2020; Ameh et al., 2017).

According to Gollakota et al. (2019), the important compositional elements of CFA, in decreasing order of abundance, are silica, alumina, iron, calcium, carbon, metallic oxides, sulphates, phosphates, dehydrated silicates, and inorganic particulate residues, regardless of coal grade or processing mechanism.

Class F

Class F fly ash is typically produced by the combustion of harder, older anthracite and bituminous coal. This fly ash is pozzolanic in nature, containing less than 7% lime (CaO) (Musyoka., 2009; Gollakota et al., 2019). Because of its pozzolanic properties, the glassy silica and alumina in class F fly ash necessitate the addition of a cementing agent, such as Portland cement, quicklime, or hydrated lime mixed with water, to react and produce cementitious compounds. A geopolymer can also be created by combining a Class F ash with a chemical activator such as sodium silicate.

Class C

Over time, Class C fly ash hardens and becomes stronger. Class C fly ash typically contains more than 20% lime (CaO) (Musyoka., 2009; Gollakota et al., 2019). In contrast to Class F fly ash, self-cementing Class C fly ash does not require an activator. Class C fly ashes have higher alkali and sulfate (SO_4) contents.

2.2.5 **Environmental concerns of CFA**

Inadequate CFA disposal can disrupt environmental cycles, posing water and soil hazards. Furthermore, it has the potential to cause smog and haze, resulting in severe air pollution (Boycheva et al., 2020; He et al., 2020; Luo et al., 2020). When CFA is dumped in landfills, heavy metals leach into the soil, which is one of the environmental concerns (Mushtaq et al., 2019). CFA is a complex anthropogenic material that is difficult to handle due to its toxicity; the toxicity is due to CFA's intricate composition, which includes organic and inorganic compounds at various scales derived from various grades of coal (Gollakota et al., 2019).

CFA landfilling degrades the state of several environmental components. it reduces soil fertility, pollutes groundwater through infiltration of poisonous components, fine dust particles dissipate in the atmosphere (Boycheva et al., 2020). As a result, it is critical to develop technologies that will allow this vast source of raw materials to be utilized rather than discarded as waste (Kunecki et al., 2018).

Trace elements in the environment come from a variety of natural and anthropogenic sources, perhaps none more so than coal. Trace levels of trace elements can be found in coal (Be, B, P, V, Cr, Mn, Co, Ni, Cu, Zn, Ga, As, Se, Sr, Mo, Ag, Cd, Ba, Hg, Tl, and Pb). Trace element emissions from coal combustion can be relatively benign under certain conditions (Finkelman, 1999; Fan et al., 2020).

Many of the trace elements listed above are extremely toxic to humans and other forms of life. As a result, fly ash produced by the combustion of this coal contains increased concentrations of these elements, and the ash's potential to pollute groundwater is significant. Finding disposal sites, the cost of long-term maintenance, unproductive land exploitation, and negative environmental effects are the factors that discourage CFA disposal (Mushtaq et al., 2019).

Toxins found in uncovered CFA are also released into the environment, lowering air quality. Furthermore, only 12% of the CFA in these impoundments is recycled into useful products, while the rest is unused and left exposed, causing ecological imbalances, and increasing natural disasters (Gollakota et al., 2019; Elavarasan et al., 2019).

2.3 **Zeolites**

Zeolites are hydrated 3D aluminosilicate frameworks with porous crystalline structures (Feng et al., 2019; Ozdemir et al., 2019; Kasneryk et al., 2019) that are widely used in adsorption, catalysis (Bai et al., 2019; Kasneryk et al., 2019), and ion exchange (Joseph et al, 2019; Bai et al., 2019). Zeolites are aluminosilicates that occur naturally or are synthesized. They have a three-dimensional framework of SiO_4 and AlO_4 that are tetrahedrally connected to each other via corner-sharing oxygen atoms (Ameh et al., 2017). These systems endow zeolites with unique properties and application areas, such as sorption capacity, ion-exchange and molecular sieve properties, and catalytic properties.

Several routes for preparing various zeolite types have been proposed based on fly ash pre-treatment, hydrothermal solution alkalinity, molarity of alkaline agents, solution/solid ratio, templating agent, time, temperature, and time of incubation (Missengue et al., 2018). The use of coal combustion fly ash as a raw material for zeolite synthesis has received a lot of attention (Zhang et al, 2019; Missengue et al., 2018).

The type of zeolite produced from CFA is determined by, but is not limited to, the following factors: (i) the alumina and silica source (ii) the Si/Al ratio (iii) the loading ratio (volume of the alkali solution to weight of CFA), (iv) the synthesis procedure, and (v) reaction conditions (i.e., reaction time and temperature) (Makgabutkane et al., 2020).

Zeolites from CFA have been synthesized using a variety of methods. The hydrothermal method, alkali fusion-assisted hydrothermal treatment, microwave-assisted hydrothermal treatment (Makgabutkane et al., 2020), molten salt method (Park et al., 2000), solvent-free method (Liu et al., 2018), and ultrasonic-assisted method (Mokgehle et al., 2020). The aforementioned synthesis methods yielded a variety of zeolites with varying purity levels, including zeolite A, sodalite, zeolite X, and zeolite NaP.1.

The Fig 1 depicts the structures of two zeolites; the pore structure varies greatly from one zeolite to the next. The pore diameters in all zeolites are determined by the free spaces formed by 4, 6, 8, 10, or 12 member rings of oxygen atoms, with maximum values calculated to be 2.6, 3.4, 4.2, 6.3, and 7.4 µm respectively (Bhatia, S., 2020). Due to puckering, the effective free space may have an oval shape.

According to Ghosal et al. (1995), CFA has a hydrophilic surface, predominantly spherical in shape, ranges in size from 0.01 to 200 m (an average diameter of 10 m), and frequently contains irregular shaped debris and porous un-burnt carbon. Zeolite's structural framework has permanent negative charges and has little or no affinity for anions or organic molecules in aqueous states (Pina et al., 2011; Medina et al., 2017).

The actual pore size is also determined by the type of cation present; molecules such as ammonia, hydrogen, oxygen, and argon can pass through the pores of almost any type of molecular sieve. Zeolites have a three-dimensional structure made up of (Si, Al) O_4 tetrahedra connected by all of their oxygen vertices, forming channels where H_2O molecules and exchangeable cations counterbalance the negative charge generated by isomorphous substitution.

Apart from their lower cost, zeolites have the advantage of ion selectivity. Zeolites have been used as water softeners and adsorbents due to their structural characteristics and adsorbent properties (Ghobarkar et al., 1999).

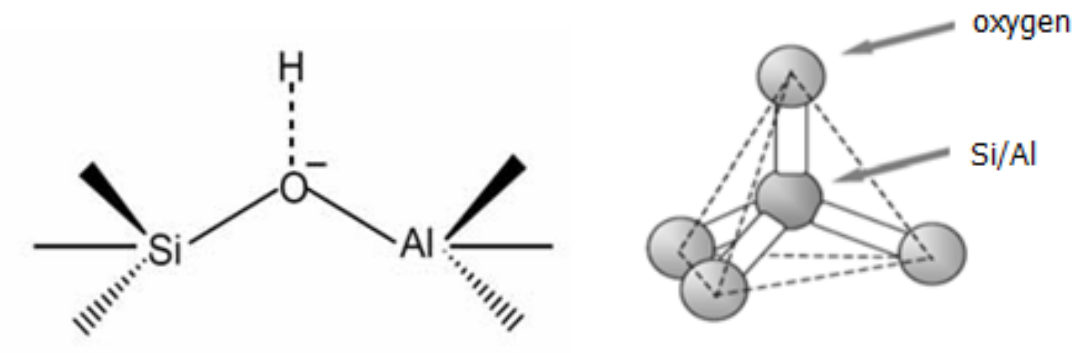

Fig 1: Zeolite's structure (Yuliani et al., 2020)

The presence of massive amounts of potentially poisonous coal-derived compounds poses a critical problem for zeolite synthesis. However, some of these methods are hampered by long reaction times and the use of high reaction temperatures. The hydrothermal synthesis of zeolite is a long reaction method in hydrothermal treatment, typically lasting up to 48 hours due to the high activation energy required to dissolve the glassy phase of Si and Al in CFA (Belviso et al., 2018; Makgabutlane et al., 2020).

Si and Al are extracted/separated with the help of reagents, resulting in an additional burden of unwanted elements in the final products. By fusing into zeolites, those undesirable elements are released into the environment sooner or later (Ferrarini et al., 2016). The alkali fusion-assisted methods that have been widely used for producing highly pure and crystalline zeolites necessitate the use of high temperatures (550°C) (Belviso et al., 2009) Although these methods produced zeolites from CFA effectively, they are no longer economically viable or environmentally friendly.

Researchers have made significant efforts to supplement traditional synthesis methods with greener methods, such as the hydrothermal method, in order to reduce synthesis time and temperature. The synthesis of zeolites from CFA has been proposed to consist of two steps: dissolution of SiO_2 and Al_2O_3, primarily from the glass phase, into an alkaline solution (e.g., NaOH); and crystallization of aluminosilicate gel to form the zeolite crystal.

2.3.1 **Uses of zeolites**

Due to its adjustable surface acidity, micropore structure, gas separation, sewage purification, ion exchange (Kobayashi et al., 2020), and hydrothermal stability, zeolite has also been successfully used in the fields of oil refining, environmental protection, and methanol to light olefins (Zhang et al., 2020). This is due to their high adsorption capacity, high selectivity, and thermal stability. It is still critical today to reduce costs in order to synthesize this zeolite with low-cost silica and aluminum raw materials (Feng et al., 2019).

Such porous products have a wide range of applications in environmental engineering, including the removal of ammonium and the protection of heavy metals from water and wastewater, as well as the separation/adsorption of gases such as CO_2 and the removal of radionuclides from mine waters (Ameh et al., 2017).

Zeolites can adsorb molecules with an infinite dipole moment and have other interaction effects with selectivity that is no longer determined in other adsorbents. The surface area of zeolites, which is determined experimentally by the Brunauer-Emmett-Teller technique (BET), which is entirely based on the relationship of adsorption of a given adsorbate under a positive set of precise conditions, plays an important role in adsorption (Musyoka., 2019).

Zeolites are suitable for adsorptions due to their high cation exchange capacity and affinity for heavy metals (including Ce^{3+}, La^{3+}, UO_2^{2+}, Co^{2+}, Sr^{2+}, Pb^{2+}, Tl^{+}, Zn^{2+}, and Cu^{2+}). The adsorption process includes three zeolite transfer phases as well as a reaction phase. The first depicts the solute's migration from the aqueous phase to the zeolite's surface (outside diffusion). The second is associated with intraparticle diffusion, and finally, the surface chemical reaction between these zeolite and metal ion functions (Ferhat et al., 2019).

One of the important of zeolite is its applications in petroleum refining. The versatility of zeolite catalysts is reflected in the Table 1 below on applications in petrochemistry. Some of the processes such as catalytic cracking, isomerisation of light gasoline and light alkenes, isobutane alkylation and conversion of methanol to gasoline or olefins are highlighted.

Table 1: Application of zeolites as a catalyst (Kianfar et al., 2020)

Inorganic reaction	Organic reactions	Hydrocarbon conversion
H_2S oxidation	Aromatisation (C_4 hydrocarbons)	Alkylation Cracking
NO reduction of NH_3	Alkylation (naphthalene, benzene ethylbenzene, aniline, biphenyl,	Dehydration
CO oxidation, reduction	polyaromatics, etc.)	
Decomposition of H_2O		Fischer-Tropsch
	Aromatics (hydrogenation, oxidation, nitration, disproportionation, hydroalkylation, hydroxylation, oxyhalogenation, etc.)	Synthesis Friedel-Crafts
	Chiral (enantioselective) Hydrogenation	
	Cyclohexane (oxidation, isomerisation, aromatisation, ring opening)	

2.3.2 **Physical properties of crystalline zeolites**

Zeolites are generally colorless, but the color of zeolites is affected by impurities. Zeolites have a crystal hardness that ranges from 4 to 5 on the Mohr scale. Zeolites have a density of about 2 to 2.3 g/cc (Breck, 1974). Exchange with other heavy ions may cause the density to rise; for example, barium zeolite has a density of 2.8 g/cc.

The cations and water molecules in the zeolite structure are relatively free to move, allowing for ion exchange and water purification. This property of zeolites is classified as a "molecular sieve." The chemical composition of the zeolites is similar to the aortic spaces of the channel (Ramanathan et al., 2020). When drained, most zeolites remain stable and have cation exchange properties. Dehydrated crystals have molecular and uniform sizes, as well as a variety of physical properties such as electrical conductivity, gas and vapor coefficients, catalytic properties, adsorption, and an ion network (Kianfar., 2019).

Zeolites are microporous aluminosilicate crystalline minerals with exchangeable cations that play critical roles as adsorbent ion-exchangers or catalysts in a variety of chemical and petrochemical industries, as well as in water treatment applications (Razavian et al., 2015; Narayanan et., 2015). The use of zeolites for applications is frequently limited due to diffusion and access issues caused by the small pore size of zeolites, which ranges from 0.3 to 1 nm, (Verboekend et al., 2013; Yin et al., 2015).

Poor diffusion of relatively large reactant molecules or ions to the active sites present in the zeolite micropores may also result in underutilization of the available zeolite internal surface area and volume, common blocking of the diffusion direction, and rapid zeolite deactivation (Le et al., 2011; Al-Jubouri et al., 2017).

By providing shorter diffusion paths for reactant and product molecules inside the pores, hierarchically porous zeolite can reduce or eliminate undesirable diffusion boundaries of the reaction rate (Ding et al., 2007). In general, hierarchical zeolite composites are made by growing a zeolite layer onto a porous support using a hydrothermal treatment (Yu et al., 2015; Rio et al., 2015).

Zeolites are three-dimensional networks of corner-sharing [TO_4] tetrahedra, where T is typically silicon or aluminum. The framework is neutral because it is made entirely of [SiO_4] units. When Al with a charge of 3^+ is an isomorphous substitute for Si with a charge of 4^+, the framework becomes negatively charged compensated by using extra-framework cations, resulting in its cation exchange capability (Hong et al., 2019).

Zeolites' inherent pores are entirely micropores. For example, the primary zeolite constructing units are sodalite cages linked with the aid of a 4-membered ring, which includes enormous cage cavities of 1.14 nm interconnected with the aid of eight-ring openings with a 0.41 nm aperture (Brunetti et al., 2018). The development of a hierarchical mesopore system may allow for larger and more numerous cations to enter the zeolites, increasing the rate and capacity of heavy metal cation removal in wastewater (Hong et al., 2019).

2.3.3 **Classification of zeolites**

2.3.3.1 **Natural zeolites**

Zeolites are hydrated aluminosilicate minerals that occur naturally. They are classified as "tectosilicates," a type of mineral. Natural zeolites are mostly formed by the alteration of glass-rich volcanic rocks (tuff) with fresh water in playa lakes or by seawater (Erdem et al., 2004).

Many countries recognize natural zeolites as low-cost treatment adsorbents. By using the ion exchange mechanism, these natural adsorbents can remove heavy metals from commercial and polluted wastewater. The primary advantages of these systems over other methods are selectivity, significantly less sludge production, and compliance with stringent discharge standards (Moazeni et al., 2020).

2.3.3.2 **Synthetic zeolites**

The ability of synthetic zeolites derived from CFA to be modified with various hydroxides, metals, and metal oxides expands the application area (Mushtaq et al, 2019). CFA-derived zeolites contain zeolite and non-zeolite fractions that can be used to remove heavy metals, cationic and anionic pollutants. The zeolite fraction (carrying negative charges) is in charge of removing cationic pollutants from water, while the non-zeolite fraction (containing Al_2O_3, CaO, and Fe_2O_3 originally derived from CFA) is in charge of removing anionic pollutants from ater (Mushtaq et al., 2019).

2.3.4 **Characteristics and modification of zeolite structures**

The structure of the framework of a zeolite can be influenced in two ways: direct synthesis and post-synthetic treatment and modification. The primary method for producing zeolites is direct synthesis. Many parameters, such as synthesis mixture composition, synthesis temperature and time, solution pH, aging and seeding, directing agent or template, all have an effect on zeolite shape (Kianfa et al., 2020).

Zeolites can be modified to improve their properties, particularly for catalytic reactions. Some modifications can be based on the formation of secondary pores via dealumination or acid leaching, or on increasing external surface area or inner pore volume by blocking pores and varying the chemical composition via isomorphous substitution of Al or Si by elements with ionic radii and coordination requirements compatible with the tetrahedral sites in the structure (Musyoka., 2019).

The direct synthesis route, in most cases, does not result in the formation of zeolites with desirable properties for final applications. In addition to direct synthesis, post-synthesis methods such as ion exchange, metal-supported zeolites preparation, dealumination, reinsertion of heteroatoms (e.g., B, Ga, Ge, or Al) into zeolite frameworks, and other modification methods provide a more practical route to modify the zeolites to accumulate desirable framework compositions and other properties (Kianfa et al., 2020).

2.4 **Metals**

Heavy metals exist in water in colloidal, particulate, and dissolved forms, and their presence in bodies of water is either natural (e.g., eroded minerals within sediments, leaching of ore deposits, and volcanic extruded products) or anthropogenic (e.g., solid waste disposal, commercial or domestic effluents, and harbour channel dredging) (Momodu and Anyakora., 2010; Rai et al., 2019).

Metals are distinct from other toxic substances in that they are not created or destroyed by humans. Alkali metals, alkaline earth metals, transition metals, noble metals, platinum metals, rare metals, rare earth metals, actinide metals, and light metals are the different types of metals.

2.4.1 **Toxicity of metals**

Heavy metals, also known as poisonous metals, are trace metals that are harmful to human health and have a density at least five times that of water (Sardar et al., 2013; Rahman et al., 2019; Bilal et al., 2020). Heavy metals enter the body through inhalation, ingestion, and pores and skin absorption after being released into the environment via the air, drinking water, food, or an infinite variety of man-made chemicals and products.

Heavy metals enter and accumulate in body tissues faster than the body's detoxification pathways can dispose of them, resulting in a slow build-up of those pollutants (Marella et al., 2020). Heavy metal accumulation in body tissues occurs steadily and, over time, can reach toxic concentration levels far beyond the permissible limits, so high concentration exposure is not required to produce a state of toxicity within the body (Suruchi et al., 2011; Ashraf et al., 2019).

2.4.2 **Sources of heavy metals**

Many industries such as mining, electroplating, pesticides, paint, agriculture, transportation, batteries, and ceramics discharge massive quantities of heavy metals in the environmental (Latif et al., 2020). The primary sources of pollution by metal into the environment include municipal wastes, fertilizers, pesticides, and sewages (Ashraf et al., 2019; Atafar et al., 2010). Table 2 shows the permissible limits for some toxic inorganics set by the United States Environmental Protection Agency (USEPA), WHO, and South African national standards (SANS) for their levels in drinking water.

Wastewaters and pollution of water bodies contain poisonous components because of the indiscriminate disposal of heavy metals that are dangerous to living creatures and environment. An increase in the level of environmental pollution has ended in an growing concern for humans well-being and for global ecosystem (Taghizadeh et al., 2017; Hassanpour at al., 2018; Tavengwa et al., 2013).

Table 2: Maximum permissible limits of different heavy metals in drinking water (Verlicchi et al., 2020; WHO, 2008)

Trace inorganic Contaminants	USEPA (mg L^{-1})	South African Standards (mg L^{-1})	WHO Limits (mg L^{-1})
Arsenic, as As	0.050	0.010	-
Cadmium, as Cd	0.005	0.003	0.005
Chromium, as Cr (VI)	0.050	0.005	0.050
Iron, as Fe	0.300	0.300	0.300
Lead, as Pb	0.050	0.010	0.050
Manganese, as Mn	0.050	0.100	0.100
Mercury, as Hg	0.002	0.006	0.010
Nickel, as Ni	0.100	0.070	0.500

Chapter three

Experimental

This chapter gives the materials and methods, chemical and reagents used in this study. It also focuses on the optimizing conditions required to form zeolites. It concludes by Kinetic and adsorption modelling which describe the adsorption process and the adsorption mechanisms that control it.

3. **Experimental**

3.1 **Synthesis of zeolites**

This fig. 2 shows the Schematic representation for synthesis and characterization of zeolites that was followed in this study.

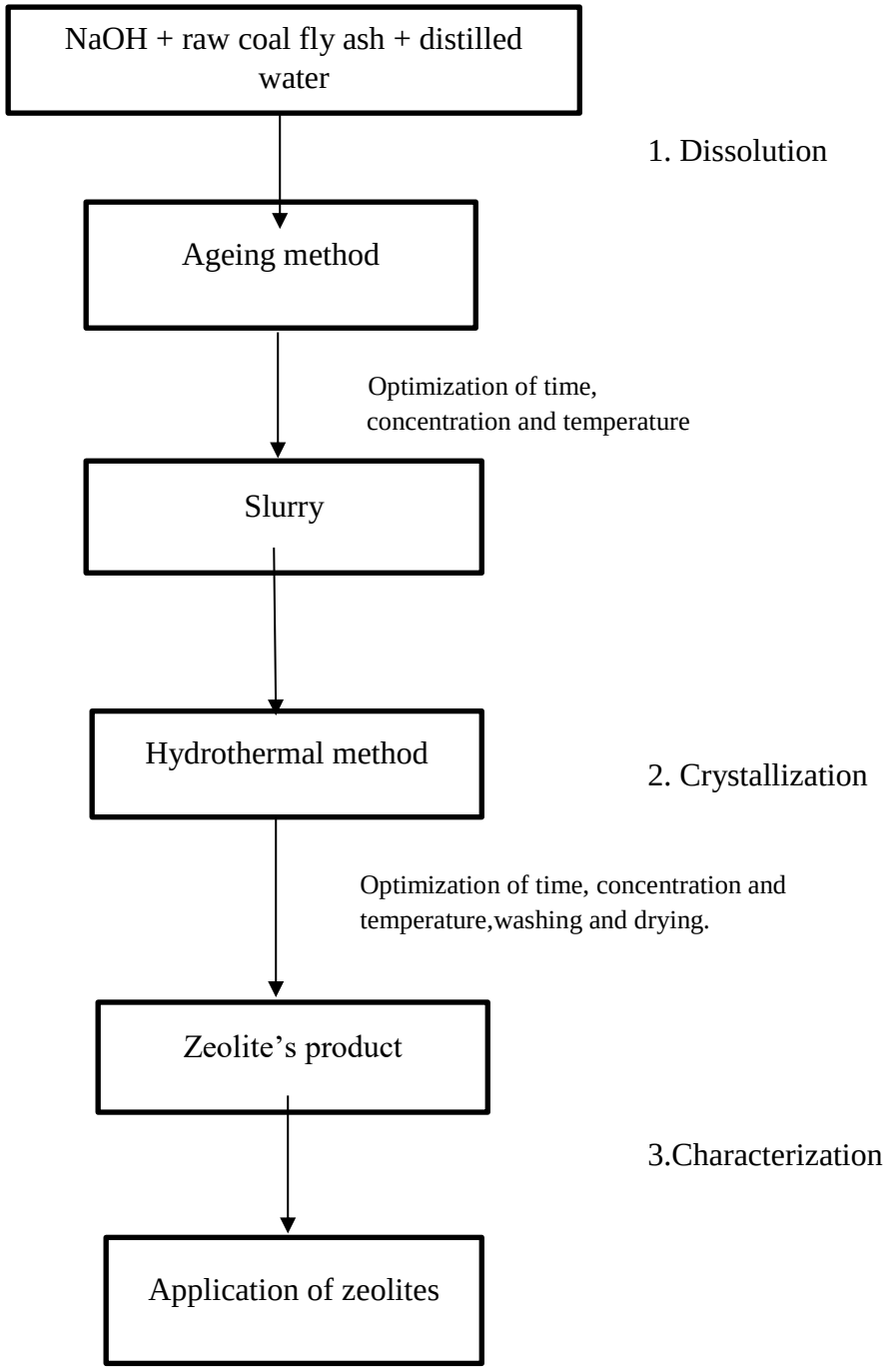

Fig 2: Schematic representation for synthesis and characterization of zeolites.

3.2 **Materials and methods**

3.2.1 **Chemicals and reagents**

Rochelle Chemicals (Johannesburg, South Africa) supplied sodium hydroxide pellets, which were used as alkaline activating agents in the dissolution of the aluminosilicate matrix in CFA. The chemicals, $Al_2(SO_4)_318H_2O$ and SiO_2, were obtained from Associated Chemical Enterprises (Johannesburg, South Africa) and Sigma-Aldrich (Johannesburg, South Africa), respectively, and were used as standards in the analysis of dissolved Si^{4+} and Al^{3+} species in alkaline solution using the flame atomic adsorption spectrometer (FAAS).

To stirrer CFA thus alkaline activating solution, a Heidolph temperature probed magnetic stirrer from Heidholph Instruments (Schwarzenberg, Germany) was used. To separate the slurry from the NaOH activating solution, a Millipore 0.2 m membrane filter was used. We used deionized water with a conductivity of 1.5 ms/cm.

To separate the slurry from the NaOH activating solution, a CN-2060 centrifuge from Monitoring and Control Laboratories (Johannesburg, South Africa) was used. The dissolved ions from the CFA aluminosilicate matrix were analyzed using a PerkinElmer PinA Acle 900T graphite furnace atomic absorption spectrometer (AAS) (Massachusetts, United States of 3America).

Crystallization experiments were carried out with a 278AC Brass Parr Bomb obtained from the Parr Instrument Company (Illinois, United States of America). Agilent (Santa Clara, United States of America) inductively coupled plasma-optical emission spectroscopy (ICP-OES) was used to analyze water samples from WWTPs.

3.2.2 **Method**

The synthesis of zeolites from CFA was carried out in two steps, the first of which was ageing, and the second of which was hydrothermal treatment. The slurry obtained from optimized ageing conditions was crystallized during the hydrothermal treatment step by transferring a 20 mL mixture into a 40 mL Teflon-lined "cup" of the Parr bomb for an appropriate time, temperature, and variation within the addition of ultra-pure water. The slurries' crystallization required optimizing the subsequent times of 6 h, 24 h, 48 h, and 72 h at 140°C.

Following that, crystallization temperatures of 25°C, 70°C, 100°C, 140°C, and 160°C at an optimized crystallization time were investigated. Following that, another optimization study was conducted in which the variation in the amount of ultra-pure water added to the slurry was investigated, with the following volumes included: 0, 3, 6, 9, 12, and 15 mL. The different water additions produced H_2O: SiO_2 ratios (v/v) of (0:20), (3:17), (6:14), (9:11), (12:8), and (15:5), where SiO_2 indicated the slurry at an optimized crystallization time and temperature.

3.2.3 **Preparation of working samples**

A wide range of working solutions were created by spiking aliquots of typically 20 mL ultra-pure water with various known concentrations of target analytes and then adjusting the pH with 0.1M NaOH and 0.1M HNO_3. Following that, zeolite removal experiments were performed on these samples.

3.2.4 **Sample handling and storage**

The CFA samples were stored in an airtight plastic container with a tight-fitting lid. Containers were kept in cool, dark places away from moisture, direct sunlight, and temperature fluctuations. This is because, when exposed to the atmosphere, many of the metastable assemblies of minerals phases in CFA that were formed at high temperatures during coal combustion will change to create thermodynamically stable minerals, potentially altering the overall initial composition of fly ash (Musyoka, 2009).

3.2.5 **Synthesis equipment**

The setup of the ageing method is shown in Fig. 3. Parr bombs with Teflon lining Fig. 4 were used in the hydrothermal treatment process. The slurry volume poured into the Teflon-lined "cup" was 20 mL on average. The hydrothermal synthesis was performed by putting filled and sealed Parr vessels in a temperature-controlled environment. Hot air oven by Memmert (1999) used a two-step synthesis method for zeolite synthesis from CFA, including ageing followed by hydrothermal treatment. The slurries were crystallized once the optimal conditions for dissolution of the CFA aluminosilicate matrix were achieved.

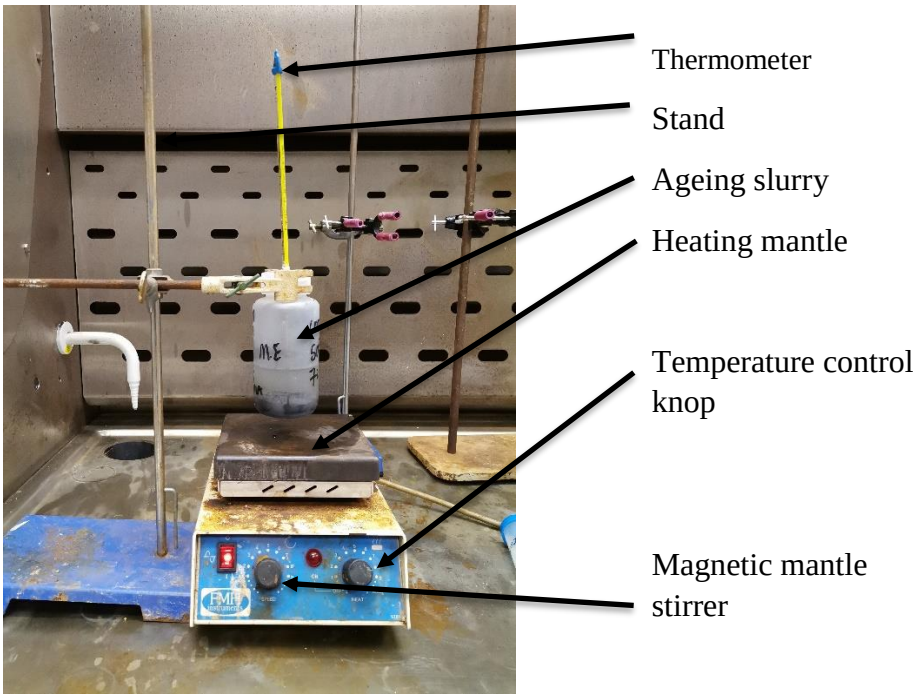

Fig 3: Experimental set-up during ageing process.

Fig 4: Parr bombs and Teflon lining used in the hydrothermal treatment process.

3.2.6 **Ageing step**

In this step, the mass ratio of fly ash to sodium hydroxide pellets was set to (w/w) 1:1. A volume of 100 mL of CFA was dissolved in sodium hydroxide in a separate beaker before being added to the CFA in a plastic 250 mL sealable bottle. The magnetic bar was added to the mixture, the bottle was sealed, and it was then placed on a magnetic stirrer to begin heating. The rotational speed was set to 800 rpm, and the heater temperature was set to 50°C and controlled by a temperature probe inserted through the lid. Temperature and aging time were kept constant at 50°C and 48 h, respectively.

3.2.7 **Hydrothermal treatment**

After ageing, varying amounts of ultra-pure water were added to the slurry while stirring, and the resulting homogeneous solution was transferred into a 40 mL Parr bomb in 20 mL aliquots. The feedstock was crystallised in sealed Parr bombs in a thermostated EcoTherm hot air oven for a set time and temperature. After ageing and before hydrothermal synthesis, the amount of water added was expressed as a molar ratio of H_2O/SiO_2.

Table 3: Variation of molar quantities of water added to the slurry during the hydrothermal treatment step, where the ratio H_2O: SiO_2 molar ratio ranged from 0 to 3.

Experiment number	Water (mL)	Slurry (mL)	H_2O/SiO_2
1	0.00	20.0	0.00
2	3.00	17.0	0.18
3	6.00	14.0	0.43
4	9.00	11.0	0.82
5	12.0	8.0	1.50
6	15.0	5.00	3.00

The slurry was shaken for 3 min to achieve a homogeneous solution before being transferred in aliquots of 20 mL into the Parr bomb's 40 mL Teflon-lined "cup." The feedstock was crystallized by placing the sealed Parr bomb in a thermostated EcoThem oven set at 140℃ for 72 h.

3.2.8 **Recovering of the zeolites**

The Parr bombs were removed from the oven and cooled to room temperature after hydrothermal treatment at the above-mentioned water content, time, and temperature. Filtration separated the liquid phase from the zeolite. The solid product was thoroughly washed with ultra-pure water until a pH of 9 - 10 was obtained in the filtrate. The solid product residue was dried at 50℃ before being transferred to an airtight plastic container for characterization. As shown in the equation below, the percentage yield of the zeolite products was calculated.

$$\text{Pecentage yield} = \left(\frac{\text{Actual yield}}{\text{Theoretical yield}}\right) \times 100 \qquad (1)$$

3.2.9 **Batch equilibrium studies**

The initial sample pH (2 - 8), contact time (10 - 90 min), adsorbent amount (10 - 150 mg), and initial concentration (0.1 – 5 mg L^{-1}) of Cr (VI) were optimized, as was the temperature, where C_o (mg L^{-1}) represents the initial concentration and C_e (mg L^{-1}) represents the final equilibrium concentration after adsorption. The percentage removal equation is shown in Equation (2).

$$R\ (\%) = \frac{(C_o - C_e)}{C_o} \text{ x } 100 \qquad (2)$$

The mass of substrate bound on a gram of adsorbent, q (mg g^{-1}), is defined as the adsorption capacity, q (mg g^{-1}). The mathematical equation for calculating adsorption capacity is shown in Eq. (2), where C_o (mg L^{-1}) and C_e (mg L^{-1}) are defined as in Eq. (1), and V (L) is the volume of the sample solution and W(g) is the mass of the adsorbent (Tavengwa et al., 2013).

$$\text{Adsorption capacity } (q_e) = \frac{(C_o - C_e)V}{W} \qquad (3)$$

3.2.10 **Kinetic and adsorption modeling**

Kinetic modeling is important for understanding the mechanisms and rate-controlling steps that affect adsorption kinetics (Tavengwa et al.,2014). Two kinetic models, pseudo first order and pseudo second order, have been used to describe the adsorption process and the adsorption mechanisms that control it, such as mass transfer and chemical reaction.

3.2.10.1 **Pseudo first order**

The linear form of the pseudo first-order kinetic model is given by equation (4).

$$\log (q_e - q_t) \log q_e - \frac{k_1}{2.303} t \qquad (4)$$

where q_e and q_t are the amounts of Cr (VI) adsorbed on adsorbent (mg g^{-1}) at equilibrium and time t (min), respectively, and k_1 (min^{-1}) is the first order adsorption rate constant. Straight-line plots of log (q_e – q_t) versus t yielded the rate constants, k_1 and q_e.

3.2.10.2 **Pseudo second order**

The pseudo second-order equation is expressed as follows by equation (5)

$$\frac{t}{q_t} = \frac{1}{k_2 q^2 e} + \frac{1}{q_e} t \qquad (5)$$

where k_2 is the second-order adsorption rate constant (g mg^{-1} min^{-1}). The intercept and slope of the kinetic plots were used to calculate the model parameters.

3.2.10.3 **Adsorption isotherm**

The sorption isotherm expresses the relationship between the amount of solute adsorbed by a unit weight of solid sorbent and the amount of solute remaining in solution at equilibrium. In this study, the Langmuir and Freundlich adsorption isotherms were used. The Langmuir and Freundlich isotherm models have both been shown to be appropriate for describing the short-term and mono-component adsorption of meatal ions materials (Khaldoun Al-Sou'od., 2012).

3.2.10.4 **Langmuir model**

The Langmuir model, on the other hand, provides a mechanistic understanding of the sorption phenomena and can be used to easily estimate the maximum chromium uptake from experimental data. The Langmuir isotherm model assumes homogeneous monolayer adsorption onto the surface with no re-adsorption of adsorbate on the surface (de Sousa et al., 2018).

This model is primarily based on two key assumptions: the forces of interaction between adsorbed molecules are negligible, and no further sorption occurs once an analyte occupies a site (monolayer sorption). The following is the linearized mathematical representation of its form:

$$\frac{1}{q_e} = \frac{1}{q_m b C_e} + \frac{1}{q_m} \qquad (6)$$

where Ce (mg L^{-1}) represents the equilibrium concentration of Cr (VI) in the solution and qe (mg g^{-1}) represents the mass of Cr (VI) retained on a unit mass of the sorbent. The maximum is q_m. The adsorption capacity (mg g^{-1}) is calculated from the slope and intercept of the straight-line plots of $1/q_e$ versus $1/C_e$, where b is the Langmuir constant.

According to the Langmuir model, the critical characteristics of the isotherm can be predicted using a dimensionless constant separation factor (R_L) to predict the favorability of adsorbent interaction. The following equation is used to represent this parameter:

$$R_L = \frac{1}{(1+b\,C_o)} \quad (7)$$

3.2.10.5 **Freundlich model**

The Freundlich isotherm is an empirical equation that has been demonstrated to be most effective at low concentrations. The stronger binding sites on the surface are occupied first, according to the Freundlich isotherm model, and binding strength decreases with increasing site occupancy (de Sousa et al., 2018). The Freundlich isotherm model has the following linear form:

$$\log q_e = \log k_f + \frac{1}{n} \log C_e$$

where C_e and q_e are synonymous; K_f and 1/n are constants that are relative indicators of adsorption capacity (or associated with the bonding energy) and adsorption intensity, respectively. A value for 1/n less than one indicates a Langmuir-type isotherm, as adsorbing additional adsorbate molecules becomes increasingly difficult at higher adsorbate concentrations (Al-Sou'od., 2012). The empirical constants k_f and 1/n can be calculated from the slope and intercept of the linear regression using a plot of log q_e vs log C_e.

3.2.10.6 **Thermodynamics**

The thermodynamic parameters for the sorption of Cr (VI) on zeolites, which include the change in enthalpy ΔH°, entropy change ΔS° and free energy ΔG° are calculated using the following equations:

$$\ln K_d = \left(\frac{\Delta S^\circ}{R}\right) - \left(\frac{\Delta H^\circ}{RT}\right) \quad (9)$$

$$\Delta G^\circ = \Delta H^\circ - T\,\Delta S^\circ \quad (10)$$

The slope and intercept (K_d I vs 1/T for prepared zeolites) are estimated by a curve-fitting program, and the values of ΔH° and ΔS° are obtained.

Chapter four

Results and discussion

This section discusses the results of experiments in which the optimum conditions for the preparation of zeolites were discussed based on chemical and mineralogical analysis of products as well as the morphological transformation of CFA during different stages of synthesis, cation exchange capacity and adsorption studies, kinetic modelling, and application

4.1 **Physicochemical and mineralogical characterization of coal**

The CFA used in these experiments was obtained from a Modderfontein steam plant which combust pulverized coal to generate steam for a nitric acid plant. The steam plant obtained its coal from the Stuart coal mine in Delmas, Witbank, Mpumalanga. The nature of the coal was subituminous, 0.5 mm – 20 mm. Additional physical and chemical properties of the coal burnt are shown in Table 4. The quantities of coal burnt, and CFA produced per annum was 32850 tons and 5585 tons, respectively. The temperature and pressure of the boiler used was 1011˚C and 32.6 kPa, respectively.

Table 4: Chemical and physical characteristics of coal burnt.

Chemical characteristics	%	Physical characteristics	
Inherent moisture	4.60	Appearance	Pieces and lumps
Ash content	17.5	Caloritic values	23.5-25.5 KJ kg^{-1}
Volatile matter	26.1	Calorific value	24.96 KJ kg^{-1}
Fixed carbon	51.8	Defomation temperature	1400 °C
Total sulfur	0.79		

4.2 **XRF analysis and loss on ignition studies on CFA**

The major metal oxides of CFA used for zeolite synthesis are shown in Table 5. The major oxides based on XRF studies; metal oxides constituted 70.39% of the composition of CFA. The ratio of SiO_2/Al_2O_3 in CFA was 1.19. The chemical composition of the zeolite plays a vital role in accommodating loosely bound ions or molecules within the cages of the zeolite framework permitting exchange without damage to the crystalline structure. Additionally, the crystalline structure determines the stability of the zeolite and the extent to which it can facilitate ion-exchange.

The low CaO composition suggested a high probability for zeolite crystallization as high amounts of Ca^{2+} could result in crystal break down during the zeolitization process. The compositional dominance of Al and Si in the CFA studied (> 60%) indicated that this material is a suitable feedstock for zeolite production.

Loss on igniton studies was conducted to determine the unburnt carbon content in CFA. The LOI for CFA was observed to be 3.29 (Table 5), This indicated that the coal burning process at the Modderfontein steam plant was efficient resulting in low fuel losses because of the combustion temperature of the boiler (1011˚C), hence the low LOI of CFA. Additionally, the low LOI of this CFA makes it a suitable candidate for cement applications due to its potentially good air entrapment performance, reducing the probability of cracks and low mechanical strength.

Table 5: Major oxide and trace elemental composition of Modderfontein steam plant CFA.

Major oxide	Composition (%)	Trace elements	Concentrations (mg L^{-1})
SiO_2	34.99	Sr	2110
Al_2O_3	29.33	Ba	1200
MgO	0.68	V	330.1
CaO	4.08	Pb	169.0
K_2O	0.86	Cd	0.101
P_2O_5	0.46	Ag	0.599
Total (%)	70.39		
LOI	3.29		
SiO_2/Al_2O_3	1.19		

4.3 **Effect of concentration of NaOH activating agent**

The effects of NaOH concentrations during the ageing synthesis are depicted in Fig. 5. The materials were prepared in the manner described in section 3.2.6, the aging step. Because the aluminosilicate layer forms the surface of the CFA particle and is the most reactive, consisting primarily of SiO_2, and the inner-most mullite layer is high in aluminium content accessibility, all Si^{4+} concentrations are higher than Al^{3+} concentrations in all concentrations. The surface-located aluminosilicate layer has greater reactivity with alkali agent (NaOH) than the Al^{3+} containing mullite phase, resulting in a high Si^{4+} content in the aqueous reaction media, and thus the relatively high concentrations observed for Si^{4+} compared to Al^{3+} as shown in Fig.5. The dissolution of the aluminosilicate layer into the alkaline solution has been observed to facilitate alkaline solution diffusion into the inner layers of the CFA. It was also discovered that 2.5 M for both Si^{4+} and Al^{3+} is greater than 0.5 M and 1.5 M, owing to the fact that the

concentrations of both Si^{4+} and Al^{3+} decrease in the following order: 2.5 M > 1.5 M > 0.5 M. The trend observed was that as alkali concentration increased, so did Al^{3+} dissolution. This was primarily due to the alkaline solution's high pH (2.5 M NaOH), which penetrated the innermost mullite phase, resulting in a higher concentration of Al^{3+} than the 1.5 M and 0.5 M NaOH alkaline solutions. (See Figure 5). The relatively higher Si^{4+} concentration in the alkaline solution compared to Al^{3+} concentration (Fig. 5) agrees with XRF data in (Table 5) which shows a Si/Al ratio of 1.19. When the 1.5 M and 2.5 M NaOH concentrations were used, there were no significant changes in the concentrations of dissolved Si^{4+}. When varying the basicity of the NaOH activator for dissolution studies of the aluminosilicate matrix of CFA, (Inada et al., 2005) observed a similar trend in the dissolved Si^{4+} concentration in the alkaline solution.

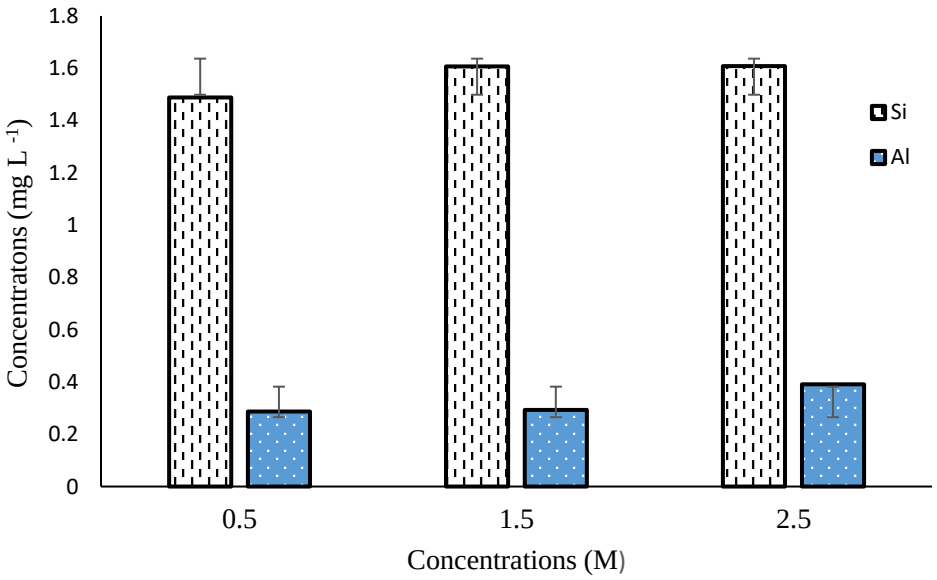

Fig 5: The optimization of ageing NaOH/CFA. Concentrations of Si^{4+} and Al^{3+} with various concentrations of NaOH (n = 3, RSD). Experimental conditions: Solution temperature = 50˚C, stirring rate = 800 rpm, time = 24 h, mass of CFA = 15 g, volume of solution = 50 mL.

4.4 **Effect of ageing time**

The results obtained while varying the time to determine the period for stabilization of CFA derived from Si^{4+} and Al^{3+} in the NaOH alkaline solution. The concentrations of Si^{4+} are all greater than the concentrations of Al^{3+}. As time passed, the concentrations of Al^{3+} increased. The results show that Al^{3+} concentrations increased with time during the initial stages of contact and only stabilized after 72 hours. (Fig.6) shows that the Si^{4+} phase was easily dissolved into the NaOH solution, as Si^{4+} concentrations remained constant from 24 h to 72 h, whereas Al^{3+} concentrations increased from 24 h to 72 h. When there was no further mass transfer of highly soluble aluminosilicates from the CFA, equilibration between the CFA and the dissolved Al^{3+} and Si^{4+} species in the activating solution was discovered. A slight increase in Al^{3+} concentrations during the first 24 h indicated that Al^{3+} from the mullite phase was involved in the reaction. According to (Musyoka, 2009), increasing the synthesis temperature is expected to increase zeolite crystal nucleation and growth. Increased mullite digestion is also expected as the synthesis temperature rises. It has also been observed that the dissolution of Si^{4+} from fly ash is greater than that of Al^{3+}, resulting in an increase in the Si/Al ratio. The solution that influences the composition of the gel and the type of zeolites that result.

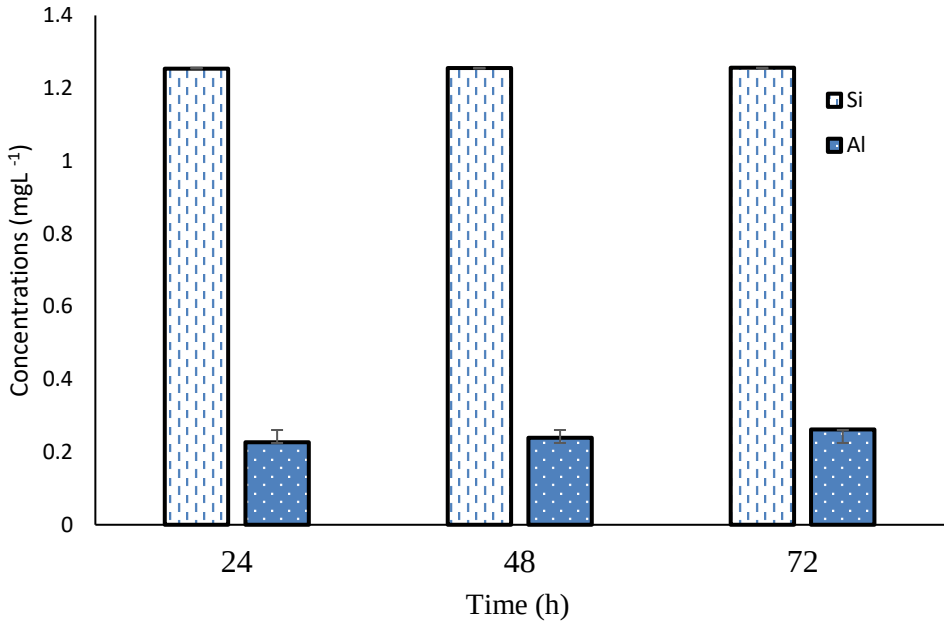

Fig 6: The optimization of time (h), Si^{4+} and Al^{3+} concentrations in the activating solutions as the volumes of NaOH solutions are varied (n = 3, RSD). Experimental conditions: (Optimum concentration = 2.5 M, Solution temperature = 50˚C, stirring rate = 800 rpm, mass of CFA = 15 g, volume of NaOH solution = 50 mL).

4.5 **Ageing as a function of S/L ratio**

The concentration of Si^{4+} and Al^{3+} in the activating agent are shown in Fig. 7 at various solid/liquid (S/L) ratios. The effect of the solid (CFA)/liquid (2.5 M NaOH) ratio on the dissolution of the aluminosilicate matrix of CFA was investigated. Fig. 7 shows that increasing the volume of the activating agent resulted in an increase in dissolved Al^{3+} concentration. This implies that increasing the activating agent volume increased the participation of the inner CFA Al abundant mullite phase in the ageing reaction. The graph also shows that the concentration of Si^{4+} is greater than the concentration of Al^{3+}. The solid/liquid (S/L) ratios of $Si^{4+}$are nearly identical for all; the high Si^{4+} concentrations observed in comparison to Al^{3+} indicated dissolution of the highly soluble aluminosilicate CFA phase into the activating agent (Murayama et al., 2002).

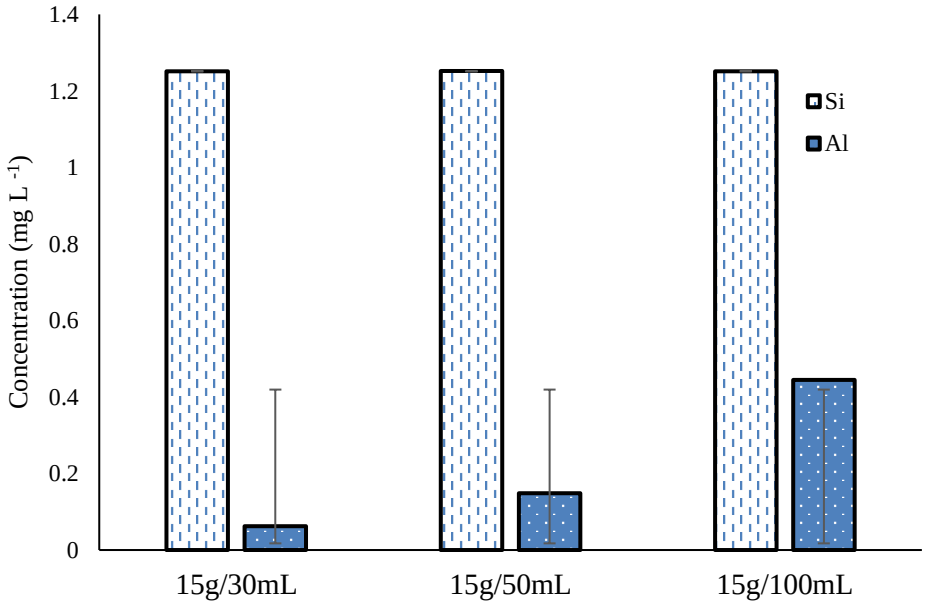

Fig 7: Solid/liquid ratio optimization (n = 3, RSD). Experimental conditions: Solution temperature = 50˚C, stirring rate = 800 rpm, mass of CFA = 15 g, volume of NaOH solution = 50 mL, optimum time = 72 h.

4.6 **FTIR results**

Optimization of NaOH concentration for dissolution of aluminosilicate matrix in CFA was done and Fig. 8 shows FT-IR spectra of solid residue as the concentration of NaOH activating agent was varied 0.5 M, 1.5 M, and 2.5 M at 50℃. The Si-O and Al-O band associated with stretching vibrations shifts (in zeolites) are visible and interpreted, and these shifts are shown to depend on the concertation of the activating agent NaOH (Fig. 6). For example, the band at around 1038 cm^{-1} of the original fly ash becomes more pronounced shifted towards lower frequencies of 971 cm^{-1} for 2.5 M, 972 cm^{-1} for 1.5 M and 983 cm^{-1} for 0.5 M in the zeolite samples. This meant more of aluminosilicate phases were converted into zeolite as the concentration of the activating agent NaOH increased, Furthermore, a band at 1450 cm^{-1} in the solid residues was observed due to (-O-H) asymmetric stretching of water from the alkaline and silanol groups, which was more prominent in the 2.5 M NaOH solid residue. At less concentration 0.5 M the peaks were less broad respectably compared to the peaks of 2.5 M. which suggest that less of aluminosilicate phase was not converted into zeolite. Hence the optimum ration for solid/liquid ratio was 2.5 M. This agrees with what was observed in FAAS analysis (Fig. 1).

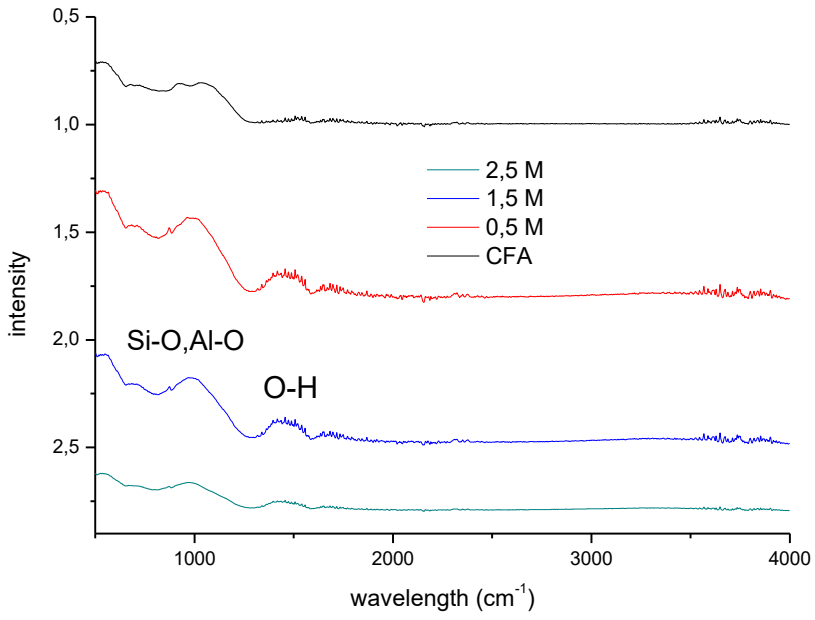

Fig 8: FT-IR spectra of solid residue as the concentration of NaOH activating agent was varied.

FT-IR spectra of solid residue as the time is varied for dissolution of aluminosilicate matrix in CFA was investigated Fig. 9. The Si-O and Al-O band associated with stretching vibrations shifted (in zeolites) are visible and interpreted, and these changes have been shown to be time dependent. For example, the approximately 1038 cm^{-1} band in the original fly ash becomes sharper and shifts at lower frequencies of 971 cm^{-1} in the zeolite samples. This meant that as time passed, more aluminosilicate phase was converted into zeolite. Additionally, a band at 1450 cm^{-1} in the solid residues was observed due to (-O-H) asymmetric stretching of water from the alkaline and silanol groups, which was more prominent for the 72-h solid residue. At 6 h the peaks were less sharp compared to the peaks at 72 h. which suggested that less of aluminosilicate phase was not converted into zeolite. Hence the optimum ration for solid/liquid ration is 72 h.

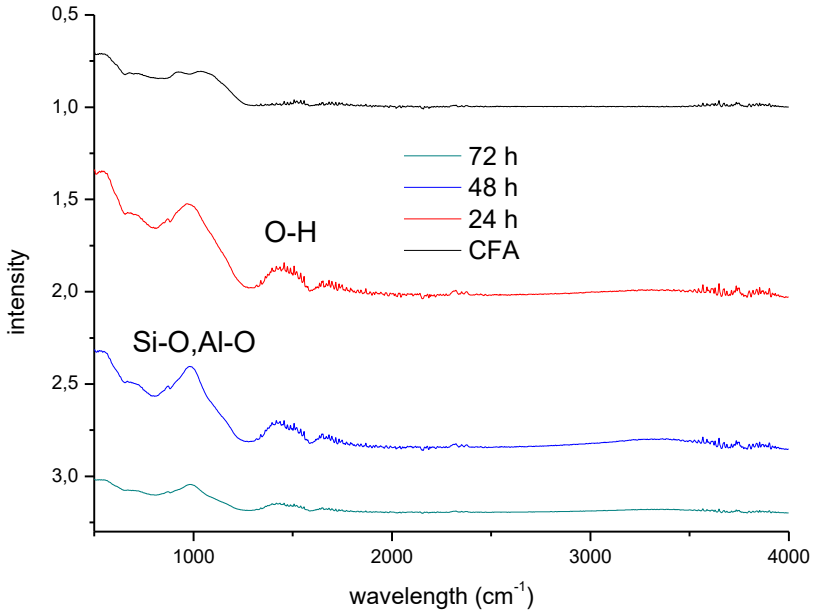

Fig 9: FT-IR spectra of solid residue as the time is varied.

The operational parameters for dissolving the aluminosilicate matrix in CFA were optimized, and Fig. 10 shows the FT-IR spectra of CFA solid residues obtained by varying the volume of the activating agent NaOH from 30 mL to 100 mL at 50°C. The Si-O and Al-O bands associated with stretching vibration shifts (in zeolites) are in interpretable ranges, and these shifts are shown to be volume dependent on the activating agent NaOH Fig. 10. In the zeolite sample, for example, the band at around 1038 cm^{-1} of the original fly ash becomes sharper and shifts to lower frequencies of 973 cm^{-1}. This means that a greater proportion of the aluminosilicate phase was converted into zeolite. Furthermore, a band at 1450 cm^{-1} in the solid residues was observed due to (-O-H) asymmetric stretching of water from the alkaline and silanol groups, which was more prominent for the 50 mL/15g and 100 mL/15g NaOH solid residues. The peak was less sharp at lower volumes (30 mL and 50 mL) when compared to the peak at 100 mL, implying that less aluminosilicate phase was not converted into zeolite. As a result, the best solid/liquid ration is 100 mL/15g.

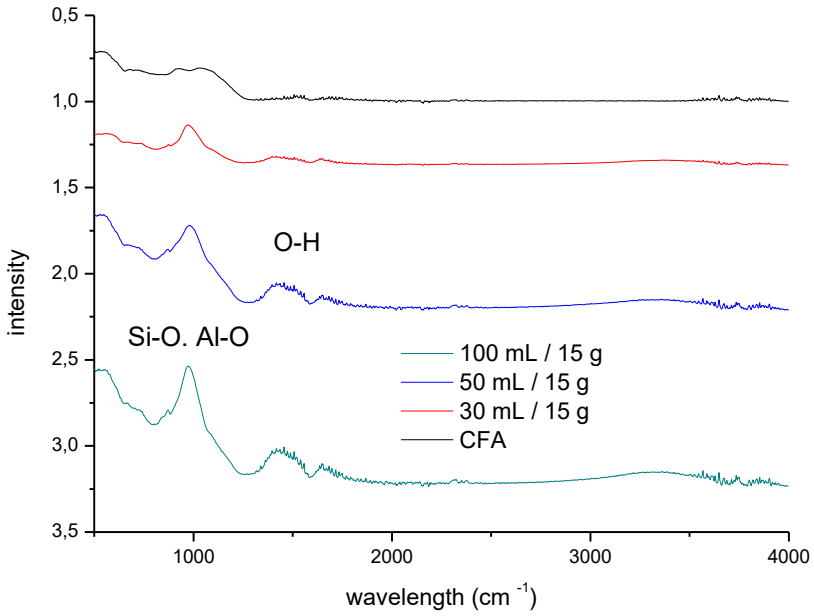

Fig 10: FT-IR spectra of the solid residue of solid/liquid.

4.7 **Hydrothermal time studies**

At 140°C, zeolites were synthesized by varying the hydrothermal time of 6 h, 24 h, 48 h, and 72 h, and the Si-O and Al-O bands associated with stretching vibrations shifts (in zeolites) are in interpretable range, and these shifts are shown according to the reaction time Fig. 11. In the zeolite sample, for example, the band of about 1038 cm^{-1} of the original fly ash becomes sharper and shifts to lower frequencies of 945 cm^{-1}. these peaks at 945 cm^{-1} were observed in all spectra due to asymmetric stretching vibrations of Al-O and Si-O (Musyoka, 2009). It was also discovered that when the peak at 1038 cm^{-1} was treated for 72 h, there was more displacement. This indicate that the vitreous component of the fly ash was forming zeolites by reacting with the alkaline activator (NaOH). At shorter hydrothermal times (6 h, 24 h, and 48 h), less of the aluminosilicate phase was converted to zeolite, as evidenced by a lower adsorption band intensity at 945 cm^{-1}; thus, 72 h was the optimum period for zeolite crystallization.

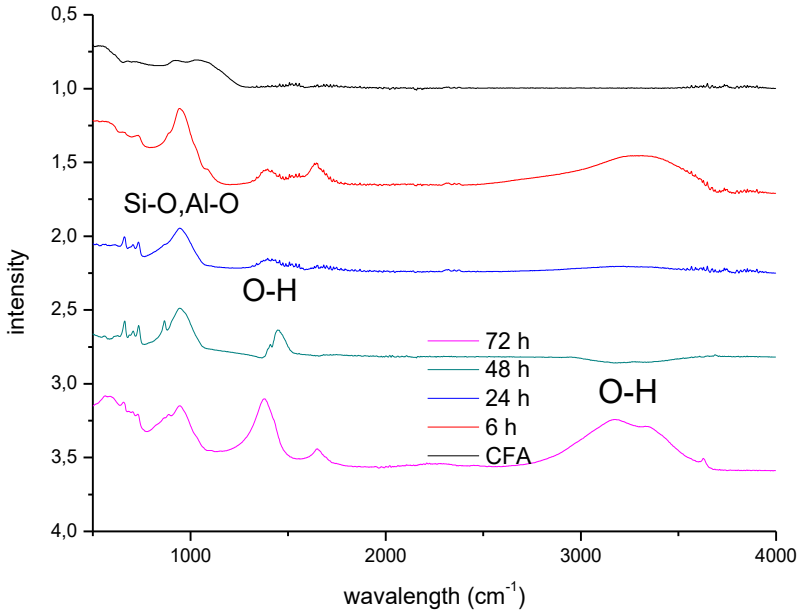

Fig 11: FT-IR spectra of zeolites synthesized at 140^{o}C by varying time of hydrothermal treatment.

The XRF data comparing the chemical composition of CFA and zeolite residues obtained at different crystallization times of 6 h, 24 h, 48 h, and 72 h revealed a significant reduction in Si and Al percentages. This indicated that not enough dissolved Si and Al crystallized on the zeolite residues. Furthermore, XRF data from the solid products for the 6 h treatment time, as shown in Table 6, revealed a higher concentration of Si and Al compared to the other periods investigated. The 72-h crystallization time was chosen as the optimum time due to the observation of a broad sharp band of asymmetric stretching of the Si-O-T (T = Al, Si) bond at 900 - 950 cm^{-1}, which indicated the formation of the Si-O-Al bond, which was also reported by Dolaberidze et al. (2017) and Singh et al. (2019).

Table 6: Chemical composition of CFA and solid products with variation in crystallization times.

Oxide compound	Composition (%) at different crystallization times				
	CFA	6 h	24 h	48 h	72 h
SiO_2	34.99	23.77	20.26	21.21	19.26
Al_2O_3	29.33	16.12	13.35	13.16	10.65
MgO	0.69	0.38	1.24	1.25	0.95
CaO	4.09	8.07	7.81	7.39	7.37
K_2O	0.87	0.41	0.41	0.46	0.49
P_2O_5	0.46	0.18	0.16	0.16	0.24
SiO_2/Al_2O_3	1.19	1.47	1.52	1.61	1.81

4.8 **Crystallization temperature**

Crystallization studies evaluating the effect of temperature carried out. Crystallization temperatures of 50°C, 70°C 100°C and 170°C for a duration of 72 h were studied. It was observed that the raw slurry persisted at lower crystallization temperatures such as 50°C and 70°C. Since the slurries were still obtained at 50°C and 70°C, probably indicated that either no crystallization or crystallization do not take place at lower temperatures. The FT-IR spectra Fig. 12 showed bands at 970 cm^{-1} which was due to asymmetric stretching vibrations of Al-O and Si-O for all the materials studied which was also reported by Musyoka. (2009). Based on FT-IR studies, the prominent peak at 970 cm^{-1} was observed for the zeolite residue crystallized at 170°C. This peak was also observed to be significantly larger relative to the other spectra as shown in Fig. 12. This suggested that optimum conversion of CFA to zeolite occurred at 170°C.

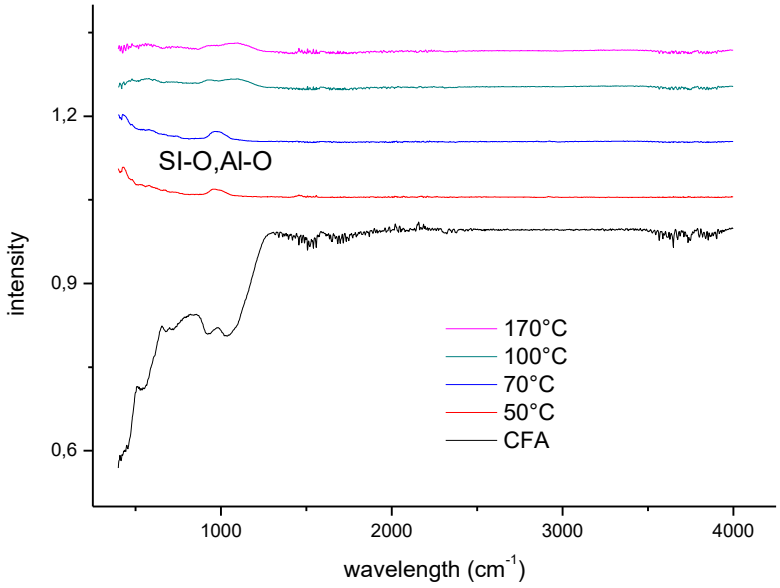

Fig 12: FT-IR spectra of zeolites synthesized at 170°C by varying temperature of hydrothermal.

.

Table 7: Chemical composition of CFA and solid products with variation in crystallization temperature.

Oxide compounds	Composition (%) at different crystallization temperature				
	CFA	50°C	70°C	100°C	170°C
SiO_2	34.99	24.41	26.70	26.19	22.56
Al_2O_3	29.33	16.03	17.41	15.86	14.29
MgO	0.69	0.66	0.24	0.34	1.01
CaO	4.09	8.18	7.80	7.39	7.56
K_2O	0.87	0.27	0.25	0.27	0.45
P_2O_5	0.46	0.13	0.18	0.19	0.16
SiO_2/Al_2O_3	1.19	1.52	1.53	1.65	1.58

4.9 **Effect of variation of water content during hydrothermal treatment process**

Fig 13: depicts the effect of ultra-pure water addition on the purity of the zeolite obtained. A H_2O/SiO_2 ratio of 0.43 produced the most intense peak in the 1200 cm^{-1} region. The peak corresponds to Si-O-Al, Si-O-Si, Si-O, and Al-O vibrations. This means that the majority of the glassy phase in the CFA reacts with the alkaline activator (NaOH) to form the zeolite. Other absorption bands, located between 3800 and 3450 cm^{-1} and 1600 cm^{-1}, are responsible for the vibrations of the hydroxyl groups Si-OH and H_2O, respectively. This 1200 cm^{-1} was observed (Ferhat et al., 2019). When no water was added (H_2O/SiO_2 = 0), the peak with the lowest intensity (Fig. 13) was observed. The addition of water indicates that the CFA improved the conversion of the glassy phase matrix to zeolite, which formed as a porous medium and allowed the crystallization of most Si^{4+} and Al^{3+} species that were dissolved in NaOH. However, large amounts of water (H_2O/SiO_2 > 0) broke down the zeolitic complex. As a result, H_2O/SiO_2 = 0.43 was chosen as the best value for future experiments.

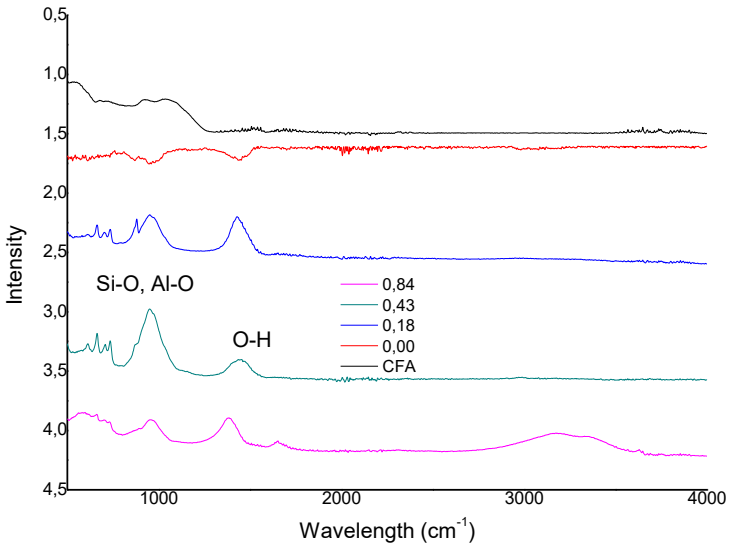

Fig 13: FT-IR spectra of zeolites synthesized at 170^{o}C by varying water content during hydrothermal treatment process.

The chemical composition of CFA and zeolite synthesized are shown in Table 8. It was observed that SiO_2 and Al_2O_3 were the main constituents of CFA as seen by the higher percentages of these oxides relative to the components. This was because of dissolution of SiO_2 and Al_2O_3 into the NaOH activating solution during ageing studies, followed by dissolution of Al^{3+} and Si^{4+} species which then condensed onto the ash surface (Remanenova et al., 2014). Additionally, the H_2O/SiO_2 = 0.43 was observed to have the highest amount of Si and Al relative to the other H_2O/SiO_2 ratios studied. The presence of these minerals was essential as they made up the backbone of the zeolite structure (Jha et al., 2016).

Table 8: XRF chemical composition of CFA and zeolites with variation of H_2O/SiO_2 ratio after ageing from 0 to 0.82.

Oxide compound	H_2O/SiO_2 ratio				
	CFA	0.00	0.18	0.43	0.82
SiO_2	34.99	18.07	19.49	22.58	11.14
Al_2O_3	29.33	10.29	11.28	14.70	6.15
MgO	0.69	1.01	1.06	0.95	0.92
CaO	4.09	7.56	7.22	6.82	5.40
K_2O	0.87	0.45	0.47	0.49	0.36
P_2O_5	0.46	0.16	0.16	0.14	0.06
SiO_2/Al_2O_3	1.19	1.58	1.73	1.69	1.81

4.10 **Effect of sample pH**

The effect of pH on Cr (VI) removal at room temperature was investigated over a pH range of 2 to 11. The results of the experiments are shown below (Fig 14). The optimal pH for Cr (VI) uptake was determined to be 4, which corresponded to 99% Cr (VI) removal by the zeolites. From pH 2 to pH 4, which was nearly maintained, but rapidly decreased to pH 5. The pH value not only determines metal ion speciation, but it also influences the surface charge of solid adsorbents. The rapid increase in adsorption with a decrease in pH was usually caused by the combined effect of changes in surface charge and ionic species shifts in the solution. A comparable observation was made (Harter at al., 2001). The removal efficiency of Cr (VI) decreased at pH values greater than 5. Beyond this pH, competition between hydroxyl ions and dichromate ions in solution was expected. Tavengwa et al. (2013). obtained similar results who demonstrated that at high acidic pH levels of 2 - 4, adsorption was extremely high and rapidly decreased after pH 5. Because pH was only used in the range of 1 to 4, the pH trend they achieved did not show a decrease in Cr (VI) absorption after pH 5.

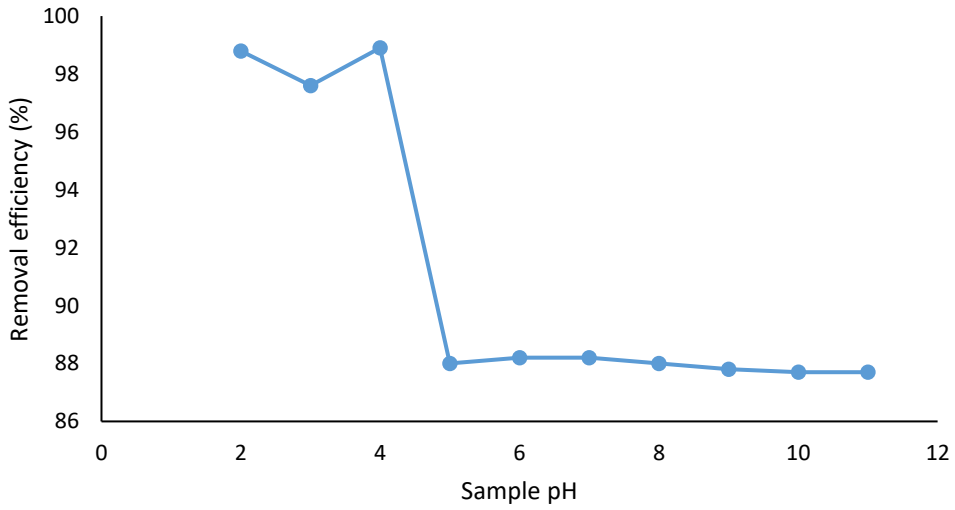

Fig 14: Effect of sample pH. (n = 3, RSD) Experimental conditions: Zeolite's amount = 50 mg, sample volume = 14 mL, concentration = 1 mgL^{-1}, contact time = 30 min, stirring speed = 800 rpm, temperature = room temperature.

4.11 **Effect of mass**

The effect of zeolites amount on Cr (VI) ion adsorption has been optimized. The removal of chromium by zeolites was investigated at various adsorbent doses (10 – 150 mg) starting from an initial Cr (VI) concentration of 1 mg L^{-1}. These findings (Fig. 15) show that the removal efficiency of Cr (VI) increased with increasing zeolites dose due to increased availability of adsorption sites within the adsorbent. As it was reported by Tavengwa et al. (2013) the effect of the amount of the magnetic polymer on adsorbing Cr (VI) has been optimized, the surface area has increased, and many empty bindings of imprinted polymeric material enhanced the removal of uranyl ions. It was also discovered that low zeolites mass has also been found to result in low recovery, which may be the result of maximum binding site occupancy. An increase from 58% to 85% in the removal efficiency of Cr (VI) ions was observed at doses of 10 to 150 mg of zeolites. The optimal amount of the zeolites was then selected to be 150 mg.

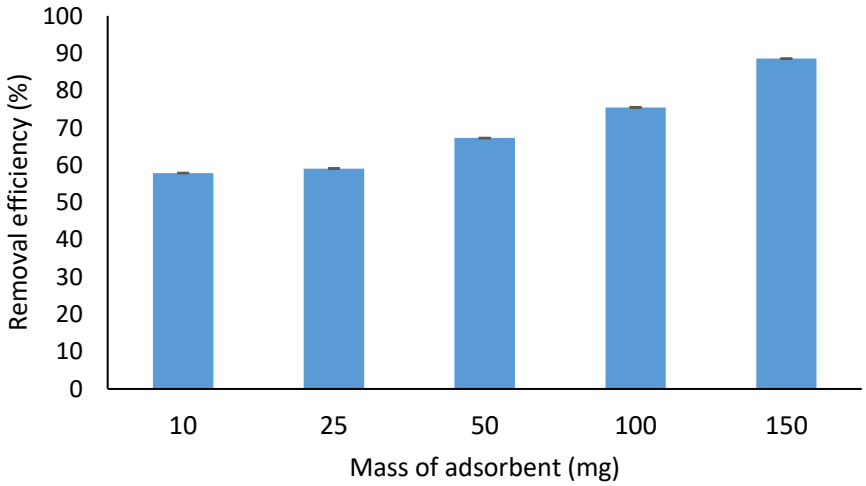

Fig 15: Chromium removal efficiency obtained by varying the mass of zeolites (n = 3, RSD). Experimental conditions: sample pH = 4, sample volume = 14 mL, concentration = 1 mgL^{-1}, contact time = 30 min, stirring speed = 800 rpm, temperature = room temperature.

4.12 **Effect of contact time**

The graph depicts the relationship between the amount of Cr (VI) adsorbed and the contact time with the zeolites (Fig. 16) Under the experimental conditions used, the amount of Cr (VI) adsorbed by the zeolites increased from 0 to 30 min before reaching equilibrium. As a result, a contact time of 60 min was selected as the optimal time because it is long enough to archive equilibrium. The initial adsorption rate may be due to the availability of anionic Cr (VI) species in the solution on the positively charged surface of the adsorbent. The slow pore diffusion of already adsorbed negatively charged adsorbate species and ions may cause electrostatic hindrance in the later slow adsorption rate part of the curve (Ghosh et al., 2005). All adsorption sites were saturated after reaching equilibrium, and Cr (VI) adsorption did not increase further. A similar pattern was observed when chromium (VI) was extracted in aqueous solution using N-propyl quaternized magnetic poly (4-vinylpyridine) (Tavengwa et al., 2013). Their findings revealed that the rate of Cr (VI) uptake was initially rapid, followed by much slower subsequent adsorption and a gradual return to equilibrium.

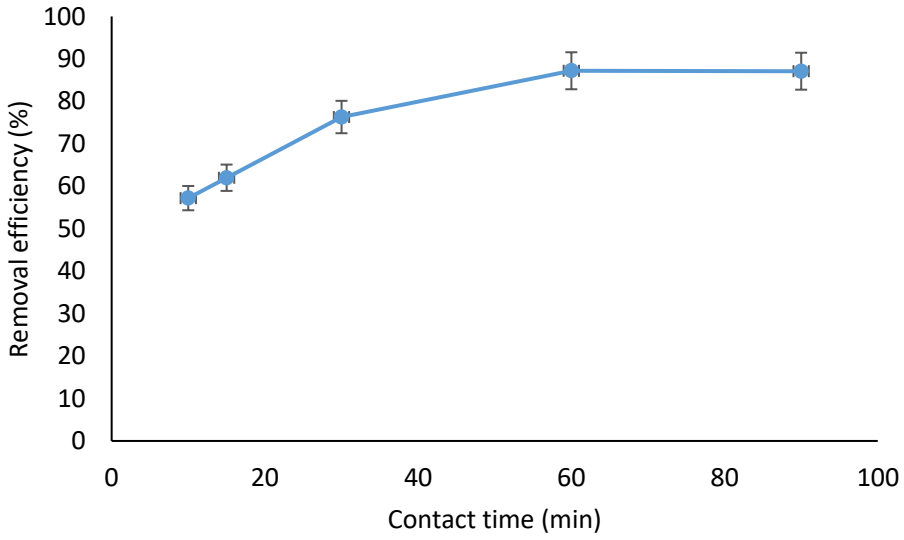

Fig 16: Effect of contact time on the up take of chromium by zeolites (n = 3, RSD). Experimental conditions: sample pH = 4, sample volume = 14 mL, concentration = 1 mg L^{-1}, zeolites amount = 150 mg, stirring speed = 800 rpm, temperature = room temperature.

4.13 **Effect of concentration**

The findings for the effect of concentration on Cr (VI) absorption by zeolites are presented in (Fig. 17). The initial Cr (VI) concentrations ranged from 0.1 to 5 mg L^{-1}. For fixed, contact time, and dose, the amount adsorbed from different concentrations of Cr (VI) ion on to zeolites was dependent on the pH of the sample. As the concentration of Cr (VI) ions increased, the percentage removal was discovered and then continue to increase. However, the absorption capacity increases with increasing initial concentration, which could be due to a greater availability of Cr (VI) ions in solution for adsorption. Furthermore, the initial adsorbate concentration provided a strong driving force to overcome the various mass transfer resistances of the metal ions from the aqueous to the solid phase. Ions of Cr (VI) are more likely to collide with active sites. This resulted in higher Cr (VI) uptake for the same amount of zeolite. This could also be attributed to an increase in the number of Cr (VI) ions in solution competing for a limited number of binding sites on the surface of zeolites. As demonstrated by Tavengwa et al. (2014), magnetic polymer was used to adsorb U (VI) ions. The removal of Cr (VI) from zeolites also resulted in a significant increase from 0.1 to 2.5 mg L^{-1}. The optimal Cr (VI) concentration was 2.5 mg L^{-1}. After this value, there was no discernible increase in the amount of analyte adsorbed on the zeolites, indicating that equilibrium had been reached.

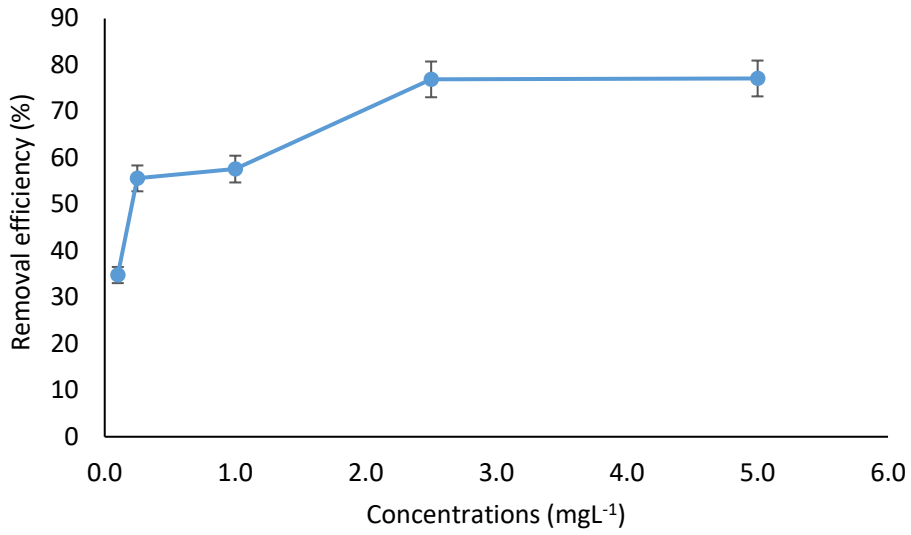

Fig 17: Effect of contact time on the up take of chromium by zeolites (n = 3, RSD). Experimental conditions: sample pH = 4, sample volume = 14 mL, zeolites amount = 150 mg, contact time = 60 min, stirring speed = 800 rpm, temperature = room temperature.

4.14 **Effect of temperature**

The removal of Cr (VI) by zeolites was investigated at various temperatures (RT - 90°C) with a Cr (VI) concentration of 2.5 mgL^{-1}, pH of 4, contact time of 60 min, and mass of 150 mg. The results shown in Fig.18 demonstrated that the removal efficiency of Cr (VI) increases with increasing temperature of the zeolites due to increased availability of adsorption sites within the adsorbent. For the zeolites, the removal efficiency of Cr (VI) ion increased from 35% to 74% at temperatures ranging from RT to 90°C. The adsorption process is greatly influenced by temperature. Higher temperatures cause the adsorbate to move more freely, resulting in desorption. The optimum amount of zeolites was then determined to be 75°C because there was no significant increase above these temperatures.

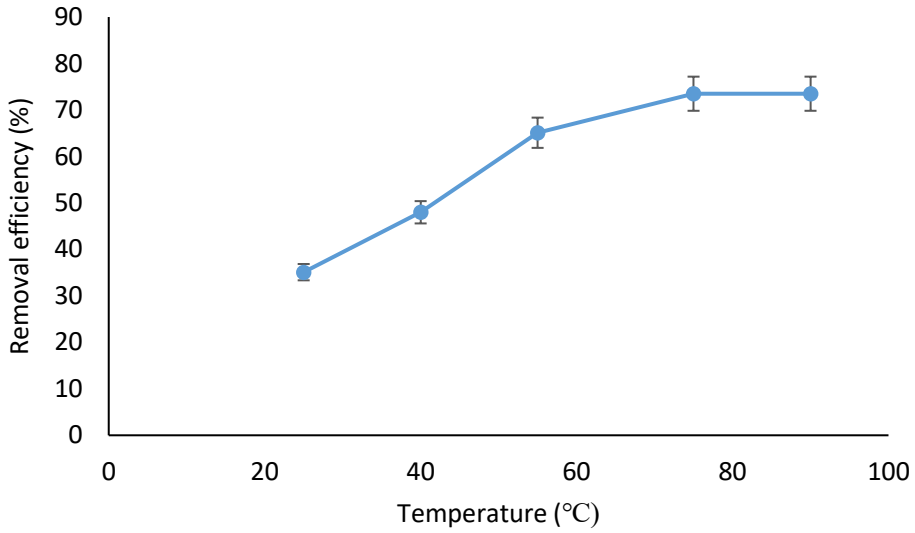

Fig 18: Effect of temperature on the up take of chromium by zeolites (n = 3, RSD. Experimental conditions: sample pH = 4, sample volume = 14 mL, concentration = 2.5 mg L^{-1}, zeolites amount = 150 mg, contact time = 60 min, stirring speed = 800 rpm, temperature = room temperature.

4.15 **Adsorption results**

To determine whether Cr (VI) adsorption on the surface of prepared zeolites was monolayer or multilayer. The adsorption data was subjected to Freundlich and Langmuir isotherm modeling. The findings are summarized in Table 9. According to Hassanpour et al (2018) and Velempini et al (2017), favorable adsorption occurs when the R_L value is between 0 and 1. The results of our study, which are summarized in Table 9, show chromium adsorption on the Cr (VI) zeolites adsorbent with R_L of 0.30.

The Freundlich isotherm was preferred over the Langmuir isotherm because the Freundlich correlation coefficients were higher than those of the Langmuir isotherm, indicating the applicability of a multi-layer Cr (VI) coating on the surface of the adsorbents. The Langmuir model is used to describe sorption data when the correlation coefficient R^2 is less than 0.997.

Table 9: Langmuir and Freundlich isotherm constants for Cr (VI) adsorption onto zeolites adsorbent.

	Langmuir isotherm model				Freundlich isotherm model		
Parameters	b (L g^{-1})	q_m (mg g^{-1})	R_L	R^2	n	K_f	R^2
	0,455	0,150	0,305	0,919	0,119	1,151	0,989

4.16 **Kinetic modelling**

The plots were used to calculate the correlation coefficients for the pseudo-first order and pseudo-second order kinetics. The graph showed that pseudo-second order kinetics produced higher correlation coefficient values for linearization than pseudo-first order kinetics.

Other researchers who used similar sorbents found the pseudo second order to be the best suitable model as well. The correlation coefficients of pseudo-first order and second-order equations can be used to predict the chromium adsorption kinetics on the zeolite. The adsorption capacity values in Table 10 were not close to each other (1.148 and 4.599 mg g^{-1}).

The results in (Table 10) show that the pseudo-second order model is the most reliable for determining the order of Cr (VI) ion adsorption kinetics onto zeolites, with a good correlation coefficient of (R^2 > 0.862). Similarly, the values of q_e calculated by the pseudo-second order model were found to be very close to the experimentally determined value q_e = 4.599. Furthermore, it justifies the fact that the kinetics of these ions are pseudo second order.

The good fit of the experimental results to the pseudo second order model suggested that Cr (VI) ion fixation on the investigated zeolite is primarily due to chemical adsorption. Indeed, Ho and McKay (1999) argue that the kinetics of most metal ions adsorbing to the adsorbent are consistent with the pseudo second-order model hypothesis that metal ions interact with various functional groups on the material's surface.

As a result, it was determined that the pseudo second order model accurately represents the experimental results. This model is widely used to simulate the kinetics of heavy metal adsorption on zeolites (Djawad et al., 2019; Fatima et al., 2013; Tajiki et al., 2017).

Table 10: Kinetic modelling parameters of the pseudo-first order and the pseudo-second-order rate equations for Cr (VI) adsorption on zeolites adsorbent.

	Pseudo-first order			Pseudo-second order		
Parameters	K_1 (min ^{1})	q_e (mg g^{-1})	R^2	K_2 (g mg ^{1}min^{-1})	q_e (mg g^{-1})	R^2
	0.088	1,148	0,827	0 ,012	4,599	0,862

4.17 **Thermodynamic results**

Table 11 shows that Negative values of the free energy ΔG° Gibbs indicate the sorption process's thermodynamic feasibility and spontaneity. A positive value of ΔH° confirms that Cr (VI) sorption is endothermic. A positive value of entropy ΔS° indicated an increase in randomness at the solid solution interface during adsorbate fixation to the active site of the adsorbent.

Table 11. Thermodynamic parameters for adsorption of Cr (VI) zeolites as function temperature

Temperature (K)	K_L	ΔG° (KJ mol $^{-1}$)	ΔH° (KJ mol $^{-1}$)	ΔS° (KJ $^{-1}$ mol $^{-1}$)	R^2
298	3,02	-2,74			
313	3,40	-3,19	3,87	22,4	0.918
328	3,67	-3,55			
348	3,77	-3,84			

* ΔG°: Gibbs free energy

* ΔH°: enthalpy

*ΔS°: entropy

4.18 **Application of the zeolites using WWTPs samples**

Before they can be mixed with biomass in an Aerated Stability Basin (ASB) or an active sludge system, many plants must keep the pH of their process effluent within an acceptable range. Even when exposed for a short period of time (less than a minute), extreme pH causes significant microbial destruction. Some influents (process influents) have pH values ranging from 9.0 to 10.5 and are slightly basic. Bacteria produce CO_2 (acidic gas) as a byproduct of metabolism, so if the pH is not high enough to completely shut down the bacteria's metabolism, it will be regulated to some extent.

The water influent and effluent water of both Makhado and Rietviei WWTPs is shown in table 12 and table 13 below. All the pH influent of both WWTPs were found to be little bit acidic as they are under 7 pH, they maybe do to the different domestic waste coming into the plants before they are treated. The pH of the effluent was found to be neutral at 7.13 for Rietviei and 6.46 for Makhado WWTP this maybe because the aim of wastewater treatment process is to achieve a treated effluent and sludge quality that is environmentally safe for disposal and/or reuse (Hassen et al., 2019).

Cr (VI) wastewaters samples were sampled from effluents discharged from WWTPs as stated above. After decanting and filtering, to remove the dissolved pollutants (e.g., organic matter) and clarify the solution, some physico-chemical properties were obtained and presented in Table 11 and Table 12. Then, Cr (VI) adsorption tests were carried out onto zeolites using optimal conditions found beforehand. the Cr (VI) removal efficiency was 69.25 % and 70.02 % for both Makhado and Rietviei WWTPs, respectively. The zeolites were found to be very effective in removing Cr (VI).

Table 12: Physiochemical properties of both inflow and final effluent of Makhado WWTP

pH meter	Influent	Effluent
pH	6.76	6.46
TDS (mg L^{-1})	5.56	5.63
EC (µS cm^{-1})	9.26	9.34
Temperature (°C)	25.9	25.5

Table 13: Physiochemical properties of both inflow and final effluent of Rietviei WWTP

pH meter	Influent	Effluent
pH	6.66	7.13
TDS (mg L^{-1})	4.43	4.99
EC (µS cm^{-1})	7.37	8,31
Temperature (°C)	26.7	27.3

Table 14 shows metals found in two WWTPs samples, analyzed using ICP-OES. The highest concentrations of most metals were found in Makhado wastewater. Among the metals studied, the most abundant element was Al (53.6 mg L^{-1}) and the lowest was iron (14.9 mg L^{-1}).

Table 15 shows the overall removal efficiency of metals at Rietviei was 70.02 % followed by Makhado 69.25 % WWTPs. This means that the removal of Cr (VI) from both WWTPs are in the following order: Rietviei > Makhado. This also mean that the zeolites used in the removal of Cr (VI) was effective in removing Cr (VI). The two WWTPs were not sufficient in the removal of heavy metals since zeolites managed to remove Cr (VI) ion with efficiencies above 60% in both WWTPs with optimized conditions.

For most individual metals found in the effluents was very low probably due to the operation of the treatment plants under stress, design weakness, and overloaded capacity. Morrison et al., (2001), found that efficiency of the treatment plant was poor, resulting in the discharge of raw sewage due to inadequate treatment works, a malfunctioning pump station, and poor planning for expansion.

Table 14: Metal composition and concentrations in real water samples using ICP-OES.

WWWPs	Metal	Co	Al	Ni	Mn	Fe
Makhado	Mean (mg L^{-1})	24.7	53.6	44.2	22.7	14.9
Rietviei	Mean (mg L^{-1})	18.3	50.7	30.5	30.3	18.1

Table 15: Application of zeolites for the removal of chromium from the effluent water samples using optimized conditions.

WWTPs	Effluent (mg L^{-1})	Treated samples	%Recovery
Makhado	22.4	4.58	69.3
Rietviei	35.5	6.57	70.0

Chapter Five

General conclusion and future work

This chapter gives general conclusions based on the research findings of this work. The recommended future work is also outlined in this chapter

5.1 **Conclusions**

The study showed that zeolite can be prepared from CFA in South Africa due to the dominance of the composition of the aluminosilicate and silicate phases. CFA obtained from Mudderfontaine steam plants was effective in removing Cr (VI) from WWTPS effluent. The optimized synthesis conditions for the preparation of zeolite were obtained when the molar regime was SiO_2 / Al_2O_3: 1.19 and ageing at 50 ℃ for 72 h under synthesis conditions. The time and temperature of the hydrothermal treatment were 72 h and 140 ℃ respectively.

It was interesting to see how the added water content after the ageing step, expressed as the H_2O/SiO_2 molar ratio, influenced the hydrothermal conversion of fly ash to zeolites. By varying the water content after ageing between the H_2O/SiO_2 molar ratios of 0 and 3.00, it was discovered that the best optimization was achieved when the molar ratio was 3.00, as confirmed by XRF studies.

The CFA was class C, according to X-ray fluorescence analysis, with a Si/Al ratio of 1.19 and a LOI of 3.29%. Optimization studies for the dissolution of Si^{4+} and Al^{3+} from the aluminosilicate matrix of CFA were conducted using the following parameters, which included the effect of activating agent concentration, ageing time, and solid/liquid ratio. 2.5 M NaOH, aged for 72 h at a S/L ratio of 15 g/100 mL, was the optimal condition.

The optimization of hydrothermal treatment parameters for crystallization of zeolite were inverstigated. During crystallization of the slurry, the dominant CFA minerals such as mullite and quartz were observed to diminish while zeolitic hydroxysodalite phase was formed. The optimized hydrothermal synthetic conditions for preparation of zeolite were achieved at a H_2O/SiO_2 molar ratio of 0.43, crystallized at 140°C for a duration of 72 h. synthesizing zeolites from CFA using the hydrothermal treatment technique was achieved.

The application was then performed using optimized parameters and applied to the absorption of Cr (VI) in influent water of Rietviei and Makhado WWTPs. Zeolites were observed to have better removal efficiency based on ICP-OES data performed with percentage obtained of 69.25% and 70.02% respectively.

5.2 **Recommendations and future work**

- The broad scope of this dissertation means that there is an excessive amount of work to be done. The investigation confirmed the possibility of synthesizing zeolite from South African CFA. Similar investigations should be conducted in South Africa for other sources of fly ash. This should be done to see if zeolite can be synthesized under the optimized conditions obtained in this study.

- If they do not produce the same zeolite under these conditions, the synthesis conditions must be optimized. To replicate the conditions used in the laboratory, pilot scale zeolite synthesis from South African fly ash should be attempted.

- The use of other zeolites synthesis techniques should be investigated to see if it is possible to reduce maturing time and temperature. This will allow for lower production costs, especially as the synthesis procedure is scaled up. To archive the proper conditions for heavy metals Cr (VI) removal from WWTP effluent water, a total optimisation study should be performed.

- Long-term stability of the zeolite-immobilized metals used in future studies will be required to determine if they can leach. Mass balances will need to be performed in future studies to determine the actual synthesis efficiency, mobility, and fate of trace elements during the synthesis process.

References

This section gives references used in chapters 1, 2, 3, 4 and 5.

References

Ahmaruzzaman, M., 2009. Role of fly ash in the removal of organic pollutants from wastewater. Energy & Fuels, 23(3), pp.1494-1511.

Ahmed, W., Neller, R. and Katouli, M., 2005. Evidence of septic system failure determined by a bacterial biochemical fingerprinting method. Journal of Applied Microbiology, 98(4), pp.910-920.

Akın, S.Ş., Magalhães, D. and Kazanç, F., 2020. A study on the effects of various combustion parameters on the mineral composition of Tunçbilek fly ash. Fuel, 275, p.117881.

Akinyemi, S.A., Gitari, W.M., Petrik, L.F., Nyakuma, B.B., Hower, J.C., Ward, C.R., Oliveira, M.L. and Silva, L.F., 2019. Environmental evaluation and nano-mineralogical study of fresh and unsaturated weathered coal fly ashes. *Science of The Total Environment*, *663*, pp.177-188.

Aldahri, T., Behin, J., Kazemian, H. and Rohani, S., 2016. Synthesis of zeolite Na-P from coal fly ash by thermo-sonochemical treatment. fuel, 182, pp.494-501.

Ali, A., Saeed, K. and Mabood, F., 2016. Removal of chromium (VI) from aqueous medium using chemically modified banana peels as efficient low-cost adsorbent. Alexandria Engineering Journal, 55(3), pp.2933-2942.

Al-Jubouri, S.M. and Holmes, S.M., 2017. Hierarchically porous zeolite X composites for manganese ion-exchange and solidification: Equilibrium isotherms, kinetic and thermodynamic studies. Chemical Engineering Journal, 308, pp.476-491.

Alnahhal, M.F., Kim, T. and Hajimohammadi, A., 2021. Waste-derived activators for alkali-activated materials: A review. Cement and Concrete Composites, p.103980.

Alzeer, M.I. and MacKenzie, K.J., 2018. Synthesis and catalytic properties of new sustainable aluminosilicate heterogeneous catalysts derived from fly ash. ACS Sustainable Chemistry & Engineering, 6(4), pp.5273-5282.

Ameh, A.E., Fatoba, O.O., Musyoka, N.M. and Petrik, L.F., 2017. Influence of aluminium source on the crystal structure and framework coordination of Al and Si in fly ash-based zeolite NaA. Powder Technology, 306, pp.17-25.

Angaru, G.K.R., Choi, Y.L., Lingamdinne, L.P., Choi, J.S., Kim, D.S., Koduru, J.R., Yang, J.K. and Chang, Y.Y., 2021. Facile synthesis of economical feasible fly ash–based zeolite–supported nano zerovalent iron and nickel bimetallic composite for the potential removal of heavy metals from industrial effluents. *Chemosphere*, *267*, p.128889.

Annadurai, G., Juang, R.S. and Lee, D.J., 2003. Adsorption of heavy metals from water using banana and orange peels. Water Science and Technology, 47(1), pp.185-190.

Anyakora, C., Nwaeze, K., Awodele, O., Nwadike, C., Arbabi, M. and Coker, H., 2011. Concentrations of heavy metals in some pharmaceutical effluents in Lagos, Nigeria. Journal of Environmental Chemistry and Ecotoxicology, 3(2), pp.25-31.

Apreutesei, R.E., Catrinescu, C. and Teodosiu, C., 2008. surfactant-modified natural zeolites for environmental applications in water purification. Environmental Engineering & Management Journal (EEMJ), 7(2).

Ashraf, S., Ali, Q., Zahir, Z.A., Ashraf, S. and Asghar, H.N., 2019. Phytoremediation: Environmentally sustainable way for reclamation of heavy metal polluted soils. Ecotoxicology and Environmental Safety, 174, pp.714-727.

Asl, S.M.H., Javadian, H., Khavarpour, M., Belviso, C., Taghavi, M. and Maghsudi, M., 2019. Porous adsorbents derived from coal fly ash as cost-effective and environmentally friendly sources of aluminosilicate for sequestration of aqueous and gaseous pollutants: A review. Journal of Cleaner Production, 208, pp.1131-1147.

Atafar, Z., Mesdaghinia, A., Nouri, J., Homaee, M., Yunesian, M., Ahmadimoghaddam, M. and Mahvi, A.H., 2010. Effect of fertilizer application on soil heavy metal concentration. Environmental Monitoring and Assessment, 160(1), pp.83-89.

Auerbach, E.A., Seyfried, E.E. and McMahon, K.D., 2007. Tetracycline resistance genes in activated sludge wastewater treatment plants. water research, 41(5), pp.1143-1151.

Ayanda, O.S., Fatoki, O.S., Adekola, F.A., Suana, E. and Ximba, B.J., 2014. comparative performance evaluation of activated carbon and fly ash/activated carbon composite for triphenyltin chloride removal by adsorption. Internal. J. Nano. Corr. Science. Engineering, 1(1), p.1.

Azizi, D., Ibsaine, F., Dionne, J., Pasquier, L.C., Coudert, L. and Blais, J.F., 2021. Microporous and macroporous materials state-of-the-art of the technologies in zeolitization of aluminosilicate bearing residues from mining and metallurgical industries: A comprehensive review. Microporous and Mesoporous Materials, p.111029.

Azizi, Seyed Naser, Ahmad Roozbehani Dehnavi, and Amir Joorabdoozha. "Synthesis and characterization of LTA nanozeolite using barley husk silica: Mercury removal from standard and real solutions." *Materials Research Bulletin* 48, no. 5 (2013): 1753-1759.

Bai, R., Song, Y., Li, Y. and Yu, J., 2019. Creating hierarchical pores in zeolite catalysts. *Trends in Chemistry*, *1*(6), pp.601-611.

Banat, K.M., Howari, F.M. and Al-Hamad, A.A., 2005. Heavy metals in urban soils of central Jordan: should we worry about their environmental risks. Environmental Research, 97(3), pp.258-273.

Bayuo, J., Pelig-Ba, K.B. and Abukari, M.A., 2019. Adsorptive removal of chromium (VI) from aqueous solution unto groundnut shell. Applied Water Science, 9(4), pp.1-11.

Belviso, C., 2018. State-of-the-art applications of fly ash from coal and biomass: A focus on zeolite synthesis processes and issues. Progress in Energy and Combustion Science, 65, pp.109-135.

Belviso, C., Cavalcante, F., Lettino, A. and Fiore, S., 2009. Zeolite synthesised from fused coal fly ash at low temperature using seawater for crystallization. Coal Combustion and Gasification Products, 1(1), pp.7-13.

Bhat, S.A., Cui, G., Li, W., Wei, Y. and Li, F., 2020. Effect of heavy metals on the performance and bacterial profiles of activated sludge in a semi-continuous reactor. Chemosphere, 241, p.125035.

Bhatt, A., Priyadarshini, S., Mohanakrishnan, A.A., Abri, A., Sattler, M. and Techapaphawit, S., 2019. Physical, chemical, and geotechnical properties of coal fly ash: a global review. *Case Studies in Construction Materials*, *11*, p.e00263.

Bhown, A.S. and Freeman, B.C., 2011. Analysis and status of post-combustion carbon dioxide capture technologies. Environmental Science & Technology, 45(20), pp.8624-8632.

Blissett, R.S. and Rowson, N.A., 2012. A review of the multi-component utilisation of coal fly ash. Fuel, 97, pp.1-23.

Boycheva, S., Marinov, I., Miteva, S. and Zgureva, D., 2020. Conversion of coal fly ash into nanozeolite Na-X by applying ultrasound assisted hydrothermal and fusion-hydrothermal alkaline activation. Sustainable Chemistry and Pharmacy, 15, p.100217.

Brunetti, A., Zito, P.F., Giorno, L., Drioli, E. and Barbieri, G., 2018. Membrane reactors for low temperature applications: An overview. Chemical Engineering and Processing-Process Intensification, 124, pp.282-307.

Cai, J., Shen, B., Li, Z., Chen, J. and He, C., 2014. Removal of elemental mercury by clays impregnated with KI and KBr. *Chemical Engineering Journal*, *241*, pp.19-27.

Cai, W., Wei, J., Li, Z., Liu, Y., Zhou, J. and Han, B., 2019. Preparation of amino-functionalized magnetic biochar with excellent adsorption performance for Cr (VI) by a mild one-step hydrothermal method from peanut hull. Colloids and Surfaces A: Physicochemical and Engineering Aspects, 563, pp.102-111.

Chakraborty, R., Asthana, A., Singh, A.K., Jain, B. and Susan, A.B.H., 2020. Adsorption of heavy metal ions by various low-cost adsorbents: a review. International Journal of Environmental Analytical Chemistry, pp.1-38.

Charerntanyarak, L., 1999. Heavy metals removal by chemical coagulation and precipitation. Water Science and Technology, 39(10-11), pp.135-138.

Chen, X., 2015. Modeling of experimental adsorption isotherm data. Information, 6(1), pp.14-22.

Chen, X.J., Guo, Y.X., Cheng, F.Q., Song, H.P., Zheng, N. and Wang, X.M., 2012. Application of modified coal fly ash as an absorbent for ammonia-nitrogen wastewater treatment. In Advanced Materials Research (Vol. 518, pp. 2380-2384). Trans Tech Publications Ltd.

Chen, Y., Dong, Y., Wu, H., Chen, C., Chi, Y. and Chen, G., 2015. Electrochemiluminescence sensor for hexavalent chromium based on the graphene quantum dots/peroxodisulfate system. Electrochimica Acta, 151, pp.552-557.

Chen, Y.W., Yu, X., Appiah-Hagan, E., Pizarro, J., Arteca, G.A., Mercier, L., Wei, Q. and Belzile, N., 2018. Utilization of coal fly ash and drinking water sludge to remove anionic As (V), Cr (VI), Mo (VI) and Se (IV) from mine waters. *Journal of Environmental Chemical Engineering*, *6*(2), pp.2470-2479.

Coedo, A.G., Dorado, T., Padilla, I. and Alguacil, F.J., 2000. Speciation of chromium in steelmaking solid wastes by selective retention on ion-exchange media and determination by isotope dilution inductively coupled plasma mass spectrometry. Journal of Analytical Atomic Spectrometry, 15(12), pp.1564-1568.

Creamer, A.E. and Gao, B., 2016. Carbon-based adsorbents for post combustion CO2 capture: a critical review. Environmental Science & Technology, 50(14), pp.7276-7289.

De Haro-Del Rio, D.A., Al-Joubori, S., Kontogiannis, O., Papadatos-Gigantes, D., Ajayi, O., Li, C., and Holmes, S.M., 2015. The removal of caesium ions using supported clinoptilolite. Journal of hazardous materials, 289, pp.1-8.

de Sousa, D.N.R., Insa, S., Mozeto, A.A., Petrovic, M., Chaves, T.F. and Fadini, P.S., 2018. Equilibrium and kinetic studies of the adsorption of antibiotics from aqueous solutions onto powdered zeolites. *Chemosphere*, *205*, pp.137-146

Ding, L. and Zheng, Y., 2007. Effect of template concentration and gel dilution on crystallization and particle size of zeolite beta in the absence of alkali cations. Microporous and mesoporous materials, 103(1-3), pp.94-101.

Ding, L. and Zheng, Y., 2007. Effect of template concentration and gel dilution on crystallization and particle size of zeolite beta in the absence of alkali cations. Microporous and mesoporous materials, 103(1-3), pp.94-101.

Djawad, F., Djamel, N., Elhadj, M. and Samira, A., 2019. Adsorption of Ni2+ Ions onto NaX and NaY Zeolites: Equilibrium, Kinetics, Intra Crystalline Diffusion, and Thermodynamic Studies. Iranian Journal of Chemistry and Chemical Engineering (IJCCE), 38(6), pp.63-81.

Dolaberidze, N.M., Tsitsishvili, V.G., Mirdzveli, N.A. and Nijaradze, N.O., 2017. Synthesis of LTA type zeolites from Georgian clinoptilolite. *Хімія, фізика та технологія поверхні*, *8*(3), pp.346-352.

Doumit, P., Clark, M.W., Yee, L.H. and Rose, A., 2019. Response surface statistical optimisation of zeolite-X/silica by hydrothermal synthesis. Journal of Materials Science, 54(24), pp.14677-14689.

Doyle, F.M. and Liu, Z., 2003. The effect of triethylenetetraamine (Trien) on the ion flotation of Cu2+ and Ni2+. Journal of colloid and interface science, 258(2), pp.396-403.

Dudley, S.P., 2011. Evaluation of fly-ash based artificial zeolite formation as treatment for salt-laden process water from eastern Montana coal operations (Doctoral dissertation, Montana Tech of The University of Montana).

Dungeni, M., van Der Merwe, R.R. and Momba, M., 2010. Abundance of pathogenic bacteria and viral indicators in chlorinated effluents produced by four wastewater treatment plants in the Gauteng Province, South Africa. Water SA, 36(5).

Dursun, S. and Pala, A., 2007. Lead pollution removal from water using a natural zeolite. Journal of International Environmental Application and Science, 7(1), pp.11-9.

Elavarasan, G., Rajakrishnamoorthy, P., Karthikeyan, D. and Saravanan, C.G., 2019. Utilization of coal fly ash as a Raw Material for the Synthesis of Zeolite like Substance. *International Journal on Emerging Technologies*, *10*(1), pp.176-182.

Erdem, E., Karapinar, N. and Donat, R., 2004. The removal of heavy metal cations by natural zeolites. *Journal of colloid and interface science*, *280*(2), pp.309-314.

Eskom (2017), Fact Sheet, Generation Communication CO 0004, Available at http://www.eskom.co.za/content/CO_0004AshManRev9.pdf. Accessed on 26th August 2017.

Fan, J., Du, M. and Liu, L., 2020. Study on the correlation between trace elements in coal and coal-forming plants: a case study. *Energy Sources, Part A: Recovery, Utilization, and Environmental Effects*, pp.1-12.

Farzadkia, M., Gholami, M., Abouee, E., Asadgol, Z., Sadeghi, S., Arfaeinia, H. and Noradini, M., 2016. The impact of exited pollutants of cement plant on the soil and leaves of trees species: a case study in Golestan province. Open Journal of Ecology, 6(07), p.404.

Fatima, H., Djamel, N., Samira, A. and Mahfoud, B., 2013. Modelling and adsorption studies of removal uranium (VI) ions on synthesised zeolite NaY. Desalination and Water Treatment, 51(28-30), pp.5583-5591.

Feng R, Chen K, Yan X, Hu X, Zhang Y. and Wu J., 2019. Synthesis of ZSM-5 zeolite using CFAas an additive for the methanol to propylene (MTP) reaction. Catalysts, 9(10), p.788.

Feng, X., Zhang, H. and Yu, P., 2020. X-ray fluorescence application in food, feed, and agricultural science: a critical review. *Critical Reviews in Food Science and Nutrition*, pp.1-11.

Ferhat, D., Nibou, D., Elhadj, M. and Amokrane, S., 2019. Adsorption of Ni2+ ions onto NaX and NaY zeolites: Equilibrium, kinetic, intra crystalline diffusion and thermodynamic studies. *Iranian Journal of Chemistry and Chemical Engineering*, *38*.

Ferrarini, S.F., Cardoso, A.M., Paprocki, A. and Pires, M., 2016. Integrated synthesis of zeolites using coal fly ash: element distribution in the products, washing waters and effluent. Journal of the Brazilian Chemical Society, 27(11), pp.2034-2045.

Finkelman, R.B., 1999. Trace elements in coal. *Biological Trace Element Research*, *67*(3), pp.197-204.

Futsaeter, G. and Wilson, S., 2013. The UNEP global mercury assessment: sources, emissions, and transport. In E3S Web of Conferences (Vol. 1, p. 36001). EDP Sciences.

Gadore, V. and Ahmaruzzaman, M., 2021. Tailored fly ash materials: A recent progress of their properties and applications for remediation of organic and inorganic contaminants from water. Journal of Water Process Engineering, 41, p.101910.

Gadore, V. and Ahmaruzzaman, M., 2021. Tailored fly ash materials: A recent progress of their properties and applications for remediation of organic and inorganic contaminants from water. Journal of Water Process Engineering, 41, p.101910.

Gallardo, H., Queralt, I., Tapias, J., Guerra, M., Carvalho, M.L. and Marguí, E., 2016. Possibilities of low-power X-ray fluorescence spectrometry methods for rapid multielemental analysis and imaging of vegetal foodstuffs. *Journal of Food Composition and Analysis*, *50*, pp.1-9.

Gautam, P.K., Gautam, R.K., Banerjee, S., Chattopadhyaya, M.C. and Pandey, J.D., 2016. Heavy metals in the environment: fate, transport, toxicity, and remediation technologies. Heavy Metals, pp.1-27.

Geary, P.M. and Gardner, E., 1998, March. Sustainable on-site treatment systems. In Proceedings of the 8th National Symposium on Individual and Small Community Sewage Systems (pp. 12-19).

Ghobarkar, H., Schäf, O. and Guth, U., 1999. Zeolites—from kitchen to space. *Progress in Solid State Chemistry*, *27*(2-4), pp.29-73.

Ghosal, S. and Self, S.A., 1995. Particle size-density relation and cenosphere content of coal fly ash. *Fuel*, *74*(4), pp.522-529.

Gollakota, A.R., Volli, V. and Shu, C.M., 2019. Progressive utilisation prospects of coal fly ash: A review. *Science of the Total Environment*, *672*, pp.951-989.

Goswami, S. and Ghosh, U.C., 2005. Studies on adsorption behaviour of Cr (VI) onto synthetic hydrous stannic oxide. water SA, 31(4), pp.597-602.

Gupta, N., Khan, D.K. and Santra, S.C., 2010. Determination of public health hazard potential of wastewater reuse in crop production. World Review of Science, Technology and Sustainable Development, 7(4), pp.328-340.

Gupta, P., Khanday, W.A., Majid, S.A., Kushwa, V., Tomar, S.S. and Tomar, R., 2013. Study of sorption of metal oxoanions from wastewater on surfactant modified analog of laumontite. Journal of Environmental Chemical Engineering, 1(3), pp.510-515.

Harizi, I., 2020. Synthèse et caractérisation des matériaux à base de zéolithe et d'hydroxydes doubles lamellaires: application à l'élimination des colorants (Doctoral dissertation).

Harter, R.D. and Naidu, R., 2001. An assessment of environmental and solution parameter impact on trace-metal sorption by soils. Soil Science Society of America Journal, 65(3), pp.597-612.

Hassanpour, S., Taghizadeh, M. and Yamini, Y., 2018. Magnetic Cr (VI) ion imprinted polymer for the fast selective adsorption of Cr (VI) from aqueous solution. Journal of Polymers and the Environment, 26(1), pp.101-115.

Hassanpour, S., Taghizadeh, M. and Yamini, Y., 2018. Magnetic Cr (VI) ion imprinted polymer for the fast selective adsorption of Cr (VI) from aqueous solution. Journal of Polymers and the Environment, 26(1), pp.101-115.

He, H., Guo, J., Xie, X. and Peng, J., 2000. Experimental study of the selective adsorption of heavy metals onto clay minerals. Chinese Journal of Geochemistry, 19(2), pp.105-109.

He, X., Yao, B., Xia, Y., Huang, H., Gan, Y. and Zhang, W., 2020. Coal fly ash derived zeolite for highly efficient removal of Ni^{2+} in wastewater. Powder Technology, 367, pp.40-46.

Hollman G.G., Steenbruggen G., Janssen-Jurkovicov M. (1999) A two-step process for the synthesis of zeolites from coal fly ash, Fuel, 78, 1225–1230.

Hong, M., Yu, L., Wang, Y., Zhang, J., Chen, Z., Dong, L., Zan, Q. and Li, R., 2019. Heavy metal adsorption with zeolites: The role of hierarchical pore architecture. Chemical Engineering Journal, 359, pp.363-372.

Hong, M., Yu, L., Wang, Y., Zhang, J., Chen, Z., Dong, L., Zan, Q. and Li, R., 2019. Heavy metal adsorption with zeolites: The role of hierarchical pore architecture. Chemical Engineering Journal, 359, pp.363-372.

Hower, J.C., 2012. Petrographic examination of coal-combustion fly ash. International Journal of Coal Geology, 92, pp.90-97.

Huang, X., Zhao, H., Hu, X., Liu, F., Wang, L., Zhao, X., Gao, P. and Ji, P., 2020. Optimization of preparation technology for modified coal fly ash and its adsorption properties for Cd^{2+}. *Journal of Hazardous Materials*, p.122461.

Hui, K.S., Chao, C.Y.H. and Kot, S.C., 2005. Removal of mixed heavy metal ions in wastewater by zeolite 4A and residual products from recycled coal fly ash. *Journal of hazardous materials*, *127*(1-3), pp.89-101.

Inada, M., Eguchi, Y., Enomoto, N. and Hojo, J., 2005. Synthesis of zeolite from coal fly ashes with different silica–alumina composition. *Fuel*, *84*(2-3), pp.299-304.

Irannajad, M. and Haghighi, H.K., 2020. Removal of Heavy Metals from Polluted Solutions by Zeolitic Adsorbents: A Review. Environmental Processes, pp.1-29.

Izadi, A., Mohebbi, A., Amiri, M. and Izadi, N., 2017. Removal of iron ions from industrial copper raffinate and electrowinning electrolyte solutions by chemical precipitation and ion exchange. Minerals Engineering, 113, pp.23-35.

Jacobs, J.A. and Testa, S.M., 2005. Overview of chromium (VI) in the environment: background and history. Chromium (VI) handbook, pp.1-21.

Jha B., Singh D.N. 2016 A review on synthesis, characterization and industrial application of fly ash zeolites, Journal of Materials Education, 33, 65–132.

Jiménez-Castañeda, M.E. and Medina, D.I., 2017. Use of surfactant-modified zeolites and clays for the removal of heavy metals from water. Water, 9(4), p.235.

Jobby, R., Jha, P., Yadav, A.K., Desai, N., 2018. Biosorption and biotransformation of hexavalent chromium [Cr (VI)]: a comprehensive review. Chemosphere 207, 255e266

Joseph, I V, Tosheva, L. and Doyle, A M, 2020. Simultaneous removal of Cd (II), Co (II), Cu (II), Pb (II), and Zn (II) ions from aqueous solutions via adsorption on fau-type zeolites prepared from coal fly ash. *Journal of Environmental Chemical Engineering*, p.103895.

Joseph, L., Jun, B.M., Flora, J.R., Park, C.M. and Yoon, Y., 2019. Removal of heavy metals from water sources in the developing world using low-cost materials: A review. Chemosphere, 229, pp.142-159.

Juang, R.S. and Shiau, R.C., 2000. Metal removal from aqueous solutions using chitosan-enhanced membrane filtration. Journal of membrane science, 165(2), pp.159-167.

Kasneryk, V., Shamzhy, M., Zhou, J., Yue, Q., Mazur, M., Mayoral, A., Luo, Z., Morris, R.E., Čejka, J. and Opanasenko, M., 2019. Vapour-phase-transport rearrangement technique for the synthesis of new zeolites. Nature Communications, 10(1), pp.1-8.

Kianfar, E. and Ali, R., 2020. Zeolite catalyst based selective for the process MTG: a review. Zeolites: Advances in Research and Applications, 8.

Kianfar, E., 2019. Nanozeolites: synthesized, properties, applications. *Journal of Sol-Gel Science and Technology*, *91*(2), pp.415-429.

Kobayashi, Y., Ogata, F., Nakamura, T. and Kawasaki, N., 2020. Synthesis of novel zeolites produced from fly ash by hydrothermal treatment in alkaline solution and its evaluation as an adsorbent for heavy metal removal. Journal of Environmental Chemical Engineering, 8(2), p.103687.

Koshy, N., and Singh, D.N., 2016. Fly ash zeolites for water treatment applications. Journal of Environmental Chemical Engineering, 4(2), pp.1460-1472.

Kostrubiak, D.E., Vacchi-Suzzi, C., Smith, D.M. and Meliker, J.R., 2017. Blood cadmium and depressive symptoms: Confounded by cigarette smoking. Psychiatry research, 256, pp.444-447.

Kunecki, P., Panek, R., Koteja, A. and Franus, W., 2018. Influence of the reaction time on the crystal structure of Na-P1 zeolite obtained from coal fly ash microspheres. Microporous and Mesoporous Materials, 266, pp.102-108.

Kurniawan, T.A., Chan, G.Y., Lo, W.H. and Babel, S., 2006. Physicochemical treatment techniques for wastewater laden with heavy metals. Chemical engineering journal, 118(1-2), pp.83-98.

Kwak, S., Yoo, J.C., Moon, D.H. and Baek, K., 2018. Role of clay minerals on reduction of Cr (VI). Geoderma, 312, pp.1-5.

Latif, A., Sheng, D., Sun, K., Si, Y., Azeem, M., Abbas, A. and Bilal, M., 2020. Remediation of heavy metals polluted environment using Fe-based nanoparticles: Mechanisms, influencing factors, and environmental implications. Environmental Pollution, p.114728.

Le Hua, Z., Zhou, J. and Shi, J.L., 2011. Recent advances in hierarchically structured zeolites: synthesis and material performances. Chemical Communications, 47(38), pp.10536-10547.

Levantesi, C., La Mantia, R., Masciopinto, C., Böckelmann, U., Ayuso-Gabella, M.N., Salgot, M., Tandoi, V., Van Houtte, E., Wintgens, T. and Grohmann, E., 2010. Quantification of pathogenic microorganisms and microbial indicators in three wastewater reclamation

and managed aquifer recharge facilities in Europe. science of the total environment, 408(21), pp.4923-4930.

Li, Y., Zeng, X., Liu, Y., Yan, S., Hu, Z. and Ni, Y., 2003. Study on the treatment of copper-electroplating wastewater by chemical trapping and flocculation. Separation and Purification Technology, 31(1), pp.91-95.

Li, Z., Qian, W., Chen, Y., Xu, P., Li, J. and Yang, J., 2021. A new treasure in industrial solid waste—coal fly ash for effective oil/water separation. Journal of the Taiwan Institute of Chemical Engineers, 118, pp.196-203.

Li, Z., Wu, L., Sun, S., Gao, J., Zhang, H., Zhang, Z. and Wang, Z., 2019. Disinfection and removal performance for Escherichia coli, toxic heavy metals and arsenic by wood vinegar-modified zeolite. Ecotoxicology and environmental safety, 174, pp.129-136.

Liu, Y., Liu, J. and Song, P., 2020. Recent advances in polysaccharide-based carbon aerogels for environmental remediation and sustainable energy. Sustainable Materials and Technologies, p.e00240.

Liu, Y., Yan, C., Zhao, J., Zhang, Z., Wang, H., Zhou, S. and Wu, L., 2018. Synthesis of zeolite P1 from fly ash under solvent-free conditions for ammonium removal from water. *Journal of Cleaner Production*, *202*, pp.11-22.

Luo, Y., Wu, Y., Ma, S., Zheng, S., Zhang, Y., and Chu, P.K., 2020. Utilization of coal fly ash in China: a mini review on challenges and future directions. Environmental Science and Pollution Research, pp.1-14.

Mainganye, D., 2012. Synthesis of zeolites from South African coal fly ash: Investigation of scale-up conditions (Doctoral dissertation, Cape Peninsula University of Technology).

Makgabutlane, B., Nthunya, L.N., Musyoka, N., Dladla, B.S., Nxumalo, E.N. and Mhlanga, S.D., 2020. Microwave-assisted synthesis of coal fly ash-based zeolites for removal of ammonium from urine. RSC Advances, 10(4), pp.2416-2427.

Makgabutlane, B., Nthunya, L.N., Nxumalo, E.N., Musyoka, N.M. and Mhlanga, S.D., 2020. Microwave Irradiation-Assisted Synthesis of Zeolites from Coal Fly Ash: An Optimization Study for a Sustainable and Efficient Production Process. *ACS omega*.

Marella, T.K., Saxena, A. and Tiwari, A., 2020. Diatom mediated heavy metal remediation: a review. Bioresource Technology, 305, p.123068.

Matjie, R.H., Lesufi, J.M., Bunt, J.R., Strydom, C.A., Schobert, H.H. and Uwaoma, R., 2018. In situ capturing and absorption of sulfur gases formed during thermal treatment of south african coals. ACS Omega, 3(10), pp.14201-14212.

Mishra, S.B., Langwenya, S.P., Mamba, B.B. and Balakrishnan, M., 2010. Study on surface morphology and physicochemical properties of raw and activated South African coal and coal fly ash. Physics and Chemistry of the Earth, Parts A/B/C, 35(13-14), pp.811-814.

Missengue, R.N., Losch, P., Musyoka, N.M., Louis, B., Pale, P. and Petrik, L.F., 2018. Conversion of South African CFA into high-purity ZSM-5 zeolite without additional source of silica or alumina and its application as a methanol-to-olefins catalyst. *Catalysts*, *8*(4), p.124.

Moazeni, M., Parastar, S., Mahdavi, M. and Ebrahimi, A., 2020. Evaluation efficiency of Iranian natural zeolites and synthetic resin to removal of lead ions from aqueous solutions. Applied Water Science, 10(2), pp.1-9.

Mokgehie, T., Gitari, W.M. and Tavengwa, N.T., 2020. Synthesis and characterization of zeolites produced by ultrasonication of coal fly ash/NaOH slurry filtrates. *South African Journal of Chemistry*, *73*, pp.64-69.

Momodu, M.A. and Anyakora, C.A., 2010. Heavy metal contamination of ground water: The Surulere case study. Research Journal Environmental and Earth Sciences, 2(1), pp.39-43.

Morrison, G., Fatoki, O.S., Persson, L. and Ekberg, A., 2001. Assessment of the impact of point source pollution from the Keiskammahoek Sewage Treatment Plant on the Keiskamma River-pH, electrical conductivity, oxygen-demanding substance (COD) and nutrients. Water Sa, 27(4), pp.475-480.

Muchuweti, M., Birkett, J.W., Chinyanga, E., Zvauya, R., Scrimshaw, M.D. and Lester, J.N., 2006. Heavy metal content of vegetables irrigated with mixtures of wastewater and sewage sludge in Zimbabwe: implications for human health. Agriculture, Ecosystems & Environment, 112(1), pp.41-48.

Murayama, N., Yamamoto, H. and Shibata, J., 2002. Mechanism of zeolite synthesis from coal fly ash by alkali hydrothermal reaction. *International Journal of Mineral Processing*, *64*(1), pp.1-17.

Muriithi, G.N., Petrik, L.F. and Doucet, F.J., 2020. Synthesis, characterisation, and CO2 adsorption potential of NaA and NaX zeolites and hydrotalcite obtained from the same coal fly ash. Journal of CO_2 Utilization, 36, pp.220-230.

Mushtaq, F., Zahid, M., Bhatti, I.A., Nasir, S. and Hussain, T., 2019. Possible applications of coal fly ash in wastewater treatment. Journal of environmental management, 240, pp.27-46.

Mushtaq, F., Zahid, M., Bhatti, I.A., Nasir, S. and Hussain, T., 2019. Possible applications of coal fly ash in wastewater treatment. Journal of environmental management, 240, pp.27-46.

Musyoka, N.M., 2009. *Hydrothermal Synthesis and Optimisation of Zeolite Na-P1 from South African CFA* (Doctoral dissertation).

Nadeem, N., Zahid, M., Bhatti, H.N., Shahid, I., Mustafa, G. and Tabasum, A., 2021. Wastewater remediation using coal fly ash nanocomposites. In aquananotechnology (pp. 149-174). Elsevier.

Narayanan, S., Vijaya, J.J., Sivasanker, S., Kennedy, L.J. and Jesudoss, S.K., 2015. Structural, morphological, and catalytic investigations on hierarchical ZSM-5 zeolite hexagonal cubes by surfactant assisted hydrothermal method. *Powder Technology*, *274*, pp.338-348.

Nasar, A. and Mashkoor, F., 2019. Application of polyaniline-based adsorbents for dye removal from water and wastewater—a review. Environmental Science and Pollution Research, 26(6), pp.5333-5356.

Ngah, W.W. and Hanafiah, M.M., 2008. Removal of heavy metal ions from wastewater by chemically modified plant wastes as adsorbents: a review. Bioresource Technology, 99(10), pp.3935-3948.

Nkongolo, E.B., 2020. Passive treatment of acid mine drainage using South African coal fly ash in a column reactor (Doctoral dissertation, Cape Peninsula University of Technology).

Ochedi, F.O., Liu, Y. and Hussain, A., 2020. A review on coal fly ash-based adsorbents for mercury and arsenic removal. Journal of Cleaner Production, p.122143.

Odlare, M., 2014. Introductory Chapter for Water Resources, Reference Module in Earth Systems and Environmental Sciences.

Ogunkunle, C.O., Abdulrahaman, A.A. and Fatoba, P.O., 2013. Influence of cement dust pollution on leaf epidermal features of Pennisetum Purpureum and Sida Acuta. Environmental and Experimental Biology, 11(1), pp.73-79.

Ojumu, T.V., Du Plessis, P.W. and Petrik, L.F., 2016. Synthesis of zeolite A from coal fly ash using ultrasonic treatment–A replacement for fusion step. Ultrasonics Sonochemistry, 31, pp.342-349.

Okoh, A.I., Odjadjare, E.E., Igbinosa, E.O. and Osode, A.N., 2007. Wastewater treatment plants as a source of microbial pathogens in receiving watersheds. African Journal of Biotechnology, 6(25).

Ou, J.H., Sheu, Y.T., Tsang, D.C., Sun, Y.J. and Kao, C.M., 2020. Application of iron/aluminum bimetallic nanoparticle system for chromium-contaminated groundwater remediation. Chemosphere, 256, p.127158.

Owoseni, M.C., Olaniran, A.O. and Okoh, A.I., 2017. Chlorine tolerance and inactivation of Escherichia coli recovered from wastewater treatment plants in the Eastern Cape, South Africa. Applied Sciences, 7(8), p.810.

Ozdemir, O.D. and Piskin, S., 2019. A novel synthesis method of zeolite x from coal fly ash: alkaline fusion followed by ultrasonic-assisted synthesis method. *Waste and Biomass Valorization*, *10*(1), pp.143-154.

Pakade, V., Cukrowska, E., Darkwa, J., Torto, N. and Chimuka, L., 2011. Selective removal of chromium (VI) from sulphates and other metal anions using an ion-imprinted polymer. Water SA, 37(4), pp.529-538.

Pandey, P.K., Sharma, S.K. and Sambi, S.S., 2010. Kinetics and equilibrium study of chromium adsorption on zeoliteNaX. International Journal of Environmental Science & Technology, 7(2), pp.395-404.

Park, M., Choi, C.L., Lim, W.T., Kim, M.C., Choi, J. and Heo, N.H., 2000. Molten-salt method for the synthesis of zeolitic materials: I. Zeolite formation in alkaline molten-salt system. *Microporous and Mesoporous Materials*, *37*(1-2), pp.81-89.

Petrik, L.F., White, R.A., Klink, M.J., Somerset, V.S., Burgers, C.L. and Fey, M.V., 2003, October. Utilization of South African fly ash to treat acid coal mine drainage, and production of high-quality zeolites from the residual solids. In Proceedings of the ash utilization symposium, Lexington, KY, USA (Vol. 2022).

Pina, M.P., Mallada, R., Arruebo, M., Urbiztondo, M., Navascués, N.D., De La Iglesia, O. and Santamaria, J., 2011. Zeolite films and membranes. Emerging applications. Microporous and Mesoporous Materials, 144(1-3), pp.19-27.

Plessis, P.W.D., Ojumu, T.V. and Petrik, L.F., 2013. Waste minimization protocols for the process of synthesizing zeolites from South African coal fly ash. Materials, 6(5), pp.1688-1703.

Poznanović Spahić, M.M., Sakan, S.M., Glavaš-Trbić, B.M., Tančić, P.I., Škrivanj, S.B., Kovačević, J.R. and Manojlović, D.D., 2019. Natural and anthropogenic sources of chromium, nickel and cobalt in soils impacted by agricultural and industrial activity (Vojvodina, Serbia). Journal of Environmental Science and Health, Part A, 54(3), pp.219-230.

Qi, X., Gao, S., Ding, G. and Tang, A.N., 2017. Synthesis of surface Cr (VI)-imprinted magnetic nanoparticles for selective dispersive solid-phase extraction and determination of Cr (VI) in water samples. Talanta, 162, pp.345-353.

Quesada, H.B., Baptista, A.T.A., Cusioli, L.F., Seibert, D., de Oliveira Bezerra, C. and Bergamasco, R., 2019. Surface water pollution by pharmaceuticals and an alternative of removal by low-cost adsorbents: A review. Chemosphere, 222, pp.766-780.

Rahman, Z. and Singh, V.P., 2019. The relative impact of toxic heavy metals (THMs) (arsenic (As), cadmium (Cd), chromium (Cr)(VI), mercury (Hg), and lead (Pb)) on the total

environment: an overview. Environmental Monitoring and Assessment, 191(7), pp.1-21.

Rahmani, K., Mahvi, A.H., Vaezi, F., Mesdaghinia, A.R., NABIZADEH, N.R. and Nazmara, S., 2009. Bioremoval of lead by use of waste activated sludge.

Rai, P.K., Lee, S.S., Zhang, M., Tsang, Y.F. and Kim, K.H., 2019. Heavy metals in food crops: Health risks, fate, mechanisms, and management. Environment International, 125, pp.365-385.

Ram, L.C. and Masto, R.E., 2010. An appraisal of the potential use of fly ash for reclaiming coal mine spoil. Journal of Environmental Management, 91(3), pp.603-617.

Rangabhashiyam, S. and Balasubramanian, P., 2018. Adsorption behaviors of hazardous methylene blue and hexavalent chromium on novel materials derived from Pterospermum acerifolium shells. Journal of Molecular Liquids, 254, pp.433-445.

Razavian, M. and Fatemi, S., 2015. Synthesis and evaluation of seed-directed hierarchical ZSM-5 catalytic supports: inductive influence of various seeds and aluminosilicate gels on the physicochemical properties and catalytic dehydrogenative behavior. *Materials Chemistry and Physics*, *165*, pp.55-65.

Rech, A.S., Rech, J.C., Caprario, J., Tasca, F.A., Recio, M.Á.L. and Finotti, A.R., 2019. Use of shrimp shell for adsorption of metals present in surface runoff. Water Science and Technology, 79(12), pp.2221-2230.

Ren, X., Qu, R., Liu, S., Zhao, H., Wu, W., Song, H., Zheng, C., Wu, X. and Gao, X., 2020. Synthesis of zeolites from coal fly ash for the removal of harmful gaseous pollutants: A review. Aerosol and Air Quality Research, 20(5), pp.1127-1144.

Ren, X., Zhang, Z., Luo, H., Hu, B., Dang, Z., Yang, C. and Li, L., 2014. Adsorption of arsenic on modified montmorillonite. *Applied Clay Science*, *97*, pp.17-23.

Reshadi, M.A.M., Bazargan, A. and McKay, G., 2020. A review of the application of adsorbents for landfill leachate treatment: Focus on magnetic adsorption. Science of The Total Environment, p.138863.

Rimayi, C.; Odusanya, D.; Weiss, J.M.; de Boer, J.; Chimuka, L. Contaminants of emerging concern in the Hartbeespoort Dam catchment and the Umgeni River estuary 2016 pollution incident, South Africa. Science. Total Environmental. 2018, 627, 1008–1017

Ríos C.A., Williams C.D., Roberts C.L. (2008) Removal of heavy metals from AMD using CFA, natural clinker and synthetic zeolites, Journal of Hazardous Materials, 156, 23–35.

Rojas, S. and Horcajada, P., 2020. Metal–organic frameworks for the removal of emerging organic contaminants in water. Chemical reviews, 120(16), pp.8378-8415.

Sajid, M., Nazal, M.K., Baig, N. and Osman, A.M., 2018. Removal of heavy metals and organic pollutants from water using dendritic polymers-based adsorbents: a critical review. Separation and Purification Technology, 191, pp.400-423.

Sangaroon, P., Srisatit, T. and Sriprom, P., 2019. Optimization Conditions for Increasing Cation Exchange Capacity of coal fly ash Zeolite Modified with Chitosan Using Box-Behnken Design. *Environment Asia*, *12*(2).

Saputro, S., Yoshimura, K., Matsuoka, S., Takehara, K., Aizawa, J. and Tennichi, Y., 2014. Speciation of dissolved chromium and the mechanisms controlling its concentration in natural water. Chemical Geology, 364, pp.33-41.

Sarbak, Z., Stańczyk, A. and Kramer-Wachowiak, M., 2004. Characterisation of surface properties of various fly ashes. Powder Technology, 145(2), pp.82-87.

Sardar, K., Ali, S., Hameed, S., Afzal, S., Fatima, S., Skhakoor, M.B., Baharwana,S.A. and Tauqeer, H.M.,2013. Heavy metals contamination and what are the impact on living organisms. *Greener Journal of Environmental Management and Public Safety*,2(4), pp. 172-179.

Sarti, E., 2014. Adsorption properties of particles for environmental applications.

Schlautman, M.A. and Han, I., 2001. Effects of pH and dissolved oxygen on the reduction of hexavalent chromium by dissolved ferrous iron in poorly buffered aqueous systems. Water Research, 35(6), pp.1534-1546.

Sen, A.K. and De, A.K., 1987. Adsorption of mercury (II) by coal fly ash. *Water Research*, *21*(8), pp.885-888.

Shah, B.A., Shah, A.V. and Singh, R.R., 2009. Sorption isotherms and kinetics of chromium uptake from wastewater using natural sorbent material. International Journal of Environmental Science & Technology, 6(1), pp.77-90.

Shanker, A.K., Cervantes, C., Loza-Tavera, H. and Avudainayagam, S., 2005. Chromium toxicity in plants. Environment International, 31(5), pp.739-753.

Siddiqui, S.I., Fatima, B., Tara, N., Rathi, G. and Chaudhry, S.A., 2019. Recent advances in remediation of synthetic dyes from wastewaters using sustainable and low-cost adsorbents. The impact and prospects of green chemistry for textile technology, pp.471-507.

Singh, S., Jain, A., Tiwari, K.R., Kumar, N. and Tomar, R., 2019. Synthesis and Characterization of Surface Modified Zeolite and its Application as Adsorbent for Pesticide. *International Journal of Materials Science*, *14*(1), pp.17-30.

Singureanu, C. and Woinaroschy, A., 2017. Simulation of Bardenpho Wastewater Treatment Process for Nitrogen Removal using SuperPro Designer Simulator. UPB Sci. Bull., Series B, 79.

Suganya, S., 2019. An investigation of adsorption parameters on ZVI-AC nanocomposite in the displacement of Se (IV) ions through CCD analysis. Journal of Industrial and Engineering Chemistry, 75, pp.211-223.

Suruchi and Khanna P., (2011). Assessment of heavy metal contamination in different vegetables grown in and around urban areas. Research Journal of Environmental Toxicology 5:162–179.

Swaroop, A., Bagchi, M., Preuss, H.G., Zafra-Stone, S., Ahmad, T. and Bagchi, D., 2019. Benefits of chromium (III) complexes in animal and human health. In the Nutritional Biochemistry of Chromium (III) (pp. 251-278). Elsevier.

Taghizadeh, M. and Hassanpour, S., 2017. Selective adsorption of Cr (VI) ions from aqueous solutions using a Cr (VI)-imprinted polymer supported by magnetic multiwall carbon nanotubes. Polymer, 132, pp.1-11.

Tahir, M.B., Kiran, H. and Iqbal, T., 2019. The detoxification of heavy metals from aqueous environment using nano-photocatalysis approach: a review. Environmental Science and Pollution Research, 26(11), pp.10515-10528.

Tajiki, A. and Abdouss, M., 2017. Synthesis and characterization of graphene oxide nano-sheets for effective removal of copper phthalocyanine from aqueous media. Iranian Journal of Chemistry and Chemical Engineering (IJCCE), 36(4), pp.1-9.

Tamjidi, S., Esmaeili, H. and Moghadas, B.K., 2019. Application of magnetic adsorbents for removal of heavy metals from wastewater: a review study. Materials Research Express, 6(10), p.102004.

Tang, X.L., Sun, Z. and Gong, L., 2018. Chromium supplementation in women with polycystic ovary syndrome: Systematic review and meta-analysis. Journal of Obstetrics and Gynaecology Research, 44(1), pp.134-143.

Tariq, S.R., Shah, M.H., Shaheen, N., Khalique, A., Manzoor, S. and Jaffar, M., 2005. Multivariate analysis of selected metals in tannery effluents and related soil. Journal of Hazardous Materials, 122(1-2), pp.17-22.

Tavengwa, N.T., Cukrowska, E. and Chimuka, L., 2013. Synthesis, adsorption, and selectivity studies of N-propyl quaternized magnetic poly (4-vinylpyridine) for hexavalent chromium. *Talanta*, *116*, pp.670-677.

Tavengwa, N.T., Cukrowska, E. and Chimuka, L., 2014. Synthesis of bulk ion-imprinted polymers (IIPs) embedded with oleic acid coated Fe 3 O 4 for selective extraction of hexavalent uranium. *Water SA*, *40*(4), pp.623-630.

Tchounwou, P.B., Yedjou, C.G., Patlolla, A.K. and Sutton, D.J., 2012. Heavy metal toxicity and the environment. Molecular, clinical, and environmental toxicology, pp.133-164.

Teixeira, E.R., Mateus, R., Camoes, A.F., Bragança, L. and Branco, F.G., 2016. Comparative environmental life-cycle analysis of concretes using biomass and coal fly ashes as partial cement replacement material. Journal of Cleaner Production, 112, pp.2221-2230.

Tkaczewska, E., Mróz, R. and Łój, G., 2012. Coal–biomass fly ashes for cement production of CEM II/AV 42.5 R. Construction and Building Materials, 28(1), pp.633-639.

Tsitsishvili, V., Dolaberidze, N., Mirdzveli, N., Nijaradze, M., Amiridze, Z., Gabunia, V. and Tsintskaladze, G., 2019. Hydrothermal transformation of natural analcime and phillipsite. *Geography. Atalante. Academic. Science*, *13*(1).

Vardhan, K.H., Kumar, P.S., and Panda, R.C., 2019. A review on heavy metal pollution, toxicity, and remedial measures: Current trends and future perspectives. Journal of Molecular Liquids, 290, p.111197.

Vasileiou, E., Papazotos, P., Dimitrakopoulos, D. and Perraki, M., 2019. Expounding the origin of chromium in groundwater of the Sarigkiol basin, Western Macedonia, Greece: a cohesive statistical approach and hydrochemical study. Environmental monitoring and assessment, 191(8), pp.1-34.

Vassilev, S.V. and Vassileva, C.G., 2005. Methods for characterization of composition of fly ashes from coal-fired power stations: a critical overview. *Energy & Fuels*, *19*(3), pp.1084-1098.

Velempini, T., Pillay, K., Mbianda, X.Y. and Arotiba, O.A., 2017. Epichlorohydrin crosslinked carboxymethyl cellulose-ethylenediamine imprinted polymer for the selective uptake of Cr (VI). International Journal of Biological Macromolecules, 101, pp.837-844.

Verboekend, D., Keller, T.C., Mitchell, S. and Pérez-Ramírez, J., 2013. Hierarchical FAU-and LTA-Type Zeolites by Post-Synthetic Design: A New Generation of Highly Efficient Base Catalysts. *Advanced Functional Materials*, *23*(15), pp.1923-1934.

Verlicchi, P. and Grillini, V., 2020. Surface water and groundwater quality in South Africa and mozambique—Analysis of the Most critical pollutants for drinking purposes and challenges in water treatment selection. Water, 12(1), p.305.

Verrecchia, G., Cafiero, L., de Caprariis, B., Dell'Era, A., Pettiti, I., Tuffi, R. and Scarsella, M., 2020. Study of the parameters of zeolites synthesis from coal fly ash in order to optimize their CO2 adsorption. Fuel, 276, p.118041.

Verrecchia, G., Cafiero, L., de Caprariis, B., Dell'Era, A., Pettiti, I., Tuffi, R. and Scarsella, M., 2020. Study of the parameters of zeolites synthesis from coal fly ash in order to optimize their CO_2 adsorption. Fuel, 276, p.118041.

Vincent, J.B., 2020. Benefits of Trivalent Chromium in Human Nutrition. Metal Toxicology Handbook.

Visa, M. and Chelaru, A.M., 2014. Hydrothermally modified fly ash for heavy metals and dyes removal in advanced wastewater treatment. Applied Surface Science, 303, pp.14-22.

Wakelin, S.A., Colloff, M.J. and Kookana, R.S., 2008. Effect of wastewater treatment plant effluent on microbial function and community structure in the sediment of a freshwater stream with variable seasonal flow. Applied and environmental microbiology, 74(9), pp.2659-2668.

Wang, N., Sun, X., Zhao, Q., Yang, Y. and Wang, P., 2020. Leachability and adverse effects of coal fly ash: A review. Journal of hazardous Materials, p.122725.

Wang, S. and Zhu, Z.H., 2005. Sonochemical treatment of fly ash for dye removal from wastewater. Journal of hazardous materials, 126(1-3), pp.91-95.

Wu, S., Dai, X., Cheng, T. and Li, S., 2018. Highly sensitive and selective ion-imprinted polymers based on one-step electrodeposition of chitosan-graphene nanocomposites for the determination of Cr (VI). Carbohydrate Polymers, 195, pp.199-206.

Xu, X., Cao, X. and Zhao, L., 2013. Comparison of rice husk-and dairy manure-derived biochars for simultaneously removing heavy metals from aqueous solutions: role of mineral components in biochars. *Chemosphere*, *92*(8), pp.955-961.

Yang L, Qian X, Yuan P, Bai H, Miki T, Men, F, Li H., and Nagasaka T, 2019. Green synthesis of zeolite 4A using fly ash fused with synergism of NaOH and Na_2CO_3. Journal of Cleaner Production, 212, pp.250-260.

Yang, L., Qian, X., Yuan, P., Bai, H., Miki, T., Men, F., Li, H. and Nagasaka, T., 2019. Green synthesis of zeolite 4A using fly ash fused with synergism of NaOH and Na_2CO_3. Journal of Cleaner Production, 212, pp.250-260.

Yang, X.J., Fane, A.G. and MacNaughton, S., 2001. Removal and recovery of heavy metals from wastewaters by supported liquid membranes. Water Science and Technology, 43(2), pp.341-348.

Yin, X., Li, Z., Wang, S., Chu, N., Yang, J. and Wang, J., 2015. Hydrothermal synthesis of hierarchical zeolite T aggregates using tetramethylammonium hydroxide as single template. Microporous and Mesoporous Materials, 201, pp.247-257.

Yu, W., Deng, L., Yuan, P., Liu, D., Yuan, W. and Chen, F., 2015. Preparation of hierarchically porous diatomite/MFI-type zeolite composites and their performance for benzene adsorption: the effects of desilication. Chemical Engineering Journal, 270, pp.450-458.

Zeremski-Škorić, T., Ninkov, J., Sekulić, P., Milić, S., Vasin, J., Dozet, D. and Jakšić, S., 2010. Heavy metal content in some fertilizers used in Serbia. Ratarstvo i povrtarstvo, 47(1), pp.281-287.

Zhang, L., Fu, F. and Tang, B., 2019. Adsorption and redox conversion behaviors of Cr (VI) on goethite/carbon microspheres and akaganeite/carbon microspheres composites. Chemical Engineering Journal, 356, pp.151-160.

Zhang, Y., Chen, Y., Kang, W., Han, H., Song, H., Zhang, C., Wang, H., Yang, X., Gong, X., Zhai, C. and Deng, J., 2020. Excellent adsorption of Zn (II) using NaP zeolite adsorbent synthesized from coal fly ash via stage treatment. Journal of Cleaner Production, 258, p.120736.

Zhang, Y., Zhou, L., Chen, L., Guo, Y., Guo, F., Wu, J. and Dai, B., 2020. Synthesis of zeolite Na-P1 from CFAproduced by gasification and its application as adsorbent for removal of Cr (VI) from water. *frontiers of chemical science and engineering*.

Zhi, S., Banting, G., Li, Q., Edge, T.A., Topp, E., Sokurenko, M., Scott, C., Braithwaite, S., Ruecker, N.J., Yasui, Y. and McAllister, T., 2016. Evidence of naturalized stress-tolerant strains of Escherichia coli in municipal wastewater treatment plants. Applied and environmental microbiology, 82(18), pp.5505-5518.

Zhou, Y., Lu, J., Zhou, Y. and Liu, Y., 2019. Recent advances for dyes removal using novel adsorbents: a review. Environmental pollution, 252, pp.352-365.

Zhou, Z., Liu, X., Zhang, M., Jiao, J., Zhang, H., Du, J., Zhang, B. and Ren, Z., 2020. Preparation of highly efficient ion-imprinted polymers with Fe_3O_4 nanoparticles as carrier for removal of Cr (VI) from aqueous solution. Science of The Total Environment, 699, p.134334

Zhu, R., Chen, Q., Zhou, Q., Xi, Y., Zhu, J. and He, H., 2016. Adsorbents based on montmorillonite for contaminant removal from water: A review. Applied Clay Science, 123, pp.239-258.

Zhu, Y., Fan, W., Zhou, T. and Li, X., 2019. Removal of chelated heavy metals from aqueous solution: A review of current methods and mechanisms. Science of the Total Environment, 678, pp.253-266.

Appendix

Supplementary data

This section gives supplementary data in this dissertation

Appendix

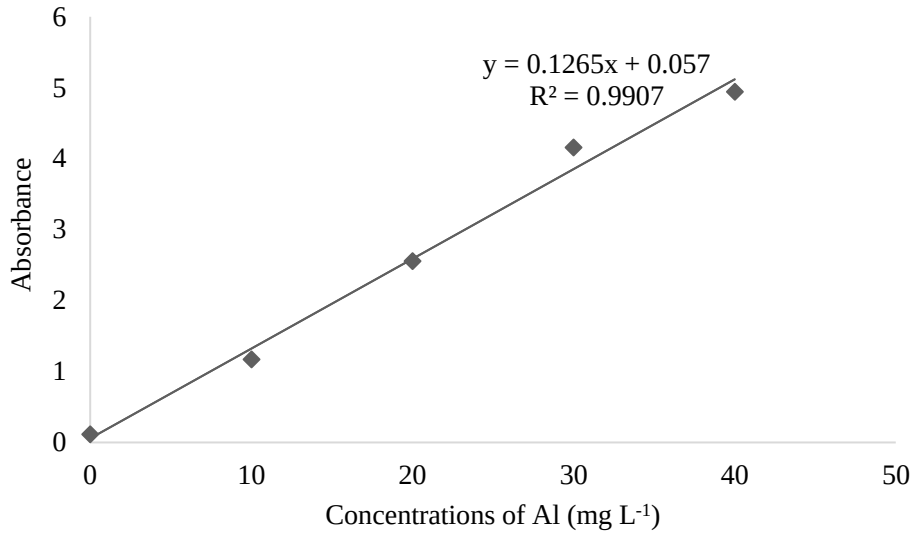

Fig. A1: Calibration curve for Aluminium for the optimization of NaOH concentration

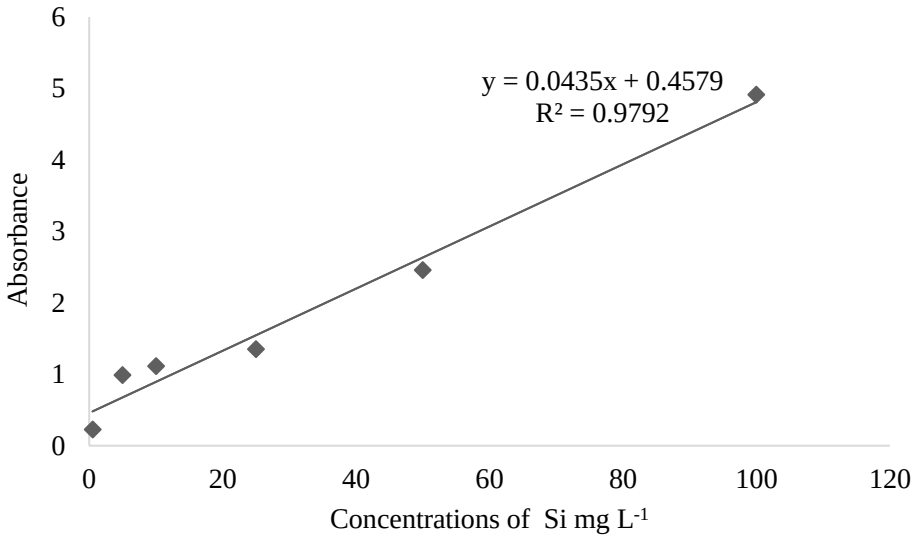

Fig. A2: Calibration curve of silicon for the optimization of NaOH concentration

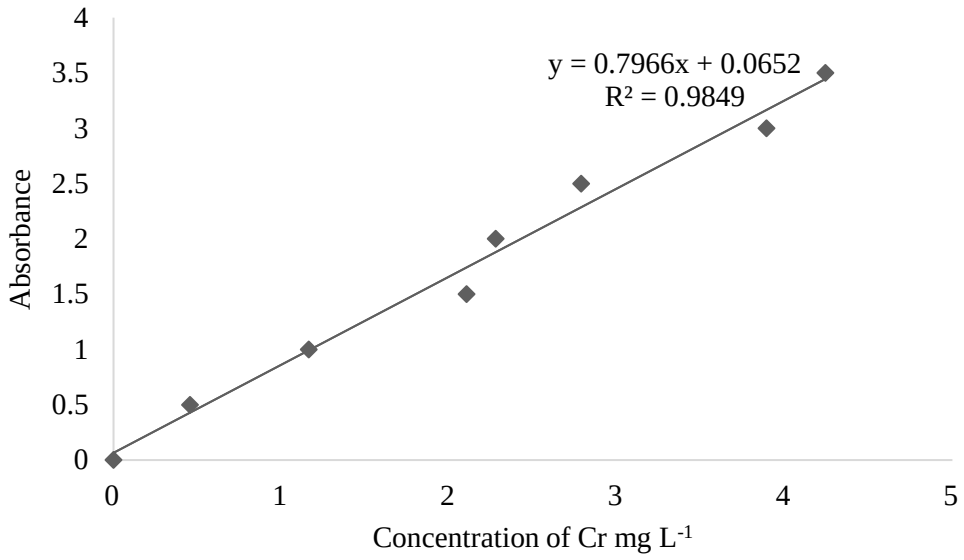

Fig.A3: Calibration curve of chromium optimization parameters for Cr (VI) uptake

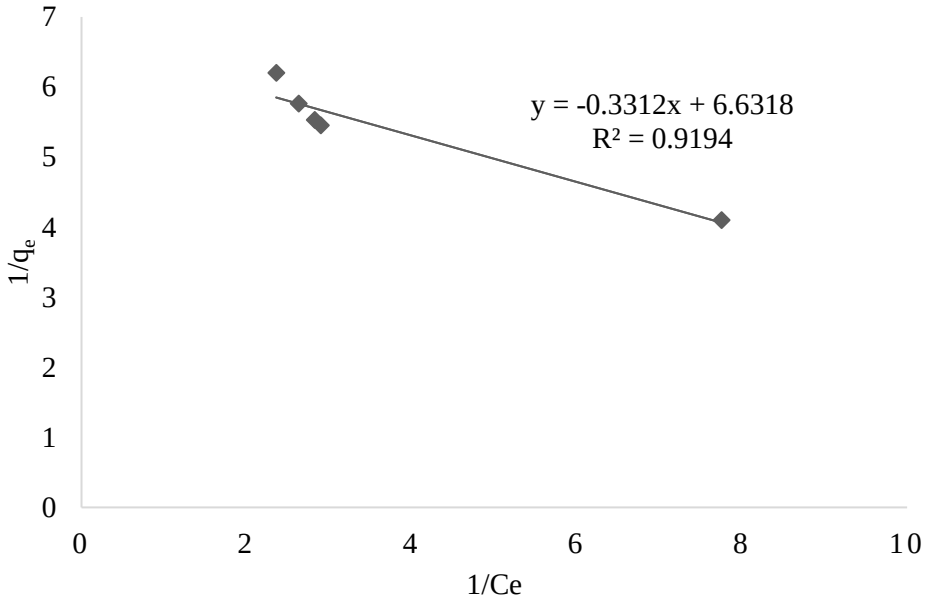

Fig. A4: Linearized form of Langmuir isotherm for the adsorption of Cr (VI) onto zeolites.

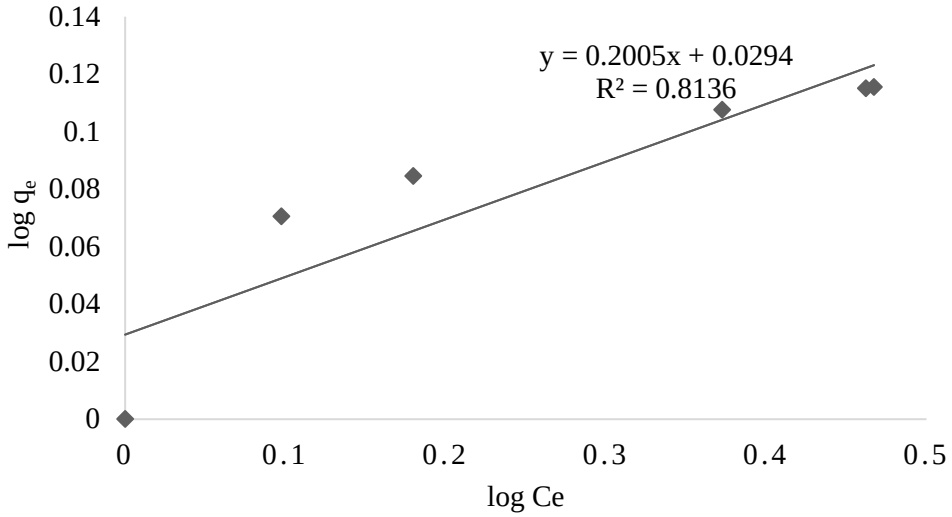

Fig A5: Linearized form of Freundlich isotherm for the adsorption of Cr (VI) onto zeolites.

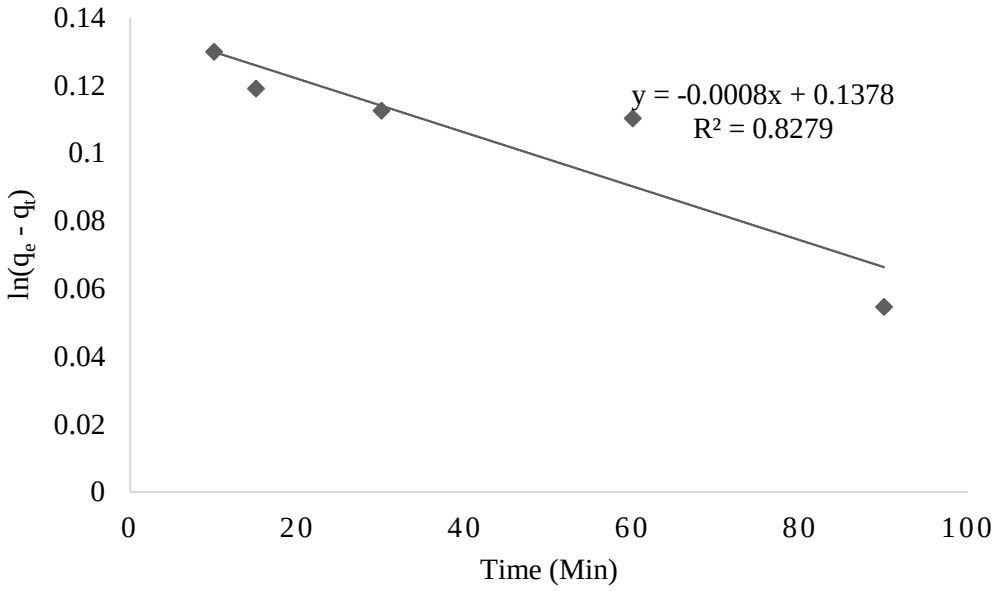

Fig A6: Pseudo first order plots for the adsorption of chromium onto zeolites.

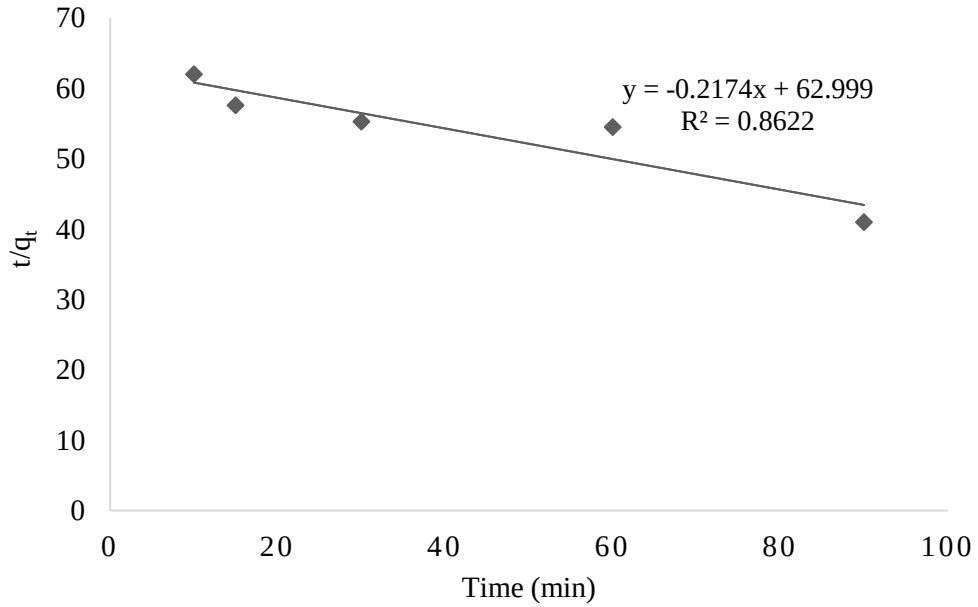

Fig A7: Pseudo second order plots for the adsorption of chromium onto zeolites.

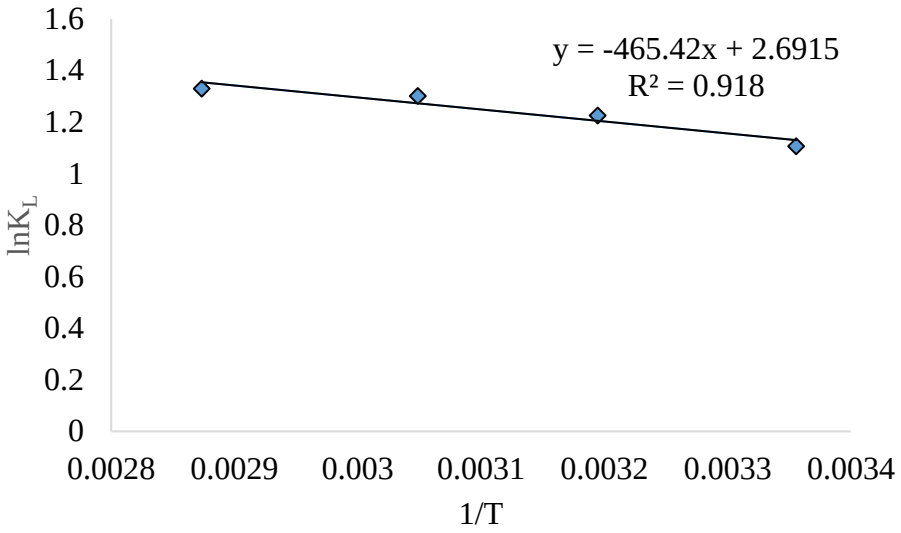

Fig.A8: Thermodynamic parameters for Cr (VI) sorption on the adsorbent.

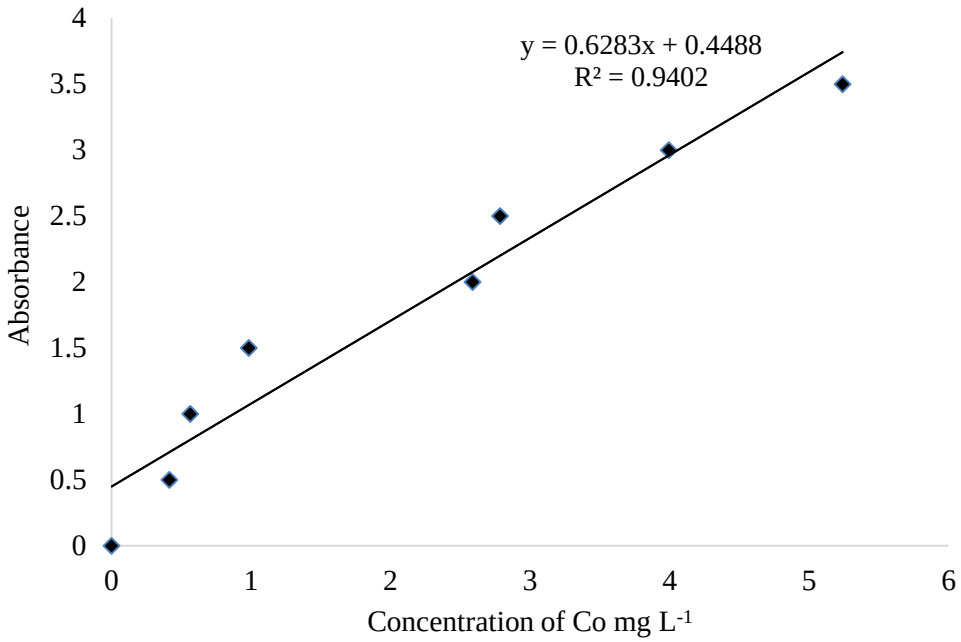

Fig. A9: Calibration curve of Cobalt

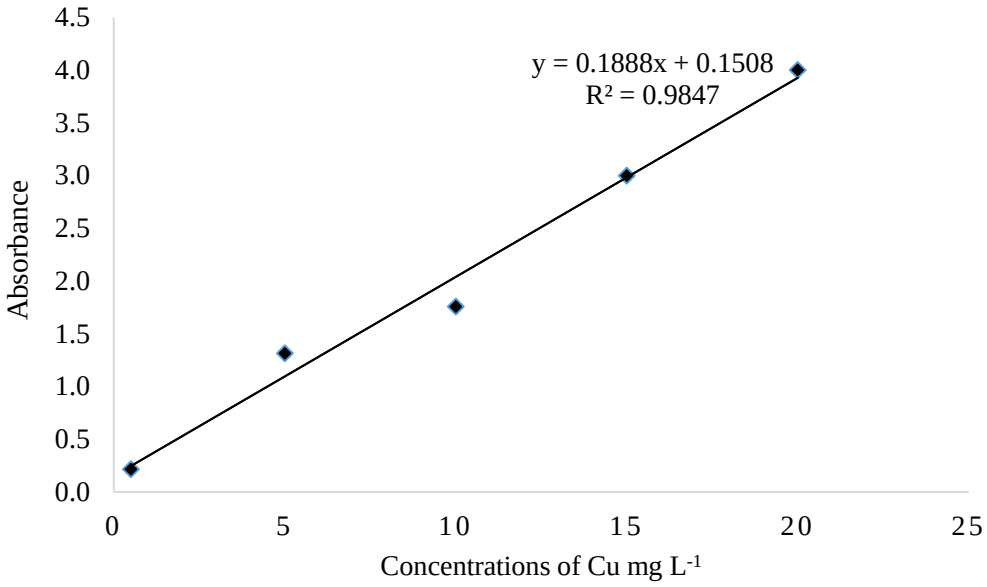

Fig. A10: Calibration curve of Copper

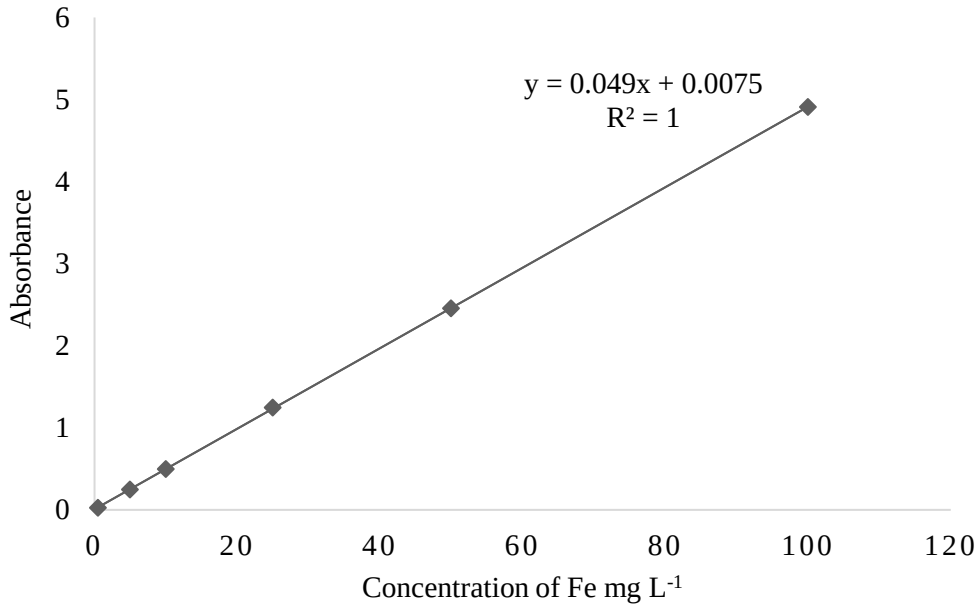

Fig. A11: Calibration curve of Iron

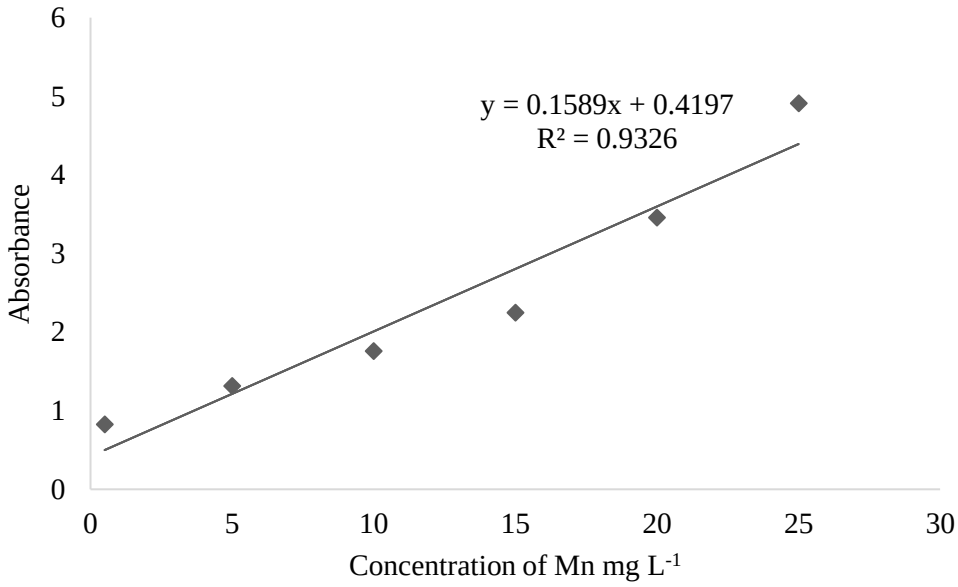

Fig. A12: Calibration curve of Manganese.

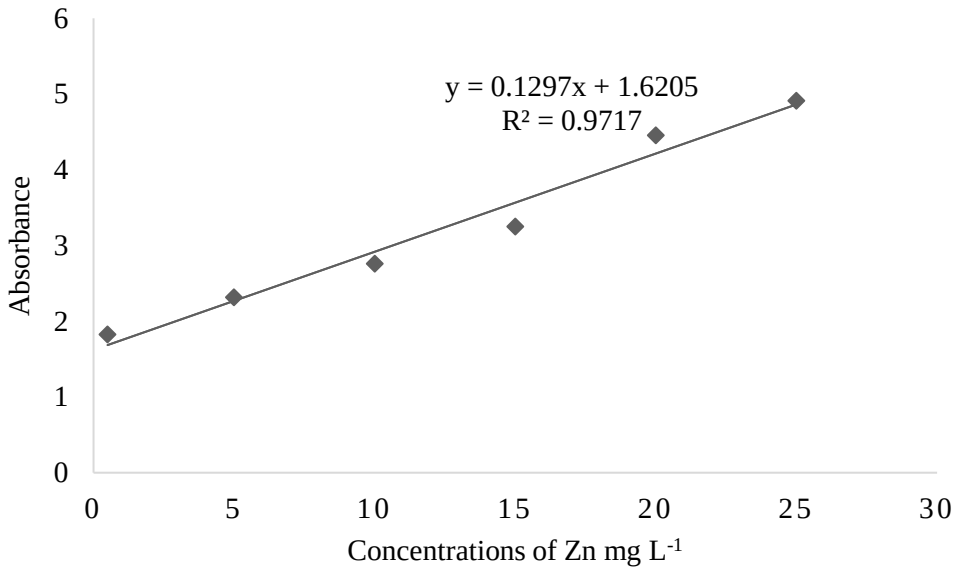

Fig. A13: Calibration curve of zinc